AD 400 459

ASD-TDR-62-1105

INVESTIGATION OF ELECTRODELESS PULSED PLASMA PROPULSION

TECHNICAL DOCUMENTARY REPORT ASD-TDR-62-1105

FEBRUARY 1963

Propulsion Laboratory
Aeronautical Systems Division
Air Force Systems Command
Wright-Patterson Air Force Base, Ohio

Project No. 3141, Task No. 314103

(Prepared under Contract No. AF 33(616)-8331 by Aerojet-General Nucleonics, San Ramon, California,
Authors: J. S. Luce, D. C. Gates, W. B. Day, J. F. Detko, O. D. Johns, J. L. Wyatt)

NOTICES

When Government drawings, specifications, or other data are used for any purpose other than in connection with a definitely related Government procurement operation, the United States Government thereby incurs no responsibility nor any obligation whatsoever; and the fact that the Government may have formulated, furnished, or in any way supplied the said drawings, specifications, or other data, is not to be regarded by implication or otherwise as in any manner licensing the holder or any other person or corporation, or conveying any rights or permission to manufacture, use, or sell any patented invention that may in any way be related thereto.

Qualified requesters may obtain copies of this report from the Armed Services Technical Information Agency, (ASTIA), Arlington Hall Station, Arlington 12, Virginia.

Copies of this report should not be returned to the Aeronautical Systems Division unless return is required by security considerations, contractual obligations, or notice on a specific document.

FOREWORD

This report was prepared by Aerojet-General Nucleonics, San Ramon, California, on Air Force contract AF 33(616)-8331, under Task No. 314103 of Project No. 3141, "Electrical Propulsion Technology." The work was administered under the direction of the Propulsion Laboratory, Aeronautical Systems Division. Mr. Richard Rivir was Task Engineer for the Laboratory.

The studies presented began in July 1961 and were concluded in November 1962. Dr. John S. Luce was responsible for research activity of Aerojet-General Nucleonics.

Dr. D. C. Gates was in charge of the experimental program. He was assisted by W. B. Day (plasma conductivity measurements and pulsed plasma source studies), J. F. Detko (d.c. plasma source development for flux trapping), O. D. Johns (superconductivity applications), and J. L. Wyatt (theory of plasma-field interactions). Contributions to the program were also made by J. A. Gray and his test engineers, and S. L. Wood, who assisted in data reduction.

This report is the final report and it concludes the work on contract AF 33(616)-8331. The contractor's report number is AN-759.

ABSTRACT

This report is a summary of the principal results of a seventeen month research program for the analytical and experimental investigation of electrodeless plasma accelerators as space propulsion devices. The investigation was directed toward the determination of the nature of the field-plasma interaction and the over-all performance characteristics of electrodeless accelerators. Progress included the design and construction of an increasing phase velocity transmission line for the study of synchronous and induction modes of acceleration.

Measurements were made of the velocity, density, and conductivity of the plasma produced by a button source to be used with the transmission line. Diagnostic equipment was constructed for the measurement of plasma velocity, density, temperature, and conductivity. The button-type sources studied proved suitable for injecting into a transmission line and capable of producing a copper plasma with densities up to 10^{15}/cc and velocities in the neighborhood of 2×10^4 m/sec. Conductivities were in the range of 1000 to 1500 mho/m.

Among the principal results of the studies of the interaction of this plasma with the transmission line was the preferential trapping of plasma on the leading portion of the traveling cusp. This result was in sharp contrast to the ineffectiveness of the trailing half of the cusp to retain and accelerate the plasma. These findings support a flux trapping concept which was devised to improve the field-plasma interaction, containment and disengagement of the plasma from the traveling field at the end of the transmission line. Also, there was found direct evidence for the presence of circulating Hall currents in the accelerator. Finally, there is strong evidence for the occurrence of a large-scale instability which developed in the reflected wave.

TABLE OF CONTENTS

TABLE OF CONTENTS
(Continued)

TABLE OF CONTENTS
(Continued)

LIST OF FIGURES

LIST OF FIGURES
(continued)

LIST OF FIGURES
(continued)

LIST OF FIGURES
(continued)

LIST OF FIGURES
(continued)

I. INTRODUCTION

The research program has been designed to investigate the problems associated with electrodeless acceleration. This program centered around the design, construction and operation of an electrodeless accelerator to be used in studies of basic containment and acceleration properties and over-all performance of such a device. A transmission line was constructed for use as either a synchronous or induction accelerator. Since the plasma source is a vital component for any electrodeless accelerator, one of the experimental tasks was to construct an efficient, reliable, long-lived plasma source. The plasma source work paralleled the accelerator program. Progress up to the time of the interim report[1] consisted largely of the design of the apparatus, procurement of materials, and fabrication and testing of the plasma source, the transmission line, and the diagnostic equipment. Some of the information in that report has been reproduced here in order to clarify various aspects of the program.

Among the major problems associated with accelerating a plasma for space propulsion are: (1) production and maintenance of a highly conducting plasma; (2) containment (i.e., insulation of the plasma from the walls); (3) effective interaction between the applied electromagnetic fields and the plasma; and (4) efficiency, i.e., the attainment of a large fraction of directed kinetic energy at the exit of the accelerator.

Although a traveling wave accelerator may be a reliable and durable system in principle, a high efficiency design has yet to be demonstrated. Directed kinetic energy, rather than thermal energy, can be effectively imparted to the plasma, but under most conditions this will be only a small fraction of the energy in the electromagnetic field. In an efficient accelerator the plasma must be highly conducting to allow maximum interaction with the applied electromagnetic fields, and minimum slippage losses. Magnetic containment of a high density plasma requires large magnetic fields and a large power source. High conductivity is necessary

---

[1] Investigation of Electrodeless Pulsed Plasma Propulsion, Interim Report for period 8 June 1961 through 28 February 1962, AN-537 (March 1962).

Manuscript released by authors (February 1963) for publication as an ASD Technical Documentary Report.

for both acceleration and containment. Therefore, if the accelerator is to perform efficiently, the plasma source must be an important component, and the plasma must be a significant segment of the electrical circuit. This criterion means that the rest of the system must have a low inductance and a high Q; development of a high Q power supply is therefore very important.

Three types of plasma sources have been studied in this program. Two of them were pulsed sources producing metal-derived plasma. These were a parallel electrode pulsed button source and a coaxial electrode pulsed source, both using copper electrodes. These sources were studied and found to have plasma velocities suitable for injection into a synchronous type traveling field accelerator. These sources are well suited to the production of plasma bursts which can be trapped and accelerated, although the sources were somewhat lacking in the volume of plasma produced and the electrical efficiency with which this was done.

A d.c. plasma source derived from the modification of a duoplasmatron-type ion source was also studied. The source was originally intended to permit experimentation on the interaction of the traveling field with a continuous plasma flow and to determine the effectiveness of the magnetic field's snowplow action on an already ionized column of gas. The effort was redirected toward testing the flux trapping concept (Section IV.B) in conjunction with the transmission line. The source was further modified and tested; determination of the properties of the emergent plasma and the flux trapping experiment await further study.

The operating characteristics of the transmission line were studied under the conditions of an initially charged line and an initially uncharged line into which a capacitor was discharged. The transmission line was then combined with the pulsed button source and studies were performed on the plasma density distribution and the magnetic field distribution within the line in the presence of plasma.

It was found that the leading half of the cusp does trap the plasma and carry it to the end of the transmission line. It was also found that when the wave reflected from the end of the transmission line, the leading half of the cusp on the returning wave exhibited a snowplow action upon the plasma within the transmission line. This suggests that plasma can be pulled along by a cusp configuration but is not pushed very well by the configuration. A theory evolved from the concept of the interception of a plasmoid initially held with the cusp by the similarly magnetized induction current in the precursor wave of the transmission line. The prime feature of this theory is the role assigned to the Hall currents and Hall polarization fields, which combine to enhance the

containment of a plasmoid riding on the precursor field and to spoil the containment of a plasmoid in the standard mid-cusp position. The distribution measurements confirm that there are circulating Hall currents present in the leading half of the traveling cusp as well as an azimuthal current. These currents are not present in the trailing half.

It was determined that the plasma which escapes from the end of the transmission line on arrival of the wave is that which is carried by the leading half of the cusp. The plasma which is trailing behind the cusp is partially returned toward the source by the reflected current wave. There is strong indication of an instability that develops in the plasma being pushed by snowplow action of the returning (reflected) wave of the unterminated line. A plausible explanation for this phenomenon is that there is some plasma trailing the returning wave which traps a significant amount of magnetic flux; the trailing half of the returning cusp is thus held away from the axis of the line by the magnetic and kinetic pressure within the plasma until the instability develops. This instability allows the plasma to leak through the leading half of the cusp after the returning wave has traveled partially down the transmission line toward the source. The instability occurred, however, after the initially accelerated plasmoid had been discharged from the end of the line and the wave had partially returned toward the source.

The over-all thrust and efficiency of the system used in this study was quite small. However, this would not necessarily be the case if a higher-density source could be used and the synchronization and wave shape optimized to take advantage of the forward-of-the-cusp location, as discussed in Section IV.B. A novel alteration, which if practicable would give a many-fold increase in thrust and efficiency, is described in the final section of this report.

II. EXPERIMENT

A. SOURCE PERFORMANCE

Three types of sources were investigated in this contract: a parallel wire button source, a coaxial button source, and a modified duoplasmatron. The electrodes of the button sources were made of copper, while argon was the material used in the d.c. source.

1. The Parallel Wire Button Source

The parallel wire button source used consists of two wires, which can be fed from outside the vacuum system, connected to a .6 μf capacitor. The charged capacitor is discharged through the source by means of a vacuum-graded switch. The vacuum-graded switch is discussed in II.A.2 below. The rise time for the current is .5 μsec, and the discharge takes 5 cycles or about 10 μsec to ring down. Most of the energy is dissipated in the first cycle, or 2 μsec.

A Johnson-Malter probe[2] was used to measure the density of the plasma. From these measurements the velocity is also determined. Figures 1 and 2 are typical oscilloscope pictures of the probe signal. In Figure 2 the sharp drop in voltage at 32 μsec indicates that arcing between the probe faces was occurring. This occurs at higher voltages on the probe, so the probe was operated at lower voltages in order to get more reliable data. Twenty volts on the probe seemed to be the maximum at which arcing would not occur. As density measurements depend on the probe current saturating, it is necessary to operate the probe at as high a voltage as possible. Twenty volts does not correspond to saturation current, so the density measurements are lower bounds only.

Figure 3 is a plot of probe distance from the source as a function of time of arrival of the plasma peak. The slope of this graph is the velocity of the plasma, and is 1.4 cm/μsec. This velocity matches the initial velocity of the transmission line quite well, as will be seen in Section II.B.1.

---

[2] E. O. Johnson and L. Malter, Phys. Rev. 80, 58 (1950).

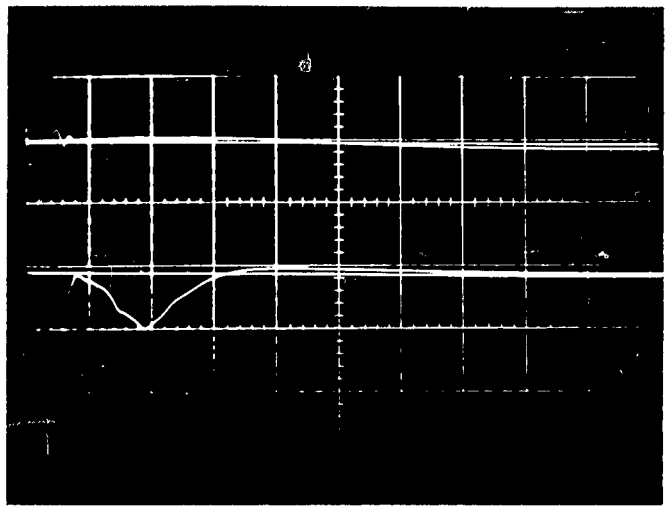

Figure 1. Signal from Johnson-Malter probe located 32 cm from the source, .5 v/cm, 10 μsec/cm. Source charged to 18 kV, 20 v on Johnson-Malter probe.

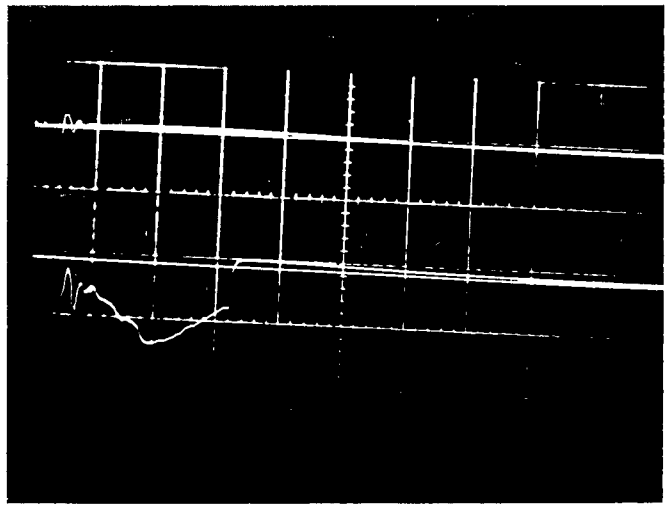

Figure 2. Signal from Johnson-Malter probe at 32 cm from source, 2 v/cm, 10 μsec/cm; source at 18 kV, 30 v on Johnson-Malter probe.

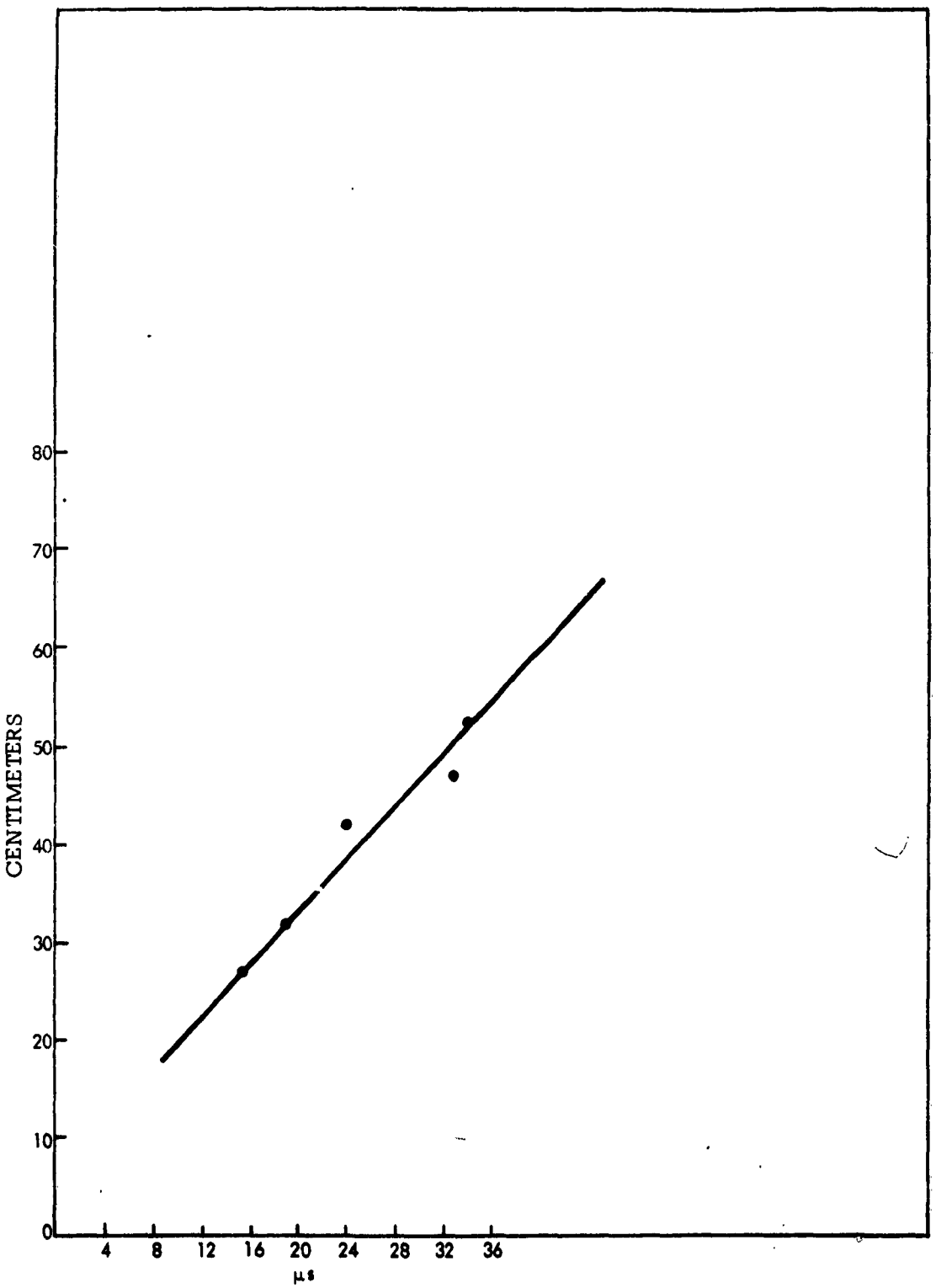

Figure 3. PROBE DISTANCE AS A FUNCTION OF TIME OF ARRIVAL OF THE PEAK PLASMA DENSITY.

As can be seen from Figures 1 and 2, measurement of ion density closer than 10 cm to the source would be obscured by the ringing of the source. Density measurements at other positions are plotted in Figure 4. Extrapolation to the source position gives n_i of approximately 10^{15} ions/cm^3, created by the source at 18 kv on the source capacitor. The variation of ion density with voltage on the source capacitor is shown in Figure 5.

The efficiency of the button source (Figure 6) is very low. For instance, if the density is 10^{15} per cm^3 and the velocity of the copper plasma is 1.4×10^6 cm/sec, the energy density is about .01 joule/cm^3. The maximum volume conceivable is about 150 cm^3, giving a total of 1.5 joules as an upper limit on the directed energy of the plasma. This is at 18 kv on the source capacitor, or 97 joules in the source. Thus, the efficiency of the source is less than 1.5 percent.

Because the density appears to vary exponentially with source voltage over the range measured, while the energy in the source varies as the square of the voltage, the higher the operating voltage the higher the efficiency for this type source.

2. The Vacuum-Graded Switch

The switch used to connect the source capacitor to the source was one section of the vacuum-graded switch described by Mather and Williams.[3]

The switch was actuated by a pulse from a 5C22 Thyratron in a conventional trigger circuit. Similar switches were used on the transmission line and as a crowbar on the coaxial source, and all operated reliably with low jitter and low inductance throughout the experimentation, needing only occasional cleaning of the spark plugs and glass insulating discs.

3. The Coaxial Source

A coaxial button source was built and its performance measured. The source consists of a center copper wire electrode and a concentric trigger electrode, both contained in an outer cylinder which acts as the ground. The outer cylinder has a copper plate on the end with a hole from which the center electrode protrudes.

---

[3] J. W. Mather and A. H. Williams, Rev. Sci. Inst. 31, 297 (1960).

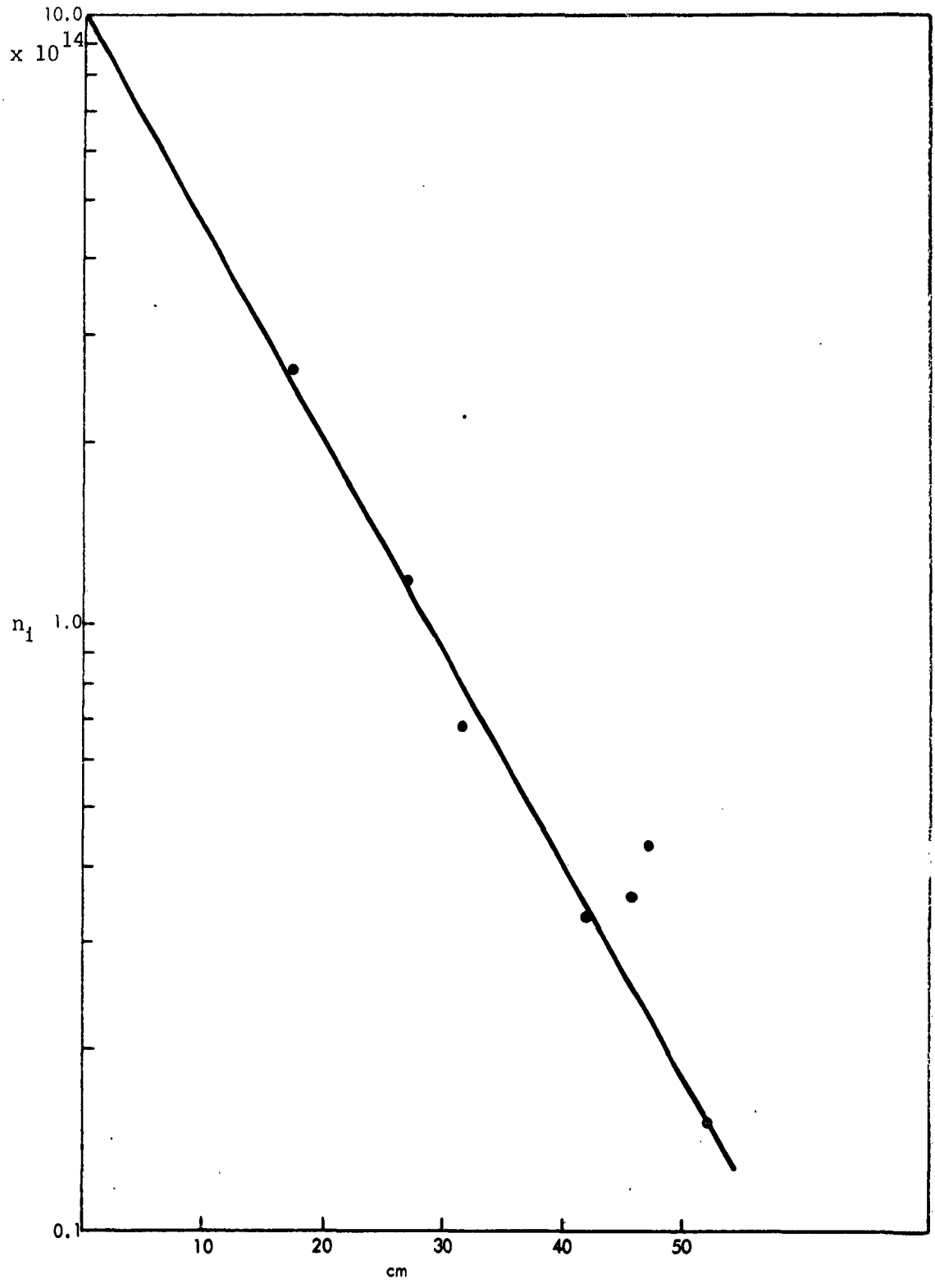

Figure 4. n_i AS A FUNCTION OF DISTANCE FROM A PARALLEL WIRE BUTTON SOURCE OPERATED AT 18 KV.

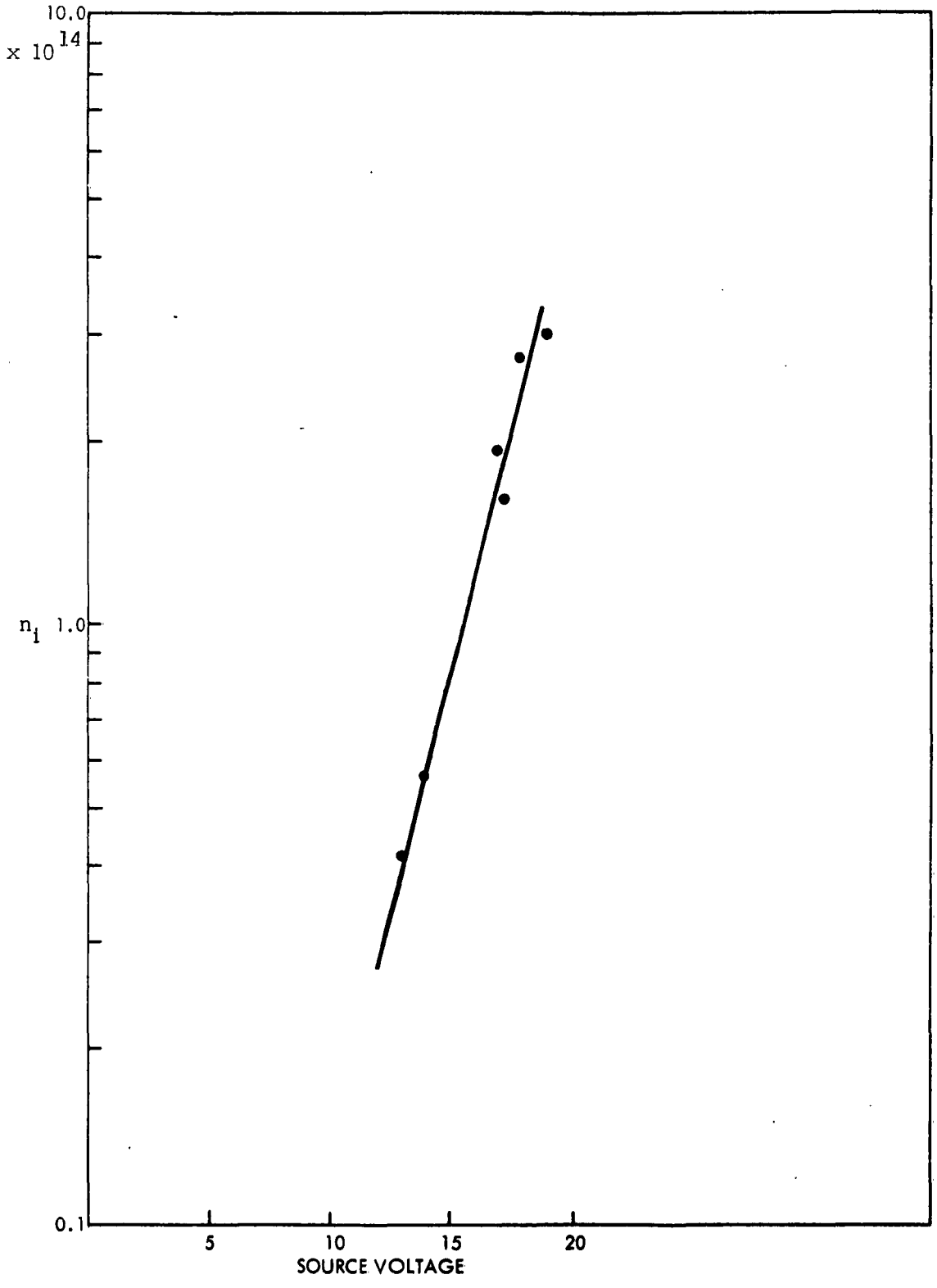

Figure 5. ION DENSITY AS A FUNCTION OF SOURCE VOLTAGE FOR A PARALLEL WIRE BUTTON SOURCE.

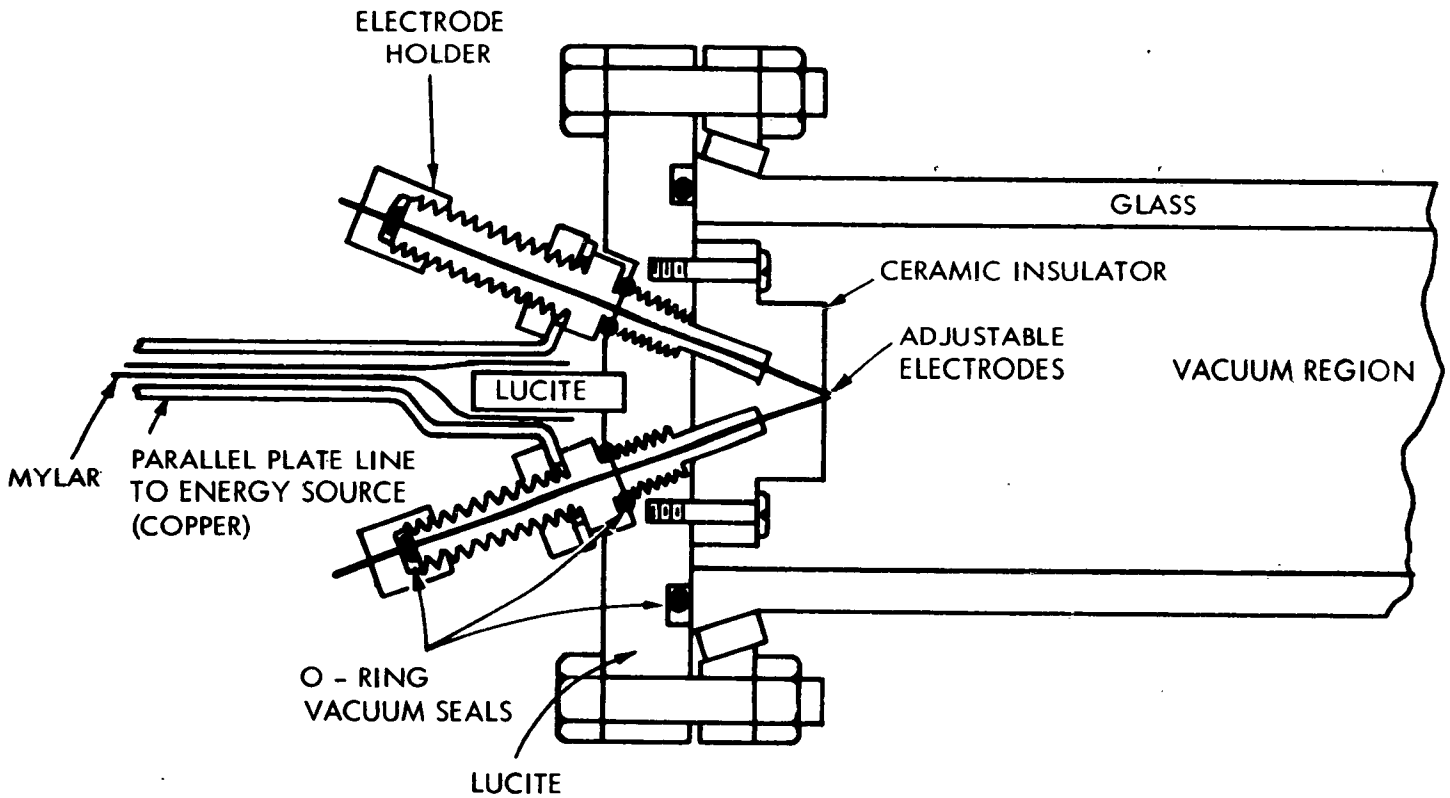

BUTTON PLASMA SOURCE WITH ADJUSTABLE ELECTRODES

FIGURE 6

The trigger electrode being in the source eliminates the need for a switch on the capacitor. A spark jumps from the trigger electrode to the center positive electrode and causes the gap between the wire and the end plate to break down. The capacitor then discharges between the wire and the plate.

Johnson-Malter probe measurements were made with this source to determine the velocity and density of the plasma. Figure 7 is a typical oscilloscope picture of the probe voltage. Figure 8 is the plot of distance from the source as a function of time of arrival of the peak plasma density. The velocity is then 3.4×10^6 cm/sec. The plasma density produced by this source is, by extrapolation, about 6×10^{14} particles/cm^3.

The conductivity of this plasma was also measured, using the method of Lin, Resler, and Kantrowitz.[4] The plasma was fired into a weak magnetic field (about 300 gauss). The displacement of the field lines by the plasma was detected by a pickup coil fed into an integrating amplifier in the oscilloscope. Figure 9 gives a typical resulting signal. For this picture the source was at 8 kv. Figure 10 is the trace of the calibration of the apparatus using an aluminum slug. Figure 11 is the plot of the conductivity as a function of voltage on the capacitor. Several measurements were taken at each voltage and averaged to give the points shown on the graph. It is probably not correct to extrapolate the conductivity to 18 kv and use that value for the conductivity of the parallel wire button source. That source was operated with only a .6 μf capacitor, so that the energy of each firing is only one and a half times that of the 2 μf capacitor at 8 kv.

The coaxial source was also operated with a vacuum-graded switch used as a crowbar. The upper beam of Figure 12 is proportional to the voltage on the capacitor. Note that the crowbar would fire only when the capacitor was positively charged. This was true regardless of the delay with which the crowbar was triggered. Figure 13 is a plot of probe distance as a function of time of plasma arrival, and gives a velocity of 6.9×10^6 cm/sec. Figure 14 is a plot of density as a function of distance from the source, and extrapolates to about 6×10^{14} particles/cm^3. This density appears to be about the same as for the source when not crowbarred, as is expected, since most of the energy is dissipated in the first cycle.

4. The Modified Duoplasmatron Plasma Source

Initial efforts to derive a high conductivity, quiescent, d.c. plasma source from a slightly modified duoplasmatron type ion source

---

[4] S. C. Lin, E. L. Resler, and A. Kantrowitz, J. Appl. Phys., 26, 95 (1955).

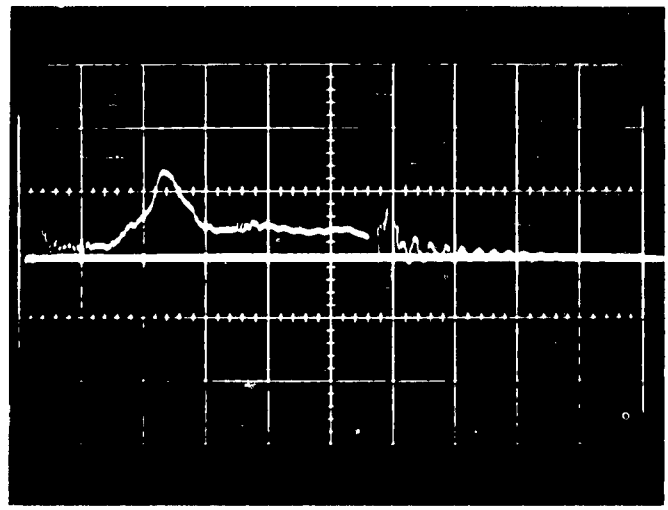

Figure 7. Johnson-Malter signal 13 cm from coaxial source, 5 v/cm, 2 μsec/cm, 30 volts on probe, source at 6 kV.

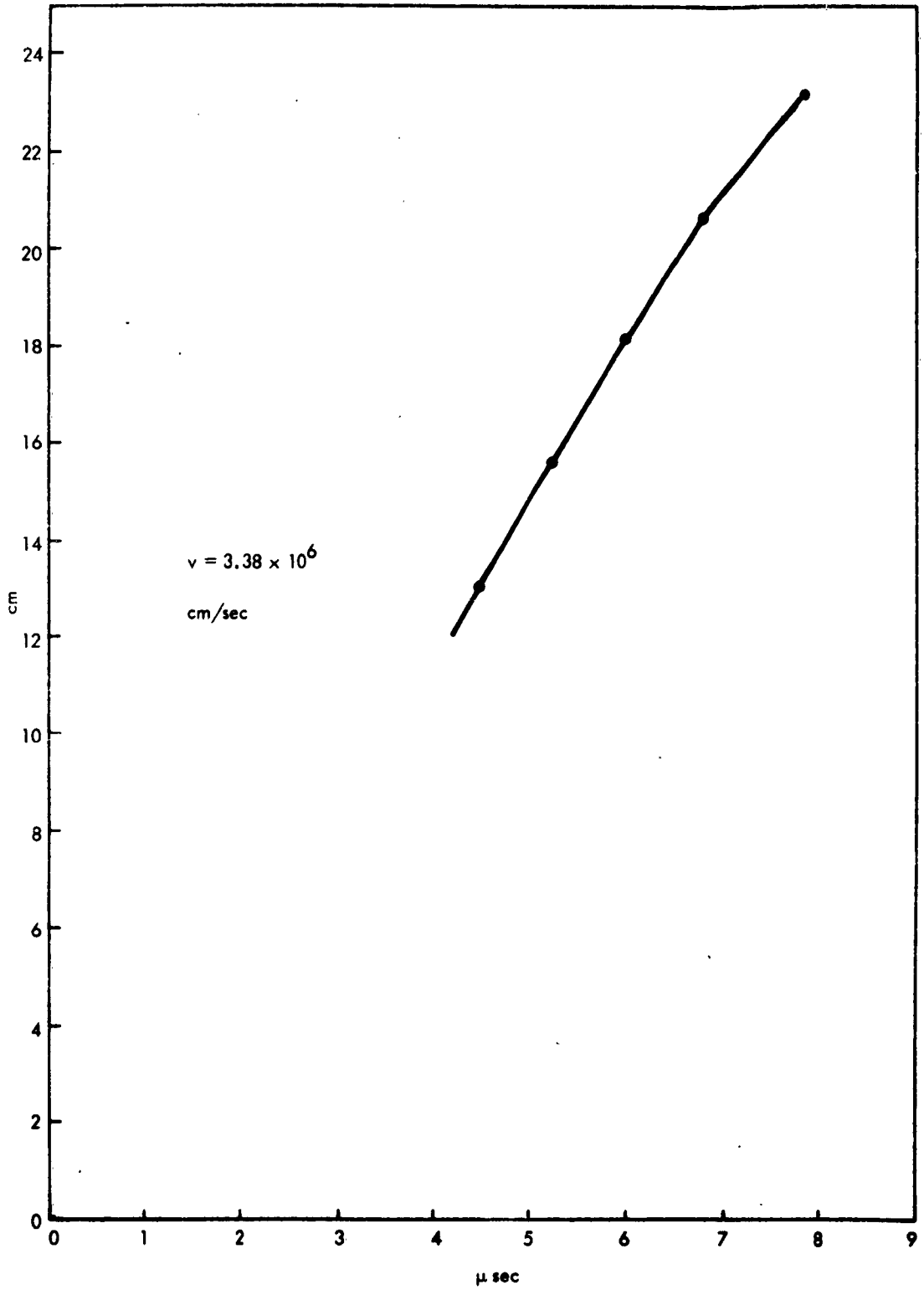

Figure 8. DISTANCE FROM SOURCE AS A FUNCTION OF TIME OF ARRIVAL OF PEAK PLASMA DENSITY FOR THE COAXIAL BUTTON SOURCE.

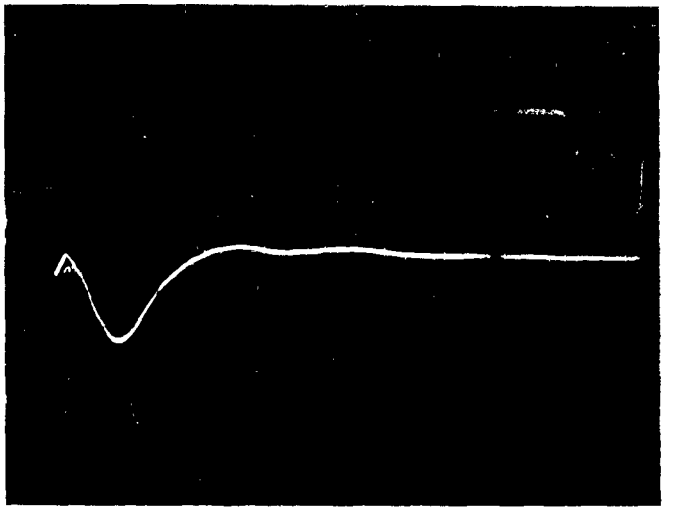

Figure 9. Conductivity signal, 2.5 v/cm, 2 μsec/cm, 8 kV on source, 300 gauss field.

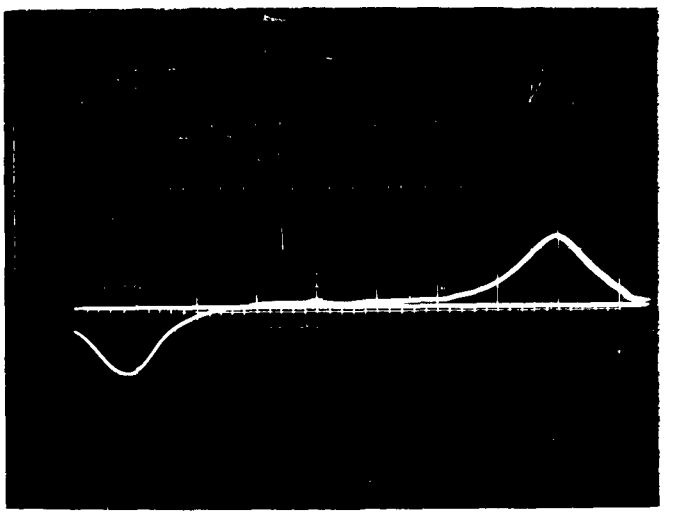

Figure 10. Calibration signal for the conductivity measurement .1 v/cm, 5 msec/cm.

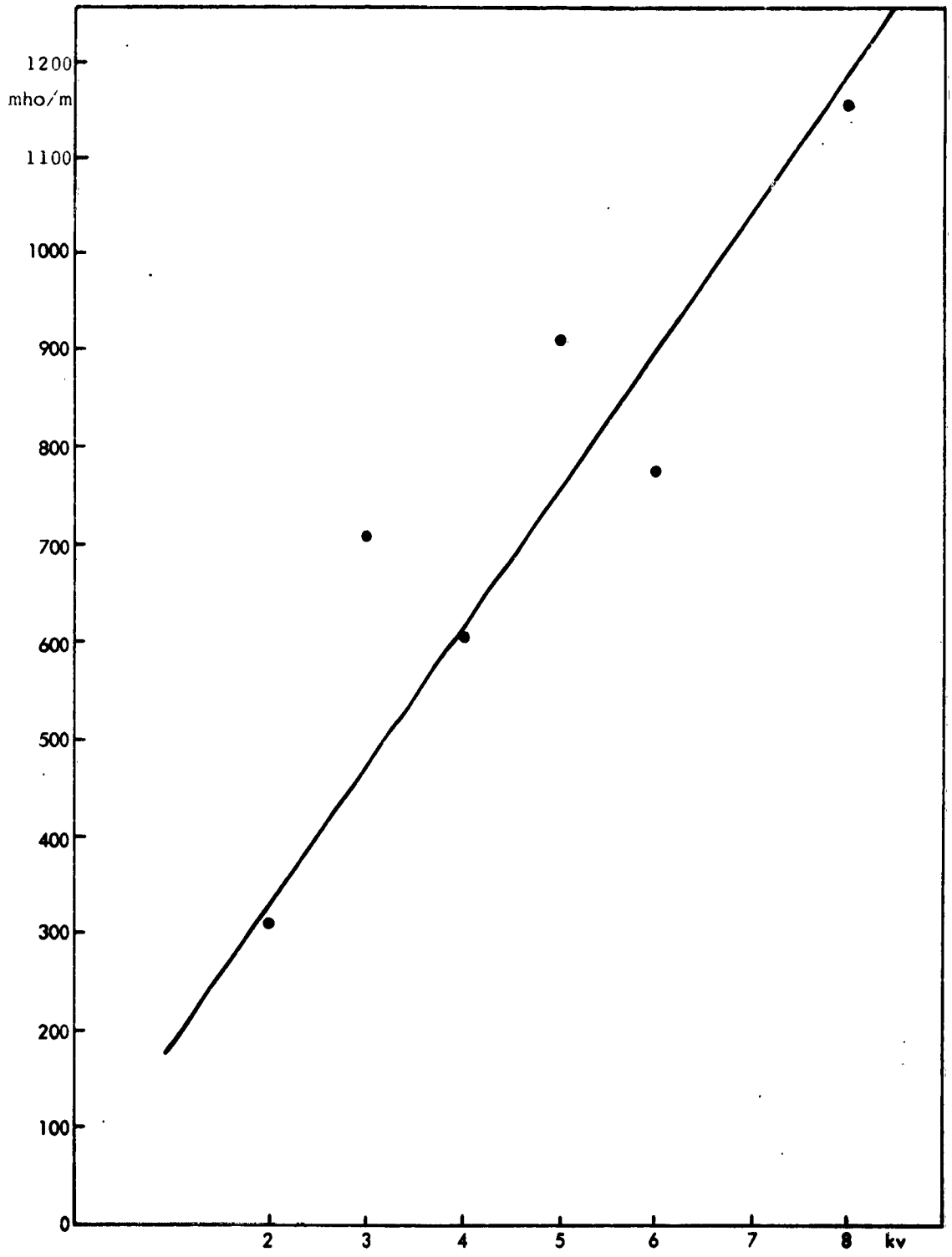

Figure 11. CONDUCTIVITY OF A PLASMA FROM A COAXIAL BUTTON SOURCE AS A FUNCTION OF VOLTAGE ON THE SOURCE CAPACITOR.

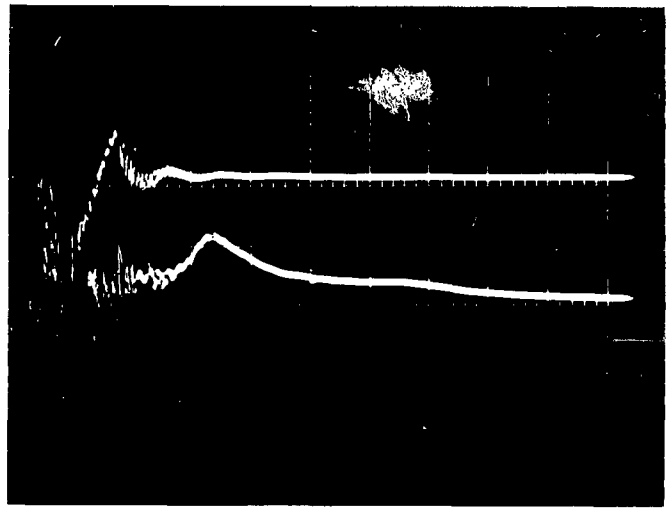

Figure 12. Upper beam is the voltage on the coaxial source capacitor with the crowbar, 2 μsec/cm, 20 v/cm. Lower beam is Johnson-Malter probe at 20 cm from source, .5 v/cm, 2 μsec/cm, 30 v on probe, source at 8 kV.

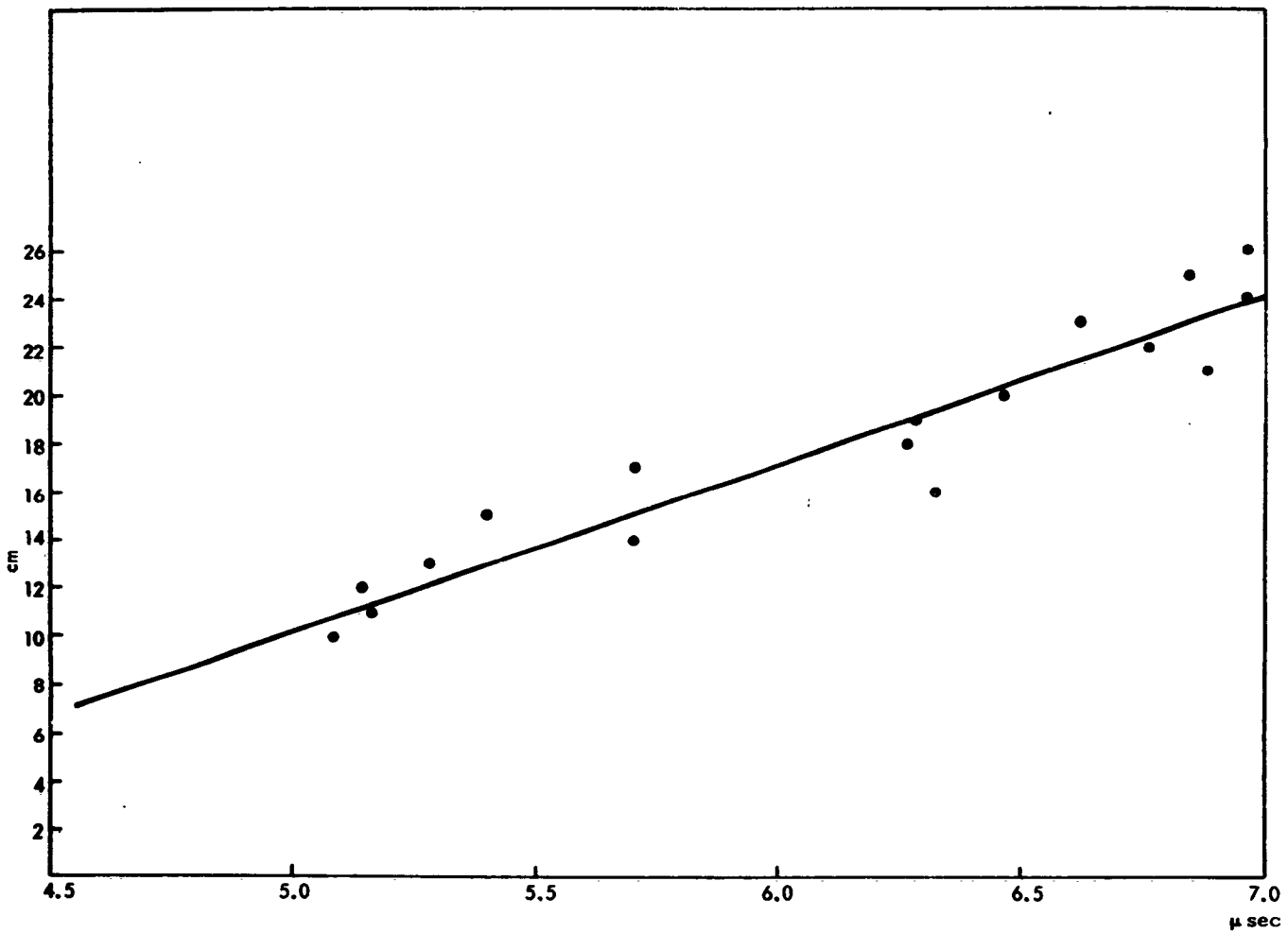

FIGURE 13

PROBE DISTANCE AS A FUNCTION OF TIME OF ARRIVAL OF PEAK PLASMA DENSITY FOR CROWBARRED COAXIAL SOURCE.

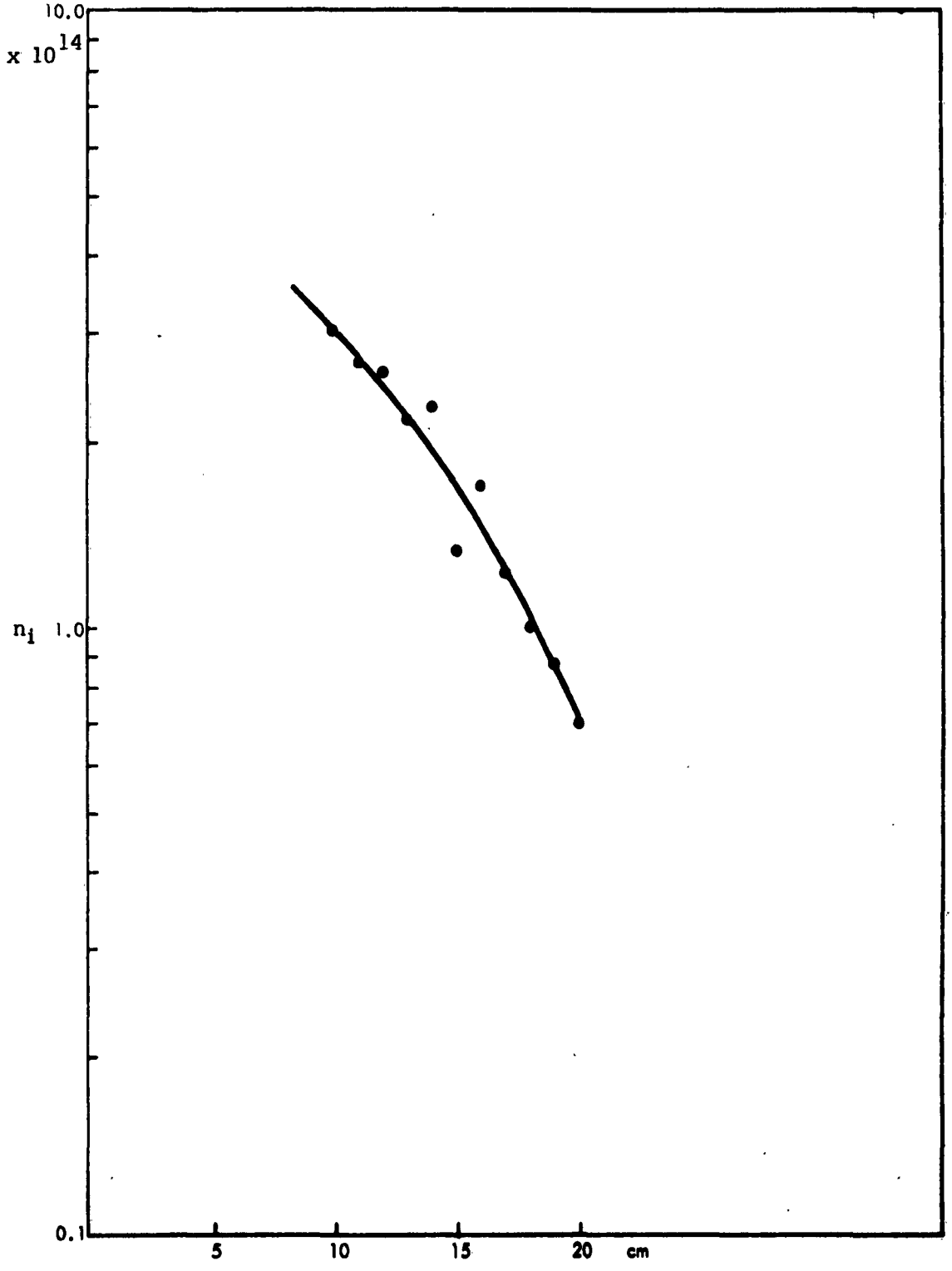

FIGURE 14. n_i AS A FUNCTION OF PROBE DISTANCE FROM THE SOURCE

were only moderately successful. Plasma volume and density levels required to determine the value of plasma flux trapping for traveling wave systems were deemed inadequate. Consequently, major modifications were undertaken on the original source geometry to circumvent several of its intrinsic deficiencies. A water cooled hollow cathode (see Figure 15) was constructed to replace the thermionic type. Changes were incorporated in the arc power supply circuit to permit radio frequency starting of the hollow cathode arc without damage to the 50 amp arc power supply. The external magnetic field, coming originally from a current coil surrounding the 2-1/2 in. iron middle electrode, was strengthened and extended by a large diameter, water cooled, high current coil constructed to replace the smaller one. The greater axial extension of the magnetic field lines is required to conduct the plasma to the injection region of the transmission line while allowing the source to operate at the required minimum distance from the transmission line. At the same time it provides the field intensity necessary to conduct flux trapping investigations with the traveling wave. The numerous details connected with these tasks prevented a performance evaluation of the injector system before the completion of this report. However, preliminary investigations have yielded arc current levels several times greater than those achieved in the previous system under equivalent conditions.

5. Summary

The coaxial source is simpler to operate than the parallel wire source, and its density is about the same when operated at the same energy. The conductivity of the coaxial source is about 1000 mho/m at a source capacitor voltage of 8 kv. As the energy in the parallel wire source capacitor is about 1.5 times the energy at which the coaxial source was operated, it is expected that the conductivity for the parallel wire source is no less than 1000 mho/m, and may be as high as 1500 mho/m. The velocity of the plasma when the source is crowbarred is about twice that when the source is allowed to ring down. The big advantage of using the parallel wire source is that the velocity of the plasma is closer to the initial velocity of the line, so that the traveling wave will be able to accelerate the plasma.

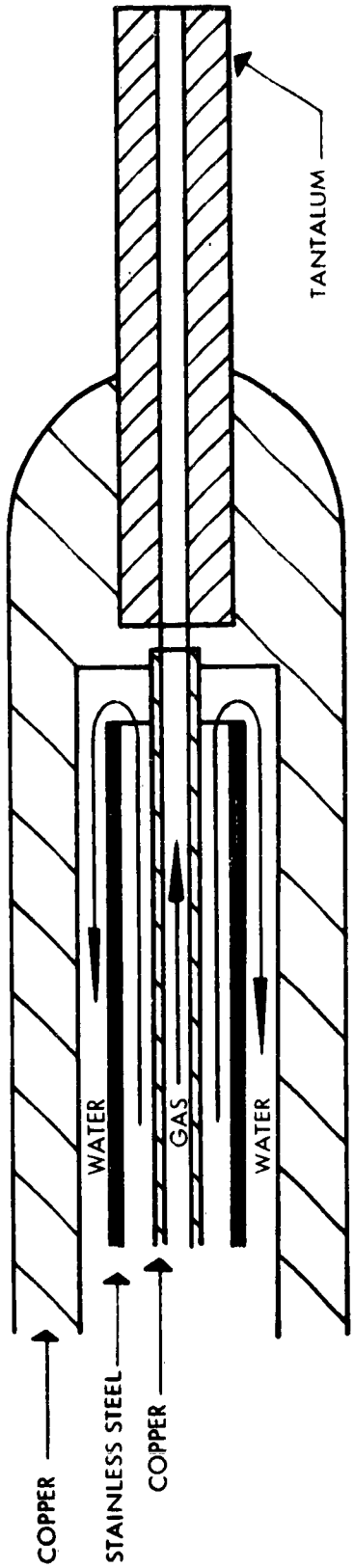

HOLLOW CATHODE

FIGURE 15

B. TRANSMISSION LINE

1. Design and Theory

a. Design

A varying phase velocity, uniform impedance, solenoidal transmission line was selected as the synchronous accelerator. Figure 16 is a schematic illustration of the operation of the line. Neglecting end effects, the requirement of varying phase velocity and uniform impedance requires that the solenoid have a varying pitch and radius. In order to produce a sufficiently large magnetic field and have the proper exit velocity, the transmission line must have a low impedance. To meet this requirement it was decided that the line should have lumped, rather than distributed capacitance. In this case a traveling magnetic field is produced by a helical transmission line loaded with capacitors. The capacitors may be initially charged and then sequentially discharged by completing the circuit. This produces a moving current step and magnetic field which travels down the line at a velocity determined by the loading of the line. Alternatively, the capacitors may be intially uncharged and a current pulse from an external power source may be propagated down the line, achieving the same result. In either case the traveling magnetic field will compress and push the plasma ahead to an extent determined by the strength and shape of the field and the conductivity and degree of ionization of the plasma. The bulk of the energy of the line goes into the magnetic field. Because this program is primarily concerned with specific impulses in the range of 1500-5000 sec, the exit velocity of the accelerator was selected as 5×10^4 m/sec.

The transmission line is designed so that a wave propagated along it begins at a velocity slightly below that of the plasma from the source and undergoes fairly constant acceleration. The requirement of uniform characteristic impedance ensures that none of the wave is reflected along the line. The impedance must be small enough so that satisfactory currents will result from operation at 20 kv. Finally, the return path for the current should help in creating the magnetic field. So that the return line can aid in supplying the magnetic field, it was made a counter-wound helix. To simplify construction, the capacitors are connected only at points where the return line crosses the helix.

The upper limit of the accelerator length is determined by the number of capacitors available; also, it should be as short as possible to minimize diffusion to the walls. The lower limit on the length is given by the physical size of the capacitors, and by the requirement that leads from the capacitors to the line be as short as

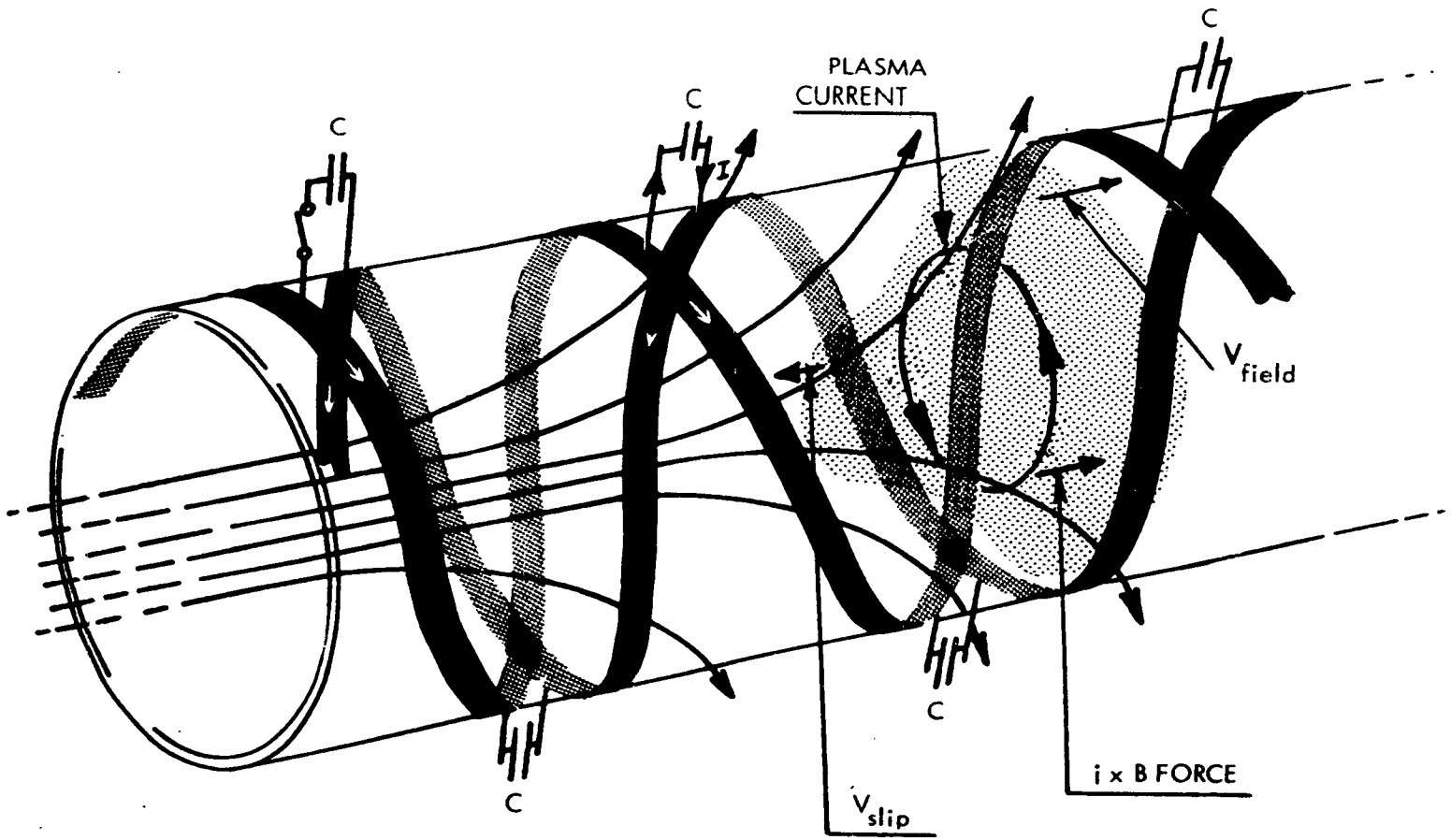

LUMPED-PARAMETER-TRANSMISSION-LINE-WITH-INCREASING-PHASE-VELOCITY FOR PLASMA ACCELERATION - SCHEMATIC DIAGRAM

FIGURE 16

possible. A length of 0.7 m was selected. As the source is to be located a few cm inside the low speed end of the line, the initial velocity, v_1, is chosen as 0.8×10^4 m/sec. The final velocity of 5×10^4 m/sec then gives an acceleration of 1.7×10^9 m/sec^2.

b. Parameters

The design of the transmission line involves calculating the inductance of two variable-pitch, variable-radius coaxial helices with different radii. The principle behind the method used is given by Harnwell.[5] The contribution to the inductance due to the region internal to the wire is computed first; then the contribution due to the region external to the wire is computed, and the two results added. To make these calculations, the size of the wire used must be known. Since the computational method uses circular wire and the transmission line is made with rectangular wire, an equivalent wire radius is needed. This is obtained by computing the size of circular wire which, in a loop, gives the same inductance as a rectangular wire with the dimensions of the wire used on the line. The inductance formulas used are those of the Bureau of Standards.[6] The wire is copper strap 3/8 x 1/32 in. in cross section. The equivalent circular wire radius is $\delta = 0.58$ in.

In the internal region of the wire, the contribution to the inductance is calculated assuming a uniform current density, $\frac{i}{\pi\delta^2}$. Then

$$H = \frac{ir}{2\pi\delta^2}$$

But

$$U = \frac{1}{2} L_i i^2 = \frac{1}{2} \mu_0 \int H^2 \, dV,$$

from which can be derived

$$L_i = \frac{\mu_0}{8\pi} \int d\ell.$$

---

[5] G. P. Harnwell, Principles of Electricity and Electromagnetism, New York, McGraw-Hill (1949), p. 330.

[6] E. B. Rosa and L. Cohen, Bull. of the Bureau of Standards, 5, 1 (1908).

Since

$$d\ell = \left[dz^2 + dr^2 + r^2 d\theta^2\right]^{1/2},$$

$$L_{il} = \frac{\mu_0}{8\pi} \int \left[1 + f'^2 + f^2 g'^2\right]^{1/2} dz,$$

where $f \equiv r(z)$ and $g \equiv \theta(z)$.

The contribution per meter is then

$$L_{il} = \frac{\mu_0}{8\pi} \left[1 + f'^2 + f^2 g'^2\right].$$

Similarly, the contribution of the return helix can be expressed

$$L'_{i2} = \frac{\mu_0}{8\pi} \left[1 + f_2'^2 + (f_2 + d)^2 f^2 g_2'^2\right]^{1/2},$$

where d is the separation of the helices, and k is the ratio of turns per unit length for the return helix to that for the main helix. The total contribution from both helices due to the internal region is then

$$L'_i = \frac{\mu_0}{8\pi} \left[1 + f_2'^2 + (f_2 + d)^2 k^2 g_2'^2\right]^{1/2} + \left[1 + f'^2 + f^2 g'^2\right]^{1/2}.$$

It is possible to compute $g(z)$ and $g'(z)$, so that the contribution to the inductance per unit length from the internal region is a function of $f(z)$ and $f'(z)$ only.

For the region external to the wire

$$L_e = \frac{\mu_0}{4\pi} \oint\oint \frac{d\ell_1 \cdot d\ell_2}{r_{12}},$$

so that

$$L_{el} = \frac{\mu_0}{4\pi} \int_0^z \int_0^z \frac{\left[1 + f_1' f_2' + f_1 (f_2 - \delta)\, g_1' g_2'\right] dz_1 dz_2}{\left[(z_2 - z_1)^2 + f_1^2 + (f_2 - \delta)^2 - 2 f_1 (f_2 - \delta) \cos(g_2 - g_1)\right]^{1/2}}$$

Then

$$L'_{e1} = \frac{\mu_0}{4\pi} \cdot$$

$$\int_0^z \frac{\left[1 + f'(\zeta)\, f'(z) + f(\zeta)\,(f(z) - \delta)\, g'(\zeta)\, g'(z)\right] d\zeta}{\left[(z-\zeta)^2 + f^2(\zeta) + [f(z) - \delta]^2 - 2f(\zeta)\,[f(z) - \delta] \cos\,(g(z) - g(\zeta))\right]^{1/2}} \cdot$$

Similarly, for the return helix

$$L'_{e2} = \frac{\mu_0}{4\pi} \cdot$$

$$\int_0^z \frac{\left[1 + f'(\zeta)\, f'(z) + (f(\zeta) + d)\,(f(z) + d - \delta)\, kg'(\zeta)\, g'(z)\right] d\zeta}{\left[(z-\zeta)^2 + (f(\zeta) + d)^2 + (f(z) + d - \delta)^2 - 2\,(f(\zeta) + d)\,(f(z) + d - \delta)\cos[k\,(g(\zeta) - g(z))]\right]^{1/2}} \cdot$$

The last term to be considered is the mutual inductance between the two helices. This term reduces to

$$L'_{e12} = \frac{\mu_0}{4\pi}$$

$$\int_0^z \frac{\left[1 + f'(\zeta)\, f'(z) + f'(\zeta)\,(f(z) + d)\, kg'(\zeta)\, g'(z)\right] d\zeta}{\left[(z-\zeta)^2 + f^2(\zeta) + (f(z) + d)^2 - 2f(\zeta)\,(f(z) + d) \cos\,(kg(\zeta) - g(z))\right]^{1/2}} \cdot$$

Then

$$L'_e = L'_{e1} + L'_{e2} + 2L'_{e12} \cdot$$

The equation,

$$Z = L'v,$$

where

$$L' = L'_e + L'_i$$

and Z is a constant, is an integral equation, the solution of which involves the use of a computer.

The problem was programmed for an IBM 7090 computer and solved for various values of the input and exit radii. The results show that a changing radius along the line has little effect on L'. The best value for the radius is about 0.055 m. An input radius of 0.050 m and an exit radius of 0.060 m give slightly better agreement with the conditions that Z be constant and that the velocity increase from v_i to v_f, but the difference is practically negligible. To simplify fabrication, the radius of the inner helix of the transmission line constructed is a uniform 0.055 m.

c. Transmission Line Equation

The differential equation for a transmission line with continuously varying inductance and capacitance per unit length can be derived in an elementary manner. If V is the voltage between helices and i is the current in the helices,

$$-\frac{\partial V}{\partial x} = L'\frac{\partial i}{\partial t}, \tag{1}$$

and

$$-\frac{\partial i}{\partial x} = C'\frac{\partial V}{\partial t} \tag{2}$$

where L' and C' are the inductance and capacitance per meter. Taking the partial derivative of (1) with respect to x and of (2) with respect to t and adding gives

$$\frac{\partial^2 V}{\partial x^2} - \frac{1}{L}\frac{dL}{dx}\frac{\partial V}{\partial x} = LC\frac{\partial^2 V}{\partial t^2} \tag{3}$$

Separating the variables by

$$V(x,t) = X(x)\,T(t)$$

gives

$$\frac{d^2 T}{dt^2} + K^2 T = 0, \tag{4}$$

and

$$\frac{d^2X}{dx^2} - \frac{L'}{L'}\frac{dX}{dx} + \frac{K^2}{v^2}X = 0 \tag{5}$$

where

$$L' = \frac{dL'}{dx},$$

$$v^2 = \frac{1}{L'C'},$$

and $-K^2$ is the separation constant.

Since the acceleration of this line is uniform,

$$v^2 = 2ax$$

with suitable choice of origin, and

$$L' = L_o x^{-1/2},$$

$$C = C_o x^{-1/2}.$$

The spatial differential equation is then

$$\frac{d^2X}{dx^2} + \frac{1}{2x}\frac{dX}{dx} + \frac{K^2}{2ax}X = 0, \tag{6}$$

The solution is

$$X = A \sin K\sqrt{\frac{2x}{a}} + B \cos K\sqrt{\frac{2x}{a}}. \tag{7}$$

As the exit end of the line is open,

$$\left(\frac{\partial V}{\partial x}\right)_{x_e} = 0, \text{ or } \left(\frac{dX}{dx}\right)_{x_e} = 0. \tag{8}$$

For an initially charged line shorted at the input end at time t_o,

$$X(x_i) = 0, \tag{9}$$

while for the case of a capacitor bank discharging into an uncharged line, the boundary condition at the input end is

$$\left(\frac{dX}{dx}\right)_{x=x_i} = L'C_b \frac{\partial^2 V_b}{\partial t^2}, \tag{10}$$

where V_b is the voltage on the bank and C_b is its capacitance. After a certain time t_o,

$$\frac{\partial^2 V_b}{\partial t^2} = 0,$$

so

$$\left(\frac{dX}{dx}\right)_{x=x_i} = 0. \tag{11}$$

The case of the initially charged line gives

$$X(x) = \sum_{n=0}^{\infty} A_n \cos K_n x \tag{12}$$

where

$$K_n = (n + 1/2) \frac{\pi a}{v_e - v_i}, \tag{13}$$

while the second case gives

$$X(x) = \sum_{n=1}^{\infty} B_n \sin L_n x, \tag{14}$$

where

$$L_n = n \frac{\pi a}{v_e - v_i} \tag{15}$$

The solution of Equation (4) is

$$T(t) = \sum_{n=0}^{\infty} C_n \sin K_n t + D_n \cos K_n t. \qquad (16)$$

Combination of (16) with either (12) or (14) gives the complete solution of the wave equation. As this solution is similar in form to the solution of the ordinary transmission line equation the existence of a traveling wave is assured.

The above analysis has been carried out for a distributed capacitance line. For an artificial line this analysis is satisfactory up to the cutoff frequency

$$K_c = \frac{1}{\sqrt{LC}},$$

where L and C are the inductance and capacitance per section. For this line,

$$K_c = \frac{1}{N\sqrt{LC}},$$

where N is the number of turns per meter. At the input end, $K_{ci} = 44 \times 10^6$, while at the exit $K_{ce} = 1 \times 10^6$. Thus for the initially uncharged line, the summation now goes from 1 to 6 at the exit end of the line. This shows that the wave may be expected to suffer considerable distortion in traveling down the line.

d. Summary

The transmission line is designed to have an initial velocity of $.8 \times 10^4$ m/sec and a final velocity of 5×10^4 m/sec. It is .7 m long and consists of two oppositely wound helices connected through capacitors at each intersection. There are a total of 24 capacitors and 24 turns on the line. The ratio of turns per meter on the outer helix to the turns per meter on the inner is 3:4, chosen to allow the intersections to be spaced evenly around the helix.

The lumped character of the impedance elements gives a cutoff frequency leading to distortion of the wave as it travels down the line. This distortion increases towards the exit end of the line.

2. Characteristics of Transmission Line Operation in the Absence of Plasma

a. Line Initially Charged

The initial studies of the characteristics of the transmission line were made for the case where the transmission line was initially charged to 6 kilovolts and then shorted at the low-speed end, using a vacuum-graded crowbar switch described in Section II.A.2. The transmission line was not terminated so that there would be no unnecessary energy dissipation at the end of the line. This results in a reflected wave which interacts with the plasma. One of the studies in this program was to determine the interaction of the reflected wave with the plasma.

Since the total capacity of the transmission line was 48 μf at 6 kilovolts, the energy stored at the beginning of the discharge amounted to 864 joules. The transmission line was designed initially to be operated at voltages up to 20 kilovolts. However, it was found that the lifetime was considerably reduced at the higher voltages due to electrical breakdown under pulse conditions. Therefore, most of the data were taken at 6 kilovolts. After the normal discharge of the transmission line there was usually a voltage remaining on the capacitors which would correspond to an energy not dissipated during breakdown. This voltage varied from pulse to pulse, ranging from 1 to 4 kilovolts. Usually about 2 kilovolts, corresponding to one-ninth of the initial energy, were retained.

With a different switch design it is believed it would not be difficult to prevent the discharge from going below 4 kilovolts, which would result in a retained energy of about 50 percent of the initial stored energy. The Q of the transmission line was determined by a measurement of the ringdown and was equal to a value of approximately 9. Using this value it was estimated that between 70 to 90 percent of the initial energy could be recovered, depending on whether the discharge was stopped at the time the wave reached the end of the line or whether it could be stopped after it had reflected and gone back to the beginning of the transmission line.

In previous reports the velocity and acceleration of the line were reported as initial velocity equal to 1.76×10^4 meters/sec, final velocity equal to 5.83×10^4 meters/sec and acceleration equal to 2.2×10^9 meters/sec^2. These values were measured by following the progress of the current peak in the arms leading from the capacitors to the transmission line. Since then the velocity has been determined by measuring the position of a cusp in the magnetic field as it progressed

down the line. Since the cusp does not fully appear on the line until a distance of approximately 4 in. from the beginning of the line, at which point the velocity was found to be 2.72×10^4 meters/sec, the velocity at the end of the line was 7.16×10^4 meters/sec, and the acceleration is given by 3.7×10^9 meters/sec^2.

The axial and radial magnetic field distributions along the axis and 2 cm from the axis of the transmission line, respectively, were measured using induction probes and integrating circuits; these results were reported previously in the Monthly Progress Report for August, AN-719 (Confidential Report). It was found that under this condition of operation with the line initially charged the wave front was rather broad, and a modification was made. A 2 μf capacitor was put in parallel with the crowbar switch. This action improved the operation of the line giving a more distinct traveling wave, apparently by virtue of the extra energy dumped initially into the spark gap switch, which lowered its resistance to a value less than the characteristic impedance of the line. However, no plasma data were taken under these conditions, as a more promising approach, described in the next section, was attempted.

The characteristic impedance of the line was measured as .35 ohms at the high speed end and .36 ohms 4 inches from the low speed end. This appears to remain reasonably constant, but is less than the .5 ohms designed.

b. Line Initially Uncharged

In this method of operation the transmission line was uncharged and a 15 μf capacitor, charged to 6 kv (270 joules), was discharged through a series switch into the input end of the transmission line.

As in the previous method of operation, the transmission line was unterminated. As before, there was energy remaining in the transmission line and the 15 μf capacitor after discharge of the bank. This was usually about 2 kv. This voltage seems to be the result of some characteristic cutoff point of the type of switch used. In this case the remaining energy was slightly less than one-half of the initial energy placed in the capacitor. Again, it is believed that a different type of switch could be used which would allow a considerably larger fraction of the initial energy to be retained after firing the transmission line.

The impedance and Q of the transmission line under this method of operation have the same values as under the previous method of operation. Axial, radial, and azimuthal magnetic distributions

were measured and these distributions are presented and discussed in the next section.

3. Transmission Line Performance with Plasma Injection by Parallel Electrode Button Source

This section describes the operating characteristics of the uncharged transmission line (discussed in the previous section) used in conjunction with the pulsed button source with copper plasma. The magnetic field distribution in the plasma free case shows a traveling cusp field. The field results from the wave front preceded by an induction wave on the transmission line which forms the leading half of the cusp on the advancing wave.

A plot of the position of the cusp in the line (actually the position of $B_z = 0$) vs time is shown in Figure 17. This plot was made in the absence of plasma, and with plasma, and it indicates that the velocity of the cusp is essentially unaffected by the presence of the plasma for the case of the advancing wave, except near the end of the line where it has slowed down slightly. However, this is not the case of the reflected wave receding from the end of the transmission line. Here there is evidence of a strong interaction between the plasma and the line, for the $B_z = 0$ position is considerably displaced from the points in the no plasma case. These phenomena are expected, for in the case of the advancing wave the timing of the discharge of the plasma and the transmission line was such that there was little plasma ahead of the cusp. However, in the case of the returning wave there is distributed along the transmission line a large volume of plasma through which this wave must pass.

Figures 18 through 21 are presented to illustrate the behavior of the magnetic field in the transmission line both with and without plasma. When the transmission line is initially discharged a traveling cusp field is initiated which travels to the end of the line in approximately 18 microseconds. This was detected by an axial magnetic induction probe located on the axis of the line and a radial magnetic induction probe located two centimeters from the axis of the transmission line. The upper trace of Figure 18 shows, from left to right, the radial field. First there is the precursor cusp, followed by the main cusp, after which the radial field reverses indicating lines passing through the solenoid. At about 25 microseconds the reflected wave passes the particular point 20 inches from the input end of the transmission line. The lower trace in the same figure is the axial magnetic field, also with its precursor. The radial peak occurs at very nearly the same time as the zero of the B_z signal. Figure 20 is the radial and axial magnetic

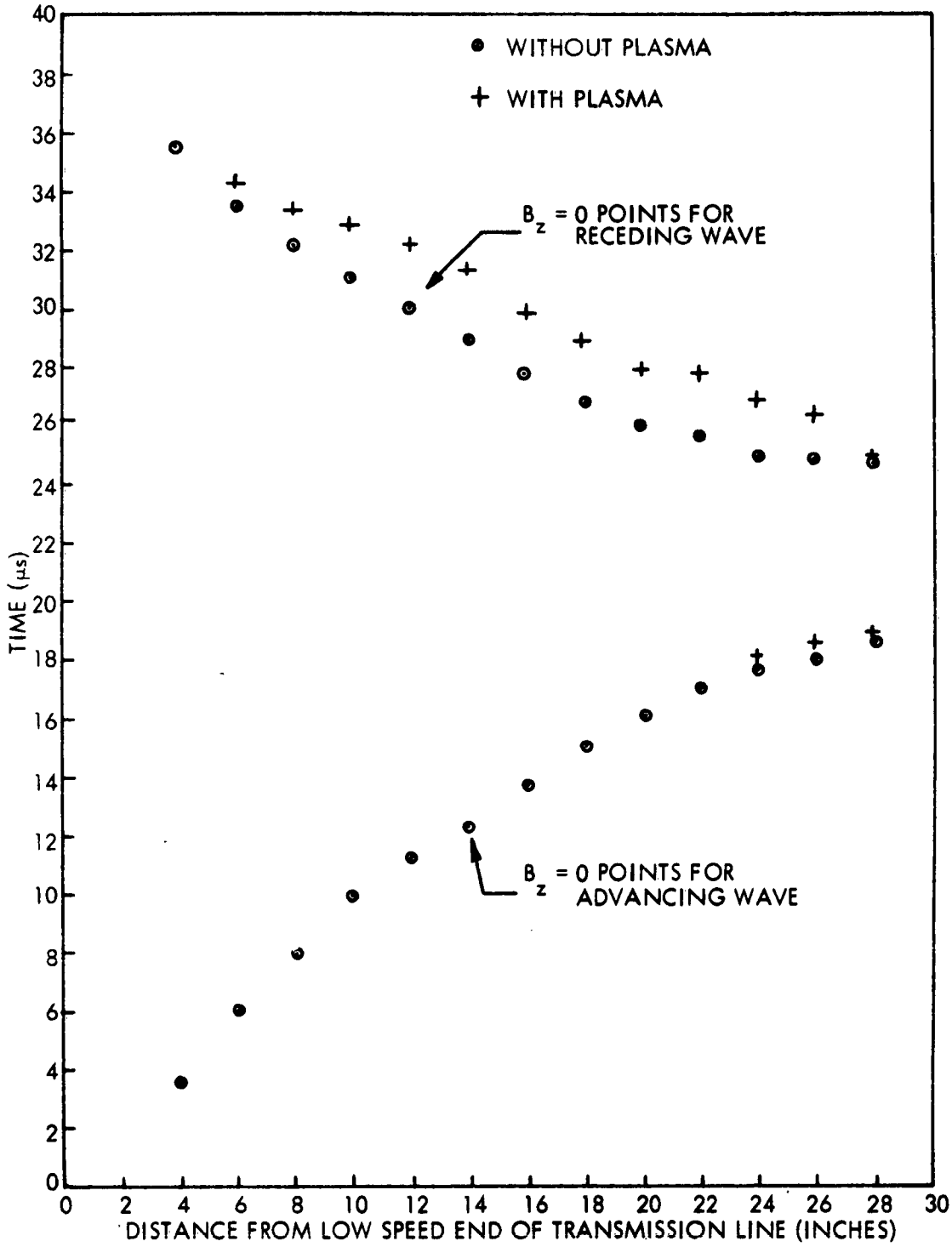

Figure 17. POSITION VS TIME PLOT OF ACCELERATING MAGNETIC CUSP IN TRANSMISSION LINE.

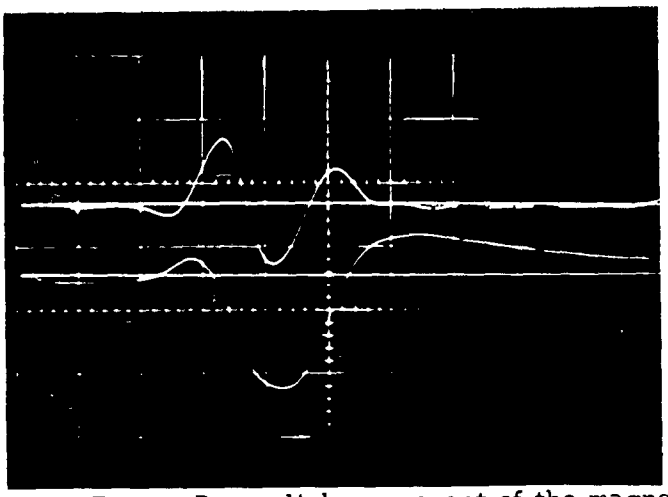

Figure 18. Upper Trace: B_r, radial component of the magnetic field 2 cm from the axis of the transmission line, 49 cm from the plasma source. Obtained from integration of an induction probe signal. Trace triggered by discharge of the transmission line, which was energized by a 15 μf capacitor charged to 6 kV. 5 μs/cm.

Lower Trace: B_z, axial component of the magnetic field at the axis of the transmission line, 49 cm from the plasma source. No plasma present. 5μs/cm.

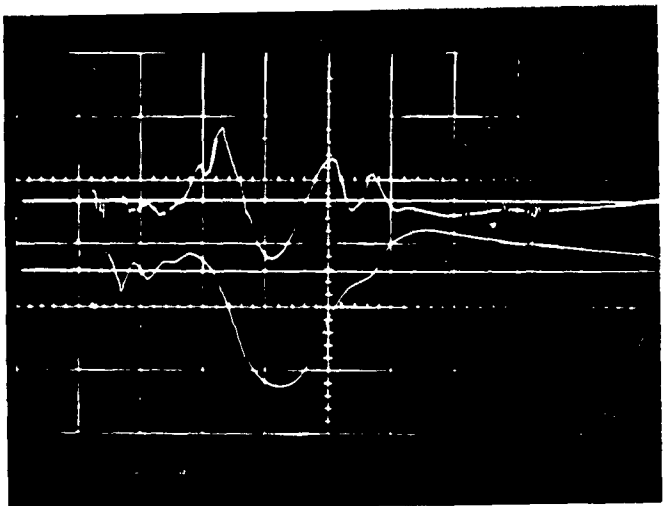

Figure 19. Same conditions as Figure 18, except the plasma source (0.6 μf charged to 18 kV) was triggered simultaneously with the line.
Upper Trace: B_r. 5 μs/cm.
Lower Trace: B_z. 5 μs/cm.

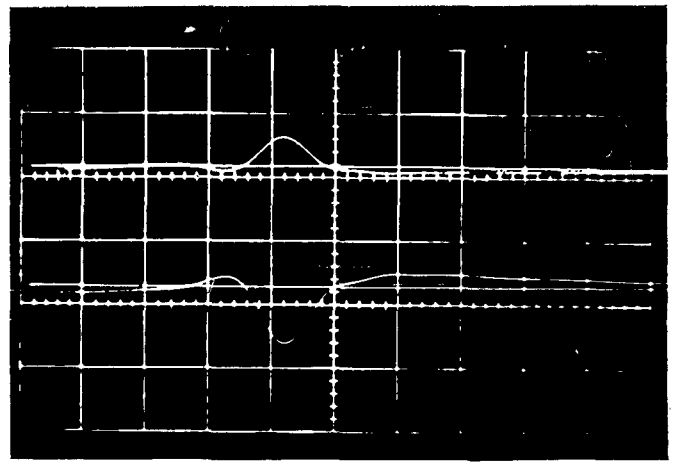

Figure 20. Upper Trace: B_r, radial component of the magnetic field 2 cm from the axis of the transmission line, 69 cm from the plasma source. 5 μs/cm.

Lower Trace: B_z, axial component of the magnetic field at the axis of the transmission line, 69 cm from the plasma source. No plasma present. 5 μs/cm.

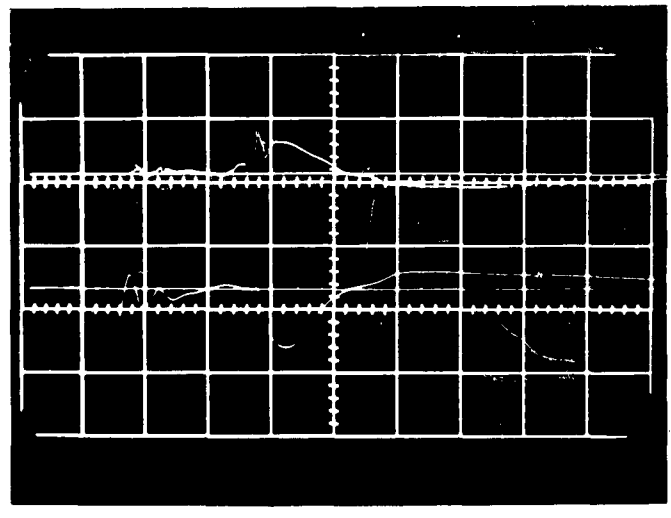

Figure 21. Same conditions as Figure 20, except the plasma source (0.6 μf charged to 18 kV) was triggered simultaneously with the line.

Upper Trace: B_r. 5 μs/cm.
Lower Trace: B_z. 5 μs/cm.

field signal 28 inches from the input end of the transmission line. Since this is approximately at the exit end of the transmission line, the advancing and receding waves are superimposed. Figures 19 and 21 also indicate dramatically the manner in which the radial and axial magnetic fields are modified by the presence of a plasma in the transmission line. In Figure 19 the upper beam is the radial magnetic field. There is a strong perturbation at approximately 16 microseconds and another at approximately 27 microseconds. Both occur approximately at the times that the wave front is passing the probes. Careful examination of this picture as well as Figure 21, where the perturbation is at approximately 18-1/2 microseconds, leads to the conclusion that the perturbation fields are due to azimuthal currents in the plasma, and are located on the leading half of the cusp on the traveling wave. This is true both for the advancing wave and the receding wave. There is no definite indication that such a ring current exists on the trailing half of the cusp in either case.

Further evidence regarding the position of the plasma on the cusp, and also indicating the presence of Hall currents in the plasma, is given by the azimuthal magnetic probe measurements shown in Figures 22 through 27. The azimuthal magnetic probe measurements were made at the same positions as were the radial probe measurements. In Figures 22 and 25 the upper beam shows the azimuthal magnetic field in the vacuum condition. Figures 23 and 26 show the azimuthal magnetic field in the presence of plasma. In Figure 23 the maximum perturbation occurs at approximately 29 microseconds, which is at the position of the receding cusp. In Figure 26 it occurs at approximately 18-1/2 microseconds, which is at the position of the advancing cusp. This figure is at the end of the transmission line, whereas Figure 23 was 20 inches from the input end of the line. Figures 24 and 27 show the plasma density at the axis of the transmission line. Figure 27 shows that approximately in the interval 14-19 microseconds, there is plasma ahead of the advancing cusp. At the time of 25 microseconds, there is plasma ahead of the receding cusp. The significance of the plasma signal in these figures at approximately 35 microseconds is explained later. The series of pictures, Figures 18 through 27, is consistent temporally and spatially with the assumption that there is an azimuthal current and plasma on the leading edges of the advancing and receding cusps. The shape of the perturbation on the magnetic field in the azimuthal case and the temporal extent of this perturbation (and its relation to the perturbation of the radial and magnetic fields) is consistent with the presence of Hall currents on the leading edge of both the advancing and receding cusps. The interaction of the field with the plasma is again indicated to be strongest in the case of the receding wave, as was indicated by the distance vs time plot in Figure 17.

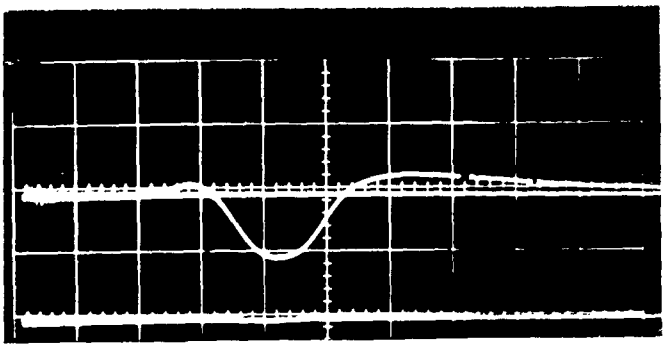

Figure 22. Upper Trace: B_θ, azimuthal component of the magnetic field 2 cm from the axis of the transmission line, 49 cm from the plasma source. No plasma present. 5 μs/cm.

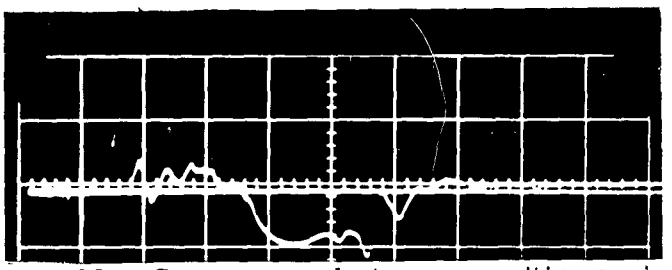

Figure 23. B_θ, measured at same position as in Figure 22, except the plasma source (0.6 μf charged to 18 kV) was triggered simultaneously with the line. 5 μs/cm.

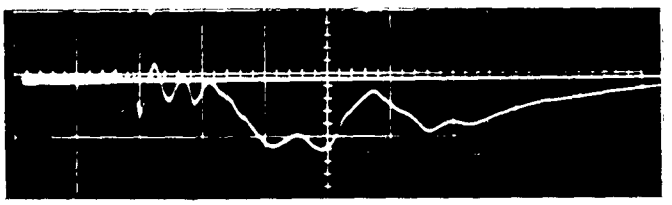

Figure 24. Plasma density (positive density is downward) 0.5 cm from transmission line axis, measured with double probe, 49 cm from the plasma source. The signal is distorted by pickup from the source discharge during the first 12 μsec. 5 μs/cm.

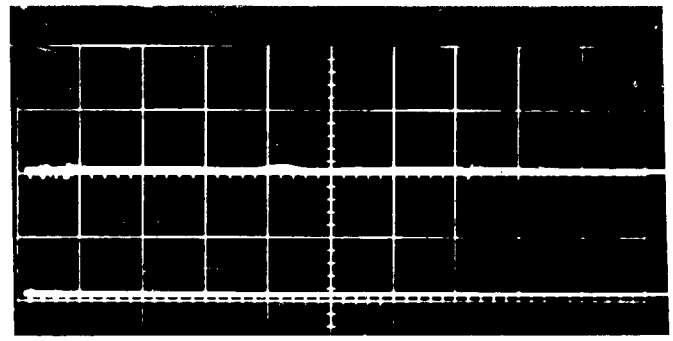

Figure 25. Upper Trace: B_θ, azimuthal component of the magnetic field 2 cm from the axis of the transmission line, 69 cm from the plasma source. No plasma present. 5 μs/cm.

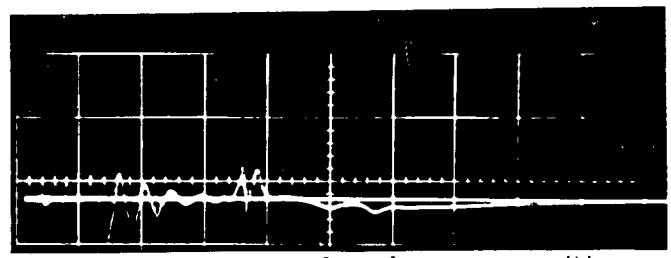

Figure 26. B_θ, measured at the same position as in Figure 25, except the plasma source (0.6 μf charged to 18 kV) was triggered simultaneously with the line. 5 μs/cm.

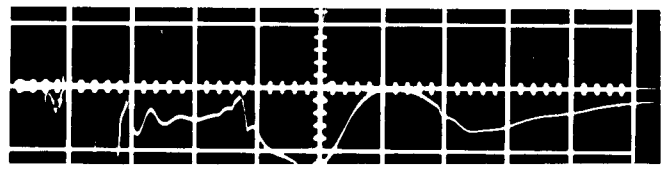

Figure 27. Plasma density (positive density is downward), 0.5 cm from transmission line axis, measured with double probe, 69 cm from the plasma source. The signal is distorted by pickup from the source discharge during the first 12 μsec. 5 μs/cm.

The results of the distribution measurements of axial magnetic field on the axis, radial magnetic field 2 centimeters from the axis, azimuthal magnetic field 2 centimeters from the axis, and the plasma density 1/2 centimeter from the axis have been plotted as space distributions at various times during the period when the wave is making its first advance and first recession in the transmission line. These measurements were made at 2 inch intervals and consequently are not able to show the fine structure in the distributions, especially at the points where the trapped plasma on the cusp fronts are located. However, they do give a good indication of the over-all characteristics of the magnetic field and the density distribution in the transmission line at successive time intervals.

These distributions are shown in Appendix B. These distributions are most useful to indicate the unusual behavior of the receding magnetic wave as it snowplows through the plasma distributed along the transmission line. The magnetic distributions are shown both in the vacuum and the plasma case. The most striking characteristic of the return wave is the large scale jump in the magnitude and direction of the axial magnetic field evidenced in the time interval between the 30 and 32 microseconds axial plots of the axial magnetic fields. A tentative explanation of this rapid change in the magnitude and direction of the axial field at this time can be formulated if one considers the progress of the returning wave from the instant of reflection of the wave at the end of the transmission line. At this time the entire wave tube is filled with a hot diamagnetic plasma and an axial field. The field direction is almost entirely toward the front of the wave tube and permeates the plasma. In the process of reflection of the wave, those axial lines not heavily tied to the plasma move upward and outward to form the precursor of the returning cusp. In so doing these lines cut the coils of the transmission line, thereby inducing the reverse currents necessary for the post-cursor of the returning cusp. However, some of the axial lines remain tied to the plasma still within the tube volume; these lines become trapped between the reverse axial field of the post-cursor of the returning cusp and the diamagnetic plasma within the tube. As this process continues with the axial precursor lines continuing to cut the coils of the transmission line, the magnitude of this exterior reverse axial field increases. The interior axial field is thus compressed by means of the plasma, to which the interior axial field is tied. This rapid compression results in considerable currents in the plasma at the interface between the two directions of axial field which now appear to the upstream end of the transmission line. Examination of the graphs shows that this compression seems to become most intense during a period on the order of one microsecond between the 30 and 32 microsecond time distributions. A simple order of magnitude calculation then shows that

the ohmic heating in the plasma during compression is sufficient to raise its conductivity to a point where the plasma can sustain the full pressure of the exterior axial field against that of the interior axial field.

This process continues with an inward radial acceleration and compression of the interior axial field to the point where this field is compressed to a magnetic pressure comparable to that of the exterior axial field. It is at this point, when the interior and exterior axial magnetic fields seem to have reached equivalent pressures through this compression, that the dramatic and complete expulsion of the interior axial field takes place.

Although no detailed explanation for the actual process of expulsion of the interior axial field completely out of the system is available at this time, the occurrence of so dramatic a change in the field distribution over a large scale distance in the wave tube during a time interval of the order of one microsecond would indicate that a violent instability mechanism is responsible. Further evidence for this phenomenon is shown in Figures 28 through 33. Shown on the upper beam is the radial magnetic field and on the lower beam the axial magnetic field (Figures 28, 30, and 32 for the vacuum fields, and Figures 29, 31, and 33 with the plasma present). Looking at the magnetic field perturbation of the radial field (in the upper beam of the lower pictures, Figures 29, 31, and 33), which is occurring at approximately 30 microseconds, one sees that there is a large perturbation in Figure 29 at 14 inches from the low speed end of the line and in Figure 33 at 10 inches from the low speed end of the line. However, this is not the case in Figure 31, for which the perturbation is 12 inches from the low speed end of the line. In Figure 31 the position of the cusp is passing at a time between 30 and 32 microseconds. The signals indicate that at this time and position there is a large discrepancy between the perturbing field due to the circulating currents in the plasma at this cusp front as compared to those at the adjacent observation points along the axis. This is another manifestation of the violent large-scale anomalous behavior which is occurring along the transmission line at the time of expulsion of the axial field from the line.

The experimental findings discussed in this section on the trapping of induced flux, the circulating currents in the leading edge of the traveling cusp, and the presence of Hall currents in electrodeless accelerator tube, as well as the instability which developed under the snowplow action of the returning wave, are summarized in Section IV. The influence of the Hall currents in the operation of a traveling wave accelerator is discussed in detail in Section III.

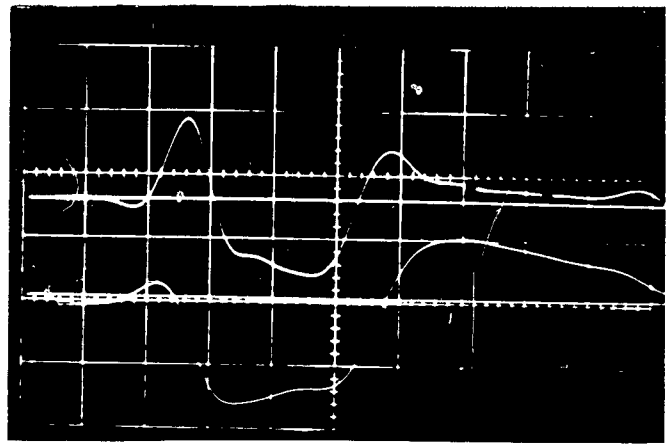

Figure 28. Upper Trace: B_r, radial component of the magnetic field 2 cm from the axis and 14 in. from the low speed end of the transmission line (33 cm from the plasma source). Obtained from integration of an induction probe signal. Trace triggered by discharge of the transmission line, which was energized by a 15 μf capacitor charged to 6 kV. 5 μs/cm.

Lower Trace: B_z, axial component of the magnetic field at the axis and 14 in. from the low speed end of the transmission line (33 cm from the plasma source). No plasma present. 5 μs/cm.

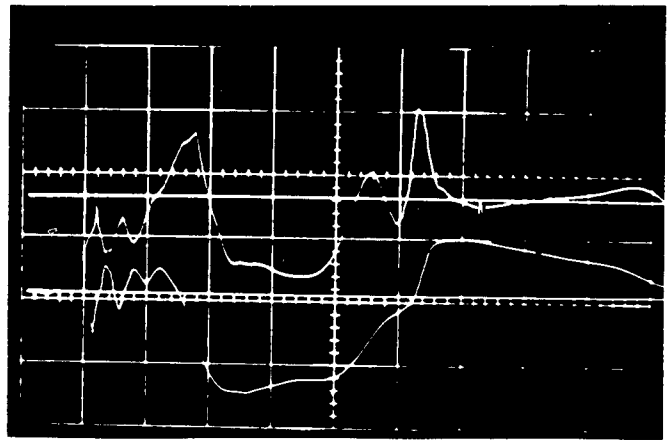

Figure 29. Same conditions as Figure 28, except the plasma source (0.6 μf charged to 18 kV) was triggered simultaneously with the line.

Upper Trace: B_r. 5 μs/cm.

Lower Trace: B_z. 5 μs/cm.

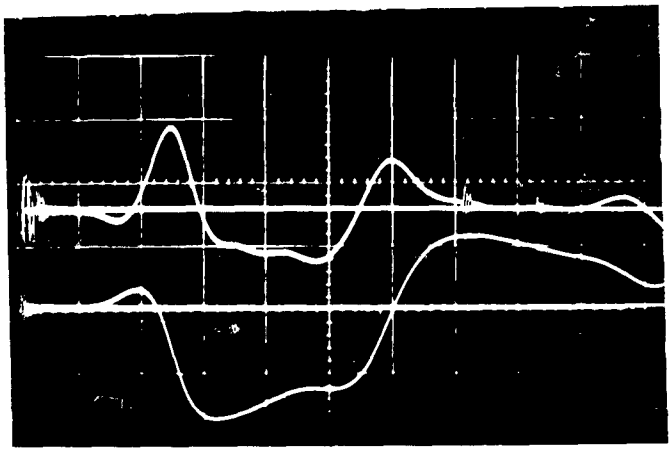

Figure 30. Upper Trace: B_r, 12 in. from the low speed end of the line (28 cm from the plasma source), without plasma. 5 μs/cm.

Lower Trace: B_z, 12 in. from the low speed end of the line (28 cm from the plasma source), without plasma. 5 μs/cm.

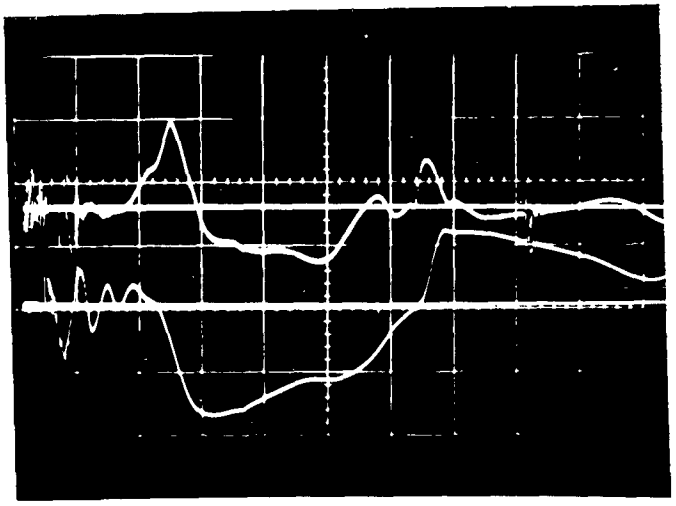

Figure 31. Same conditions as Figure 30, except with plasma.

Upper Trace: B_r. 5 μs/cm.

Lower Trace: B_z. 5 μs/cm.

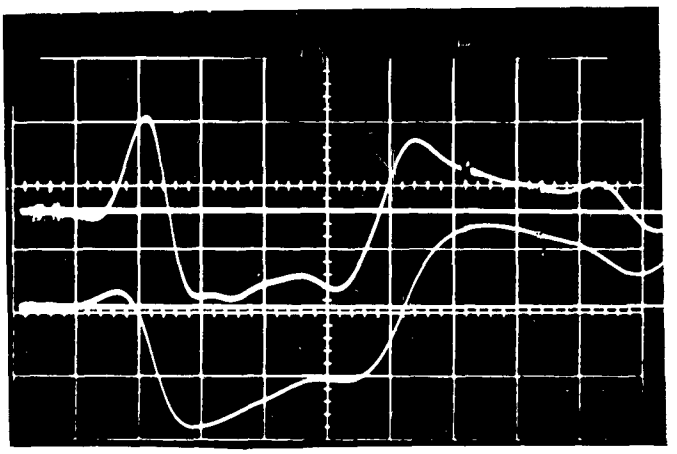

Figure 32. Upper Trace: B_r, 10 in. from the low speed end of the line (23 cm from the plasma source), without plasma. 5 μs/cm.

Lower Trace: B_z, 10 in. from the low speed end of the line (23 cm from the plasma source), without plasma. 5 μs/cm.

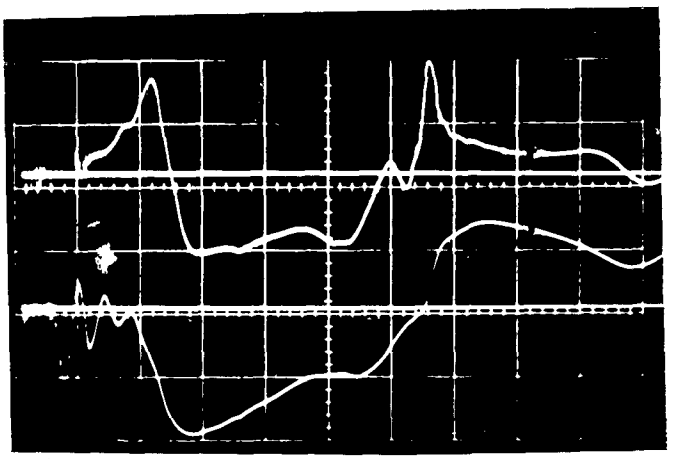

Figure 33. Same conditions as Figure 32, except with plasma.

Upper Trace: B_r. 5 μs/cm.

Lower Trace: B_z. 5 μs/cm.

III. DESCRIPTIONS OF PROPULSION MECHANISMS

The magnetic induction accelerator is a traveling field device that normally derives acceleration of a plasmoid through an appreciable amount of slippage of the field through the plasmoid. The changing pattern of magnetic field in the plasma will cause azimuthal currents to flow. These currents in turn interact with the non-axial components of the field to produce a body force on the plasmoid. This body force will generally take a direction which attempts to bring the plasmoid up to the velocity of the magnetic field.

The synchronous accelerator is a traveling wave accelerator operating within the limits of very small slip velocities. There is little relative motion of plasma and field. The temperature of the plasma must be so high that the magnetic field is either "frozen" in the plasma or is effectively excluded from the plasma. While the magnetic field in an induction accelerator moves at a recognizably greater velocity than the plasmoid to provide the induced electric field, the magnetic field in a synchronous accelerator, being either "frozen" in the plasma or excluded from it, moves at almost the same velocity as the plasma. Thus, if the plasma velocity is to increase, the velocity of the moving magnetic field must increase. The synchronous accelerator, then, is a booster device which receives a blob of the plasma (plasmoid) at a low velocity supplied by another plasma accelerator, and delivers it at higher velocity. Here the principal currents responsible for interaction between the field and plasmoid are the thermal diamagnetic currents at the surface of the plasmoid. The problem is to produce a plasma with a conductivity high enough to prevent the plasma from slipping through the magnetic field.

While containment of the plasma is desirable in an induction accelerator, it is essential in a synchronous accelerator. If the plasma is in contact with a material wall, heat conduction will cool the plasma and lower its conductivity, making it incapable of excluding the magnetic field or preventing relative motion of plasma and field. Contact with a wall or a cooler plasma can also spoil the diamagnetic currents in the plasma. The plasma will then slip behind the field, and further acceleration will proceed as in an induction accelerator. Heat loss to walls can be tolerated in an induction accelerator because the joule heating of the induced currents continuously supplies energy to the plasma. Conceivably, if containment could be assured, a machine comparable to an induction

accelerator could begin to accelerate plasma until the joule heating raised the plasma conductivity to a point at which a synchronous accelerator could take over by raising the propagation velocity of the field.

Several conceptually distinct models exist for the coupling of a body of plasma to a traveling magnetic field. Since these models yield neither identical results nor identical design criteria, it is important to understand the conceptual basis of each.*

A. PROPULSION OF A DIAMAGNETIC PLASMOID

If one first considers the behavior of a homogeneous plasma in a uniform magnetic field, it is clear that the net result of the oppositely oriented cyclotron motions of the ions and electrons combine to give a volume-distributed magnetic dipole density. If the plasma and the field are truly homogeneous (infinitely extended) and uniform, then the net contribution of all these dipoles to the field vanishes. If, however, the plasma has a boundary, there will be a net contribution of these dipoles from the region of non-uniform density near the boundary. The magnitude of the contribution of these currents is proportional to the density of plasma within the boundary and to the kinetic energy of motion of the charges in the plane perpendicular to the magnetic field in such a way that the quantity

$$\frac{B^2}{2\mu_o} + nkT$$

is constant across the boundary.

This is, of course, an elaboration of the standard confinement mechanism of controlled thermonuclear research. In cases of interest for plasma propulsion, however, there are several points of divergence from the simple diamagnetic scheme outlined above.

In the first place, the temperature and magnetic field strength are usually such that the most probable ion gyromagnetic radius is comparable to the over-all dimensions of the plasmoid. This results in a somewhat altered containment on which electrical attraction between the

---

*See, for example, "Plasma Propulsion by a Rapidly Varying Magnetic Field," Milton Klein and Keith Brueckner. There three systems of first-order effects leading to a propulsive force were considered. The resulting performance showed some degree of divergence according to the model used.

ions and the more tightly held electrons plays a large role on confining the ions to the main body of plasma.

Secondly, even the containment of electrons, which would be almost complete in the absence of collisions,* is increasingly reduced by collisions as plasmas of lower and lower temperature are considered. This is a result of the rapid increase in the occurrence of strong, distinctly two-body interactions with decreasing average energy of the plasma.

Returning now to the somewhat altered picture of the diamagnetic confinement of a plasma, we can identify the mechanism by which such a plasma can be accelerated by a magnetic field. If some imbalance of pressure exists between the forward and trailing edges of such a plasmoid, due for instance to a pressure gradient in the plasma setup as a reaction to the relative motion of the field and plasma, then the plasmoid experiences a net force in such a direction as to counter this relative motion. The pressure imbalance could also be due to a greatly decreased value of the magnetic field to one side of the plasmoid. This also results in a net force on the body of plasma, but unless the magnetic lines are set in motion, the motion of the body of plasma would mainly be merely one of redistribution along the field lines.

B. PROPULSION OF AN INDUCED CURRENT RING

Another simple model on which the propulsion of a plasma by a traveling magnetic field might be based is that of the Lorentz forces of the field acting on an induced current ring in the plasma. In this model, the transport coefficient of dominant importance is the electrical conductivity of the plasma. If there is relative motion of the traveling wave and the plasma at a position of non-zero fringing field (i.e., if $(\underset{\sim}{v} - \underset{\sim}{u}) \times \underset{\sim}{B} \neq \underset{\sim}{0}$ where $\underset{\sim}{v}$ is the velocity of motion of the wave, and $\underset{\sim}{u}$ the local average (number of signed charges) velocity of the plasma, then local electric fields appear in a reference frame moving with velocity $\underset{\sim}{u}$. This field results in an electrical current in the plasma.**

---

*Assuming that the plasma itself is non-turbulent and free from sharp non-uniformities.

**This current is easily seen to be distinct from the diamagnetic surface currents which arise as a result of the thermal energy of the plasma even in a static magnetic field. These diamagnetic surface currents are present in any case when a plasma is in contact with a magnetic field, and, since they alter the field, should in principle be included in a proper analysis of the system.

For an axially symmetric traveling wave this current may have on the average an azimuthal direction, and will generally have the proper direction to compensate for relative motion of the plasma and the field. However, the induced currents are strongly influenced by the existence of magnetic fields and density and temperature gradients in the plasma.

The simplest of these influences is that of the magnetic field. If one accepts the classical results for the transport coefficients in the presence of a magnetic field, then the conductivity tensor requires that the induction electric field in the plasma should produce not only an azimuthal current, j_θ, but also a current of magnitude $\sim\omega\tau j_\theta$ in the direction normal to both the electric and magnetic fields. This is the Hall current, which can easily be as large or even much larger than the azimuthal current under conditions of interest in an induction accelerator, since for such conditions typically $1 < \omega\tau < 50$ for the electrons. It will be shown in Section III.D that the Hall current gives rise to some unexpected phenomena which have important consequences for the design and operation of a traveling wave accelerator. For example, the presence of the Hall currents can alter both the magnitude of the azimuthal current and the nature of the fields in which this current moves.

Besides the system of electrically induced currents predicted by the classical form of the conductivity tensor, there will also be present currents due to gradients of electron density and electron temperature.* For example, in the case of a sharp boundary, there will occur surface currents distinct from those due to the diamagnetic motion of the charges,** but having the same direction--i.e., in the proper sense to reduce the magnetic field within the plasma. The relative magnitude of this current compared to the diamagnetic current will vary approximately as c/BT^4, where c is a constant. Thus the diamagnetic current becomes rapidly more important than the current due to transverse diffusion as the plasma becomes hotter. Actually, it is already substantially larger for any temperature at which appreciable ionization can be maintained in all but the smallest magnetic fields.

---

*The behavior of the ions on this model, as before, will be largely the result of electrostatic interaction with the electrons, which are almost solely responsible for the currents flowing, and hence receive the burden of forces acting on the plasma.

**This can be seen, for instance, by considering a collisionless plasma, for which the diffusion tensor has zero components for both the direct and transverse directions, so that the current due to diffusion effects vanishes, while the diamagnetic currents remain.

The existence of a temperature gradient in the plasma leads not only to a thermal flow, but to a net flow of charge as well. As with the other transport coefficients, the thermal conductivity acquires a tensor form in the presence of a magnetic field, so that the thermal flow is no longer in the direction of the temperature gradient, but has components along ∇T_e and $\nabla T_e \times B$ of relative magnitude q and $\omega\tau q$. The associated electrical currents* have the same relative components in these directions. Because of the rather non-uniform distribution of currents expected in the plasmoid, ohmic heating could result in large, steady thermal gradients. This is especially true if $\omega\tau >> 1$, so that thermal transfer across lines of force becomes difficult. In this case, the electrons could be fairly well thermalized along a given field line, since heat transfer parallel to the field proceeds at the normal rate which is always greater than the rates for transverse conduction. However, the persistence of thermal gradients perpendicular to the magnetic field could give sizable transverse electric currents.

C. COMPARISON OF THE TWO MODELS

Although several variations of these approaches to the analysis of an inductive accelerator are possible, the current systems which have been described rather exhaust the possible sources of interaction between a plasmoid and a traveling field, so that little new would be expected by new interpretation. One further point should by now be apparent--the two techniques are by no means equivalent, but rather supplementary. That is, the balance by means of diamagnetic currents of kinetic pressures and magnetic pressures is quite independent of the operation of the azimuthal and Hall currents, while the currents due to spatial non-uniformities in the plasma will be present in any case.

However, some consideration of the relative magnitudes of the currents involved reveals that:

1. In most cases of interest for inductive propulsion, the diamagnetic currents will be considerably larger than those produced directly by either density or temperature gradients.

---

*The production of an electrical current by a temperature gradient in a non-magnetized plasma is well known as the thermoelectric effect. In the presence of a strong magnetic field the phenomenon of the electrical current flow perpendicular to ∇T has been well verified, and is sometimes known as the Mernst effect.

2. The relative magnitudes of the diamagnetic and inductive currents will be a strong function of the relative velocity between the plasmoid and the traveling wave.

The effects of both in producing a force on the plasmoid vary as B_r^2 so that the relative importance should be practically independent of the field strength. But since the diamagnetic effect is primarily a surface phenomenon, while the $j_\theta \times B_r$ force is a volume distributed one, some geometric influences favoring the latter according to the depth of penetration of the B_r field into the plasma will occur. The dependence of j_θ on the electron temperature is $\sim T_e^{3/2}$, while that of the dielectric current is $\sim T^{1/2}$, so that high temperature favors the induction currents.

The only dynamical variable that enters into the relation between the diamagnetic and induction current is the relative velocity between the plasmoid and the field. As this velocity goes to zero, the induction currents disappear, while the diamagnetic currents persist. Indeed, if one considers, for example, a standard magnetic mirror geometry, for which the containment of plasma is primarily due to the invariance of single particle magnetic moments,* it is easy to imagine an "adiabatic" translation (i.e., a motion of infinitely small acceleration) of the entire magnetic geometry which simultaneously displaces the body of plasma contained in it, and involves induction currents in no way. Such a motion only requires that the mirrors be displaced by a small distance relative to the field gradients at the mirrors during one period of transit of a particle between the mirrors. On the other hand, any erratic or rapid impulsive motion of the magnetic field will undoubtedly produce important inductive effects in the plasmoid. Such motions of the field will certainly occur in the rather imperfectly propagating waves which practical considerations force upon the experimenters. These impulsive modes could easily be amplified by oscillations in the plasmoid--for instance, oscillations in the electric fields which hold the massive, magnetically passive ions to the electrons being acted on by the induction and magnetic fields.

It thus appears that in general one must consider both the induction and diamagnetic interactions of the plasma with the traveling field--although for certain shapes of the plasmoid and certain periods of the course of the wave, one may predominate over the other.

---

*This diamagnetic phenomenon will amost certainly determine any containment of the electrons in the immediate vicinity of the "hole" on the axis of the traveling field, where all radial and azimuthal components of the magnetic field must vanish.

D. INFLUENCE OF THE HALL CURRENTS

As mentioned in Section III.B, if induction fields are dominant in the plasma, then Hall currents will be set up. To understand how this phenomenon could influence the traveling wave, consider the traveling cusp fields and plasmoids shown at the top of Figures 34 and 35. In both cases the field is traveling to the right and there is a relative velocity, $\underset{\sim}{u}$, with which the plasmoid is trying to slip through the cusp. The direction of the induced azimuthal electric field and current is as indicated in the figures. If we first suppose that the Hall current flows freely, then the relation between E_θ and j_θ will be:

$$j_\theta \approx \frac{\sigma_o}{1 + (\omega\tau)^2} E_\theta$$

The direction and magnitudes of the Hall currents are then determined from

$$j_H \approx \frac{\sigma_o \omega\tau}{1 + (\omega\tau)^2} E_\theta \times B.$$

These are also indicated in the diagrams for several points in the plasmoids.

Now these Hall currents as drawn are evidently not solenoidal, i.e., $\nabla \cdot j_H \neq 0$, so that there must be an accumulation of charge. In a short time the axis becomes charged with respect to the periphery of the plasmoid, so that electric fields are established as shown in the lower portion of the figures. The general dependence of the magnitude of the Hall currents on the fields is determined by:

$$j_H \sim \frac{|E_\theta|}{|B|} \sim \frac{|\dot{B}|}{|B|} \sim \frac{|B_r|}{|B|}.$$

Since B_r is greatest and B smallest in the part of the plasmoid nearest the center of the cusp, if one assumes an otherwise uniform plasmoid, then the Hall currents will be greatest in these regions. Furthermore, examination of the line integral of B_r/B around a path over which the plasma properties are sensibly constant, gives an approximate evaluation of $\nabla x j_H$ as:

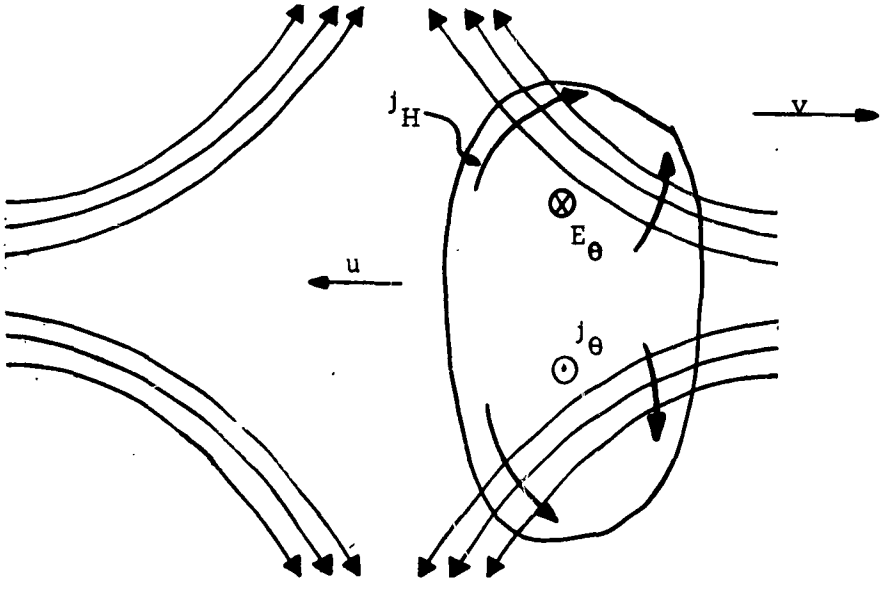

A. INITIAL FLOW OF HALL CURRENTS WITH PLASMOID IN FORWARD CUSP POSITION

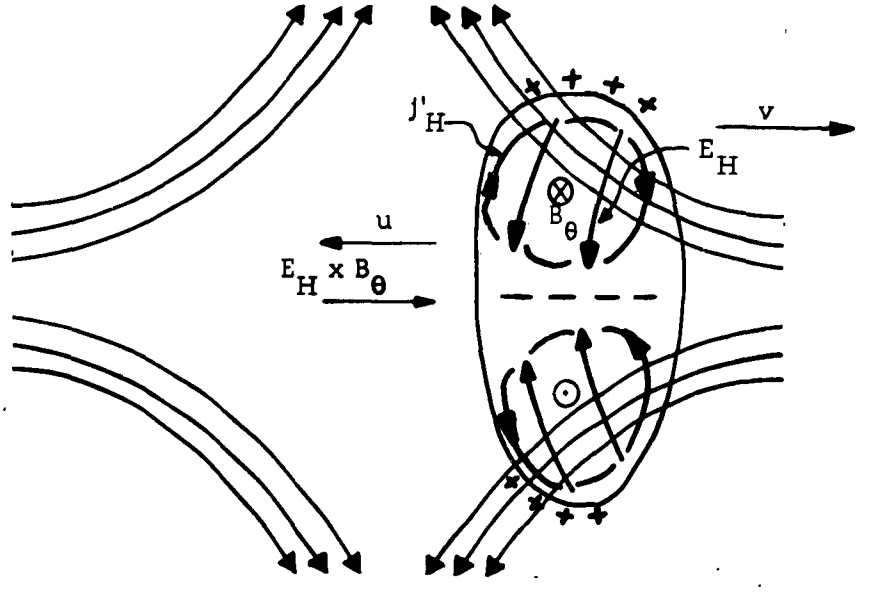

B. PERSISTENT HALL CURRENTS, SYSTEM OF FIELDS, AND DRIFT DIRECTION RESULTING FROM HALL EFFECTS

FIGURE 34

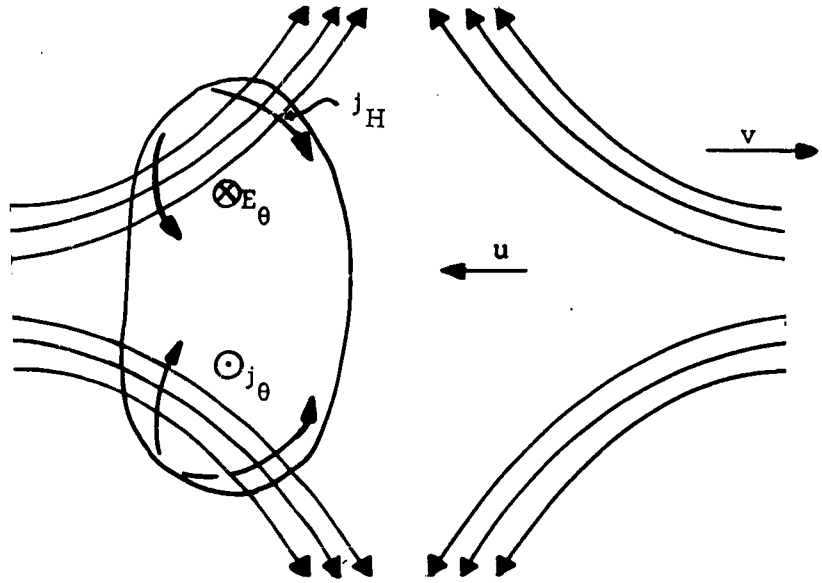

A. INITIAL FLOW OF HALL CURRENTS WITH PLASMOID IN STANDARD CUSP POSITION

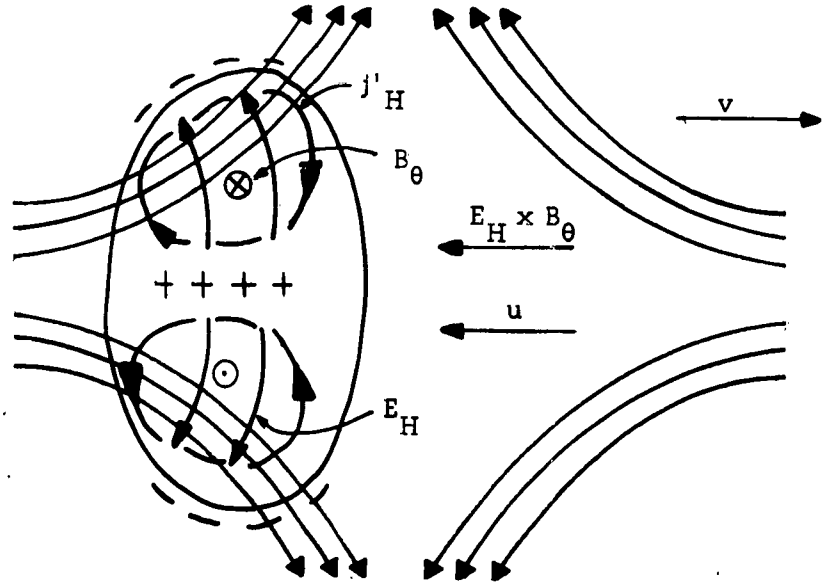

B. PERSISTENT HALL CURRENTS, SYSTEM OF FIELDS AND DRIFT DIRECTION RESULTING FROM HALL EFFECTS

FIGURE 35

$$\left|\nabla x j_H\right| \sim \left|\frac{1}{B}\left(1 - \frac{B_r}{B}\right)(B \cdot \nabla) B_r\right|,$$

which is in general zero only on the midplane of the cusp, where $B_r = B$. The implication here is that although it is generally possible to set up a charge distribution in the plasmoid to give an E_H field which can remove the divergence of j_H, so that the new distribution of currents and charges will be steady, it is generally known to be impossible to set up a steady charge distribution which can give an E_H field to cancel the rotational part of j_H. So the altered Hall current, after the polarization field has halted the accumulation of peripheral charges, will still possess non-zero, solenoidal components as shown in the lower portions of the diagrams. This solenoidal current will have a magnitude roughly equal to the difference in the initial Hall currents at the points of greatest and least current flows, i.e., at the axial extremities of the plasmoid,

$$j'_H \approx (j_H)_{max} - (j_H)_{min}.$$

This resultant Hall current can easily be of the same order of magnitude as the original Hall current, and hence of an order comparable to the azimuthal current. It should be easily observable experimentally, since it is the only sizable current present capable of generating a distinctly azimuthal magnetic field. This magnetic field was indeed observed in the course of the experiments on the AGN device, and agrees in general magnitude, extent, and direction with that predicted by the above current.

The average magnitude of the electric field developed by the Hall currents will be roughly determined by the average of these two extreme currents from the condition that the net current flow in the radial direction be cancelled by the field:

$$\frac{\sigma_o}{1 + (\omega\tau)^2} E_H = \frac{1}{2}\left((j_H)_{max} + (j_H)_{min}\right)$$

This electric field will in turn produce a transverse current, j'_θ, which is along the direction of the original induction field, E_θ. This current is of magnitude:

$$j'_\theta \approx \frac{\sigma_o \omega\tau}{1 + (\omega\tau)^2} E_H \approx \frac{\sigma_o \omega\tau}{1 + (\omega\tau)^2} \cdot \frac{(j_H)_{max} + (j_H)_{min}}{2\sigma_o} \cdot \left|1 + (\omega\tau)^2\right|$$

$$j'_\theta \sim \frac{\sigma_o (\omega\tau)^2}{\left|1 + (\omega\tau)^2\right|} \cdot E_\theta$$

So for the net azimuthal current, one has:

$$(j_\theta)_{tot} = j_\theta + j'_\theta \sim \frac{\sigma_o}{1 + (\omega\tau)^2} E_\theta + \frac{\sigma_o (\omega\tau)^2}{1 + (\omega\tau)^2} E_\theta \quad (j_\theta)_{tot} \sim \sigma_o E_\theta .$$

That is, the polarization field due to the Hall currents restores the azimuthal current to roughly the same value it would have in the absence of the magnetic reduction of the conductivity.

But although it would here seem to have come full circle, there are a number of sizable currents and fields which the Hall effect has left along the way, as illustrated in the lower diagrams of Figures 34 and 35. If now the interaction of the material within the plasmoid with the E_H and B_θ fields is considered, it is seen that:

> For the plasma situation in front of the cusp, as in the first figure, the direction of the $E_H \times B_\theta$ drift is to the right, that is, the drift tends to counter the relative motion of the plasma and field.
>
> For the plasma situated within the cusp, as in the second figure, the direction of the $E_H \times B_\theta$ drift is to the left, that is, the drift tends to exaggerate the slippage of the plasma through the cusp.

From the preceding, it is easily seen that the relative magnitudes of E_H and E_θ are determined from

$$E_H \sim \omega\tau E_\theta ,$$

so that this drift effect may under some circumstances, such as $\omega\tau >> 1$, be of considerable importance to the operation of the device.

The cusp shapes and direction of travel in the AGN induction accelerator were substantially as shown in the figures. The data showed that the plasma which moved with the line was consistently carried as in the first figure, for which the Hall currents are favorable to the propulsion, and that no detectable plasmoid was carried in the position within the cusp, for which the Hall currents are unfavorable.

IV. CONCLUSIONS AND RECOMMENDATIONS

A. HALL CURRENTS

A considerable amount of theoretical and experimental evidence has been amassed indicating the presence of circulating Hall currents in this type of traveling field accelerator. Furthermore, there are theoretical indications that the presence of Hall currents in an induction accelerator need not always oppose the operation. Actually, for some geometries of field and plasmas, Hall currents can assist in the acceleration of a plasma by a traveling magnetic field. On the basis of these observations and theoretical findings, further study of the Hall effect in traveling field accelerators is desirable. Since the presence of Hall currents in such a device can be either beneficial or detrimental to the performance of the accelerator, it is worthwhile to pursue a study which would enable the controlled use of these currents or their elimination, when proved necessary.

B. FLUX TRAPPING CONCEPT

It will be useful to recall briefly the problem of escape cone leakage encountered in attempting to accelerate a high conductivity plasma with the traveling magnetic wave. This has reference to pushing a plasma with a configuration such as that belonging to the post-cursor of the wave achieved in this program and described in Section II. The plasma, being highly conductive, inhibits the diffusion of the traveling wave's magnetic field lines into its volume. The mechanism involved is one of induced sheath currents which produce opposing fields. The net effect is a kind of pileup of magnetic lines outside the bulk of the plasma volume implying a magnetic pressure upon the plasma. This pressure both compresses the plasma radially (raising its internal pressure) and drives it ahead of the advancing wave.

Another equally valid qualitative view of the interaction is implied by seeing that the plasma penetrates the field poorly in directions perpendicular to the field lines. Losses through the wave occur, however, because the particles of the plasma are not prevented from moving freely along the field lines. Therefore, significant losses

occur where the field lines converge, somewhat as if through a hole in the wave front. These losses would occur even if the field shapes were left essentially undisturbed by the presence of the plasma. However, it is possible for the plasma to aggravate the escape region losses by forcing the field lines apart there, and making them ride up over its surface (as the wave passes) while a large part of the plasma slips through the widened loss area (moving generally parallel to the lines as it does). This behavior is the more likely the higher the plasma conductivity, depending directly upon the plasma's capacity to exclude field lines. In this loss mechanism the plasma may be thought of as behaving approximately like a fluid in a magnetic funnel whose walls exert a pressure on its contents and whose own thermal pressure keeps the walls out. Under this pressure the plasma moves out both ends of the funnel; the losses out the narrow end can prove disastrous for traveling wave systems which do not include some means to check this leakage.

In this research program evidence has been accumulated which shows that the trapping of the plasma on a precursor type magnetic configuration is superior to the concept of pushing the plasma with a post-cursor type of configuration. The precursor trapping configuration is not entirely adequate, however. The flux lines that thread the plasma, in leaving, pass out through the transmission line and are linked with the conductors on the transmission line. This allows the plasma to ride out to the walls along the field lines as the acceleration process proceeds and also involves problems of the removal of the plasma from the field at the end of the accelerator. The method of trapping flux in the plasma was conceived to improve upon this type of trapping and acceleration. Essentially this idea involves an attempt to reduce the effective fluidity of the plasma by keeping it together with magnetic field lines which are trapped within it when it is generated. These field lines do not link the transmission line coils with the plasma as in the precursor case, but complete their loop within the transmission line just outside of the plasma. Thus, there are formed closed magnetic lines with plasma keeping the lines apart. This allows the acceleration of the plasma in a fashion somewhat similar to the precursor case. However, it does not invite the problems of the plasma running out to the wall and also the disengagement of the plasma from the field of the traveling wave device at the end of the line. In a sense the plasma has the escape region plug built into it.

Because of the attractiveness of the concept of flux trapping and its general potential application to this type of accelerator, it is recommended that further investigations be directed toward achieving flux trapping both in the manner described and in evaluation of other techniques for establishing these persistent dipole currents.

C. SOURCES

Much of the work in this program related to the Bostick type pulsed plasma sources. It is concluded that sources of this type are not sufficiently efficient to be useful as a plasma source in an advanced propulsion unit. However, it has been found that these sources are quite useful in fundamental studies of the interaction of finite extent plasmas under pulsed plasma injection conditions. This type of source can still be quite useful when studies of field interactions with heavy ions are desired. Many different types of metal-derived plasmas may be produced with this method. They are, however, somewhat limited as to attainable plasma conductivity and volume, that is, total number of particles produced. Consequently, they will not be useful for all types of studies. With regard to the d.c. plasma source studied in this program, the hollow cathode plasma source seems to be a quite promising method of producing a continuous plasma stream of fully ionized gas in the density range of 10^{12} to 10^{14} ions/cc. This type of source has potential for being useful both in pulsed transmission line and continuous wave type accelerators. Further studies of the hollow cathode plasma source are recommended to determine its feasibility as an advanced propulsion unit plasma source.

D. STUDIES OF DENSITY AND TEMPERATURE GRADIENTS AS THEY AFFECT THE OPERATION OF ELECTRODELESS ACCELERATORS

Theoretical considerations indicate that although strong currents can arise from the presence of gradients in the plasma, the magnetic fields can largely stifle any net loss of particles or thermal energy by these currents, except in regions where collisions are too frequent or where the field lines do not take the proper direction to provide the desired insulation from walls. This magnetic insulation could break down, however, if sufficient large-scale oscillations take place within the plasma. Especially under the influence of strong density and temperature gradients, the usual thermal spectrum of perturbations to the distribution function is subject to amplification by a dispersion relation containing strong resonances, and even singularities. The resulting large-amplitude excursions can result in a greatly increased

diffusion of the particles or thermal energy. This phenomenon of turbulent diffusion is still imperfectly understood, but it is often observed in real plasma systems.

However, unless signs of anomalous diffusion appear in an inductive accelerator, there seems to be as yet little that theory has to offer in this area with regard to practical design.

There may be some benefit from studying in more detail the classical diffusion mechanisms, especially as they relate to the production of electrical currents in a plasmoid interacting with a traveling field.

APPENDIX A

APPLICATION OF SUPERCONDUCTIVITY TO TRAVELING FIELD DEVICES

I. INTRODUCTION

The applications of superconductors to traveling magnetic field accelerators appear limited. Two typical traveling field devices which can be mentioned are:

(1) The pulsed accelerator in which individual wave fronts are caused to travel down an accelerating tube containing plasma, and

(2) Steady state devices in which the coiled line surrounding the plasma acceleration region is driven by an a.c. source to provide a regularly spaced series of traveling magnetic wave peaks.

The use of superconducting wire in the coiled transmission lines of these devices will result only in the total elimination of ohmic heating of the coils and its attendant energy loss. The efficiency or plasma output velocity of these devices will be changed, then, only if such ohmic heating was an important energy loss mechanism.

It seems that any practical device of the second type above would have to include a termination for the line, chosen to prevent reflection. The primary energy sink would then undoubtedly be in the terminating resistor. The first type of line, however, can be operated with no termination. A pulse is sent down the line which discharges the capacitors as it travels. The plasma is expelled from the end of the device and the magnetic wave is reflected, partially recharging the capacitors on its return. In this regime of operation, the ohmic losses in the coil would have to be compared with:

(1) Losses to heating of the plasma,

(2) Dielectric losses in the capacitors.

It seems likely that the first of these will be dominant. However, the possibility that ohmic losses could be important in some such devices makes it desirable to consider the use of superconductors. The gain in efficiency from their use would, of course, have to be balanced against the power required to keep them at cryogenic temperatures. It is possible that, for short missions, a tank of liquid helium or hydrogen could perform that task.

While the uses of superconductors in the accelerator coils themselves may be interesting but problematical, the use of superconductors in any steady field solenoids (in the ion source, in d.c. biases for the accelerator, in exhaust field shaping devices, etc.) would almost certainly be advantageous.

II. PULSED AND ALTERNATING CURRENTS IN PURE SUPERCONDUCTORS

The superconducting state in a very pure metal is one of zero electrical resistance. It occurs in the temperature range from zero degrees Kelvin to 18° Kelvin. Each superconducting metal has a definite critical temperature at which, in the absence of a magnetic field or of currents, it passes abruptly into the superconducting state. The passage of electrical current through a superconductor, or its immersion in a magnetic field, lowers the temperature of transition. A curve can be drawn dividing the T-H plane into superconducting and normal areas.

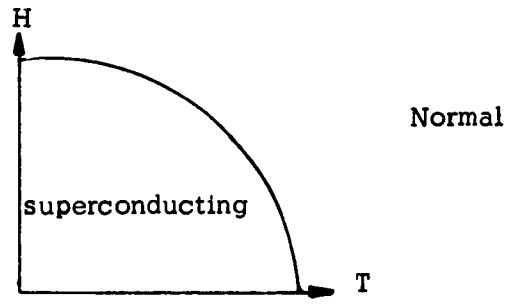

Another property of pure superconductors is their complete exclusion of magnetic flux lines. They are nearly perfect diamagnets, allowing the magnetic field to penetrate only a small distance ($\approx 10^{-6}$cm) into the bulk of the metal. The magnetic screening is accomplished by currents established in the penetration layer. The electrons in a superconductor are in a collective state which can be described as a condensation of pairs of virtual particle states formed from electron states. The

condensed, or paired, situation is stable against breakup. Between the condensed ground state and the first excited state of a superconductor is a gap of 3.5 kT_c (T_c is the critical temperature, k is Boltzmann's constant). Thus, energy of 3.5 kT_c or so must be supplied to the metal (e.g., in the form of photons) before pairs are broken and the first excited (and non-superconductive) state is possible. The energy gap, as it is called, will give an idea of the effect of an alternating electric current in a superconductor.

Experiments have been done in which radiation in the near infrared spectrum was transmitted through thin films of superconductors.[1] These experiments measured the energy gap ΔE by observing the absorption edge which presented itself at a frequency ω_c given by

$$\hbar\omega_c = \Delta E.$$

It might be concluded from these experiments that superconductors would maintain zero resistance to all frequencies into the far microwave-near infrared region. Important experiments by Pippard, however, show that at a lower frequency (~1000 mcs) an effect analogous to the anomalous skin effect in ordinary metals begins to produce resistance.[2] It would seem, therefore, that superconducting wire can carry alternating current up to 1000 mcs without resistance. The ability of superconducting wires to carry pulses can be estimated by assuming the wire's response to be linear and Fourier-analyzing the pulse into its spectrum. Then the wire can be expected to absorb that part of the spectrum which lies above 10^9 cps. In other words, the wire would pass pulses whose rise time was greater than 10^{-9} secs. Such a prediction must, however, be considered skeptically in the case of very high voltage pulses in transmission lines. In the absence of experimental data, one can only warn that the mechanical shock and high voltages present may introduce non-linear effects which would invalidate the above analysis.*

The discussion so far pertains to the special case of a straight piece of superconducting wire. When wire is wound into a solenoid, other problems arise. They arise primarily because of the locking-in of flux lines which can happen whenever an island of normal metal appears in a superconductor. This phenomenon is a result of the zero resistance of superconductors.

[1] R.C. Glover, III and M. Tinkham, Phys. Rev., 108, 243 (1958).

[2] See, for example, Shoenberg, Superconductivity, Cambridge Univ. Press, Cambridge, England, 2nd edition, 1952, p 11.

*For example, the writer knows of no experiments on cold field emission of electrons from superconductors, or similar high voltage effects.

Such islands can be formed in spots of abnormally high fields or currents which may temporarily exist in a solenoid. The island may be maintained, after the abnormal conditions disappear, by the locked-in flux intensity. Alternatively, and more important, any impurity or point of mechanical strain or plastic deformation of a superconducting wire may alter its properties locally so as to produce islands. These islands will result in hysteresis and unpredictable and undependable performance of the wire.

The discussion above has pointed out the limitations of superconductors in alternating and pulsed current traveling wave devices. A suggestion can now be made of the conditions under which superconducting wire can be useful. Niobium is a superconductor which, at 4°K, has a critical field for destruction of superconductors of around 2000 gauss. It can be made very pure, and has good mechanical properties. This wire could perhaps be used in a traveling wave device. It would be necessary, most likely, to provide a rigid support assembly for the wire. Care would have to be taken in the winding of the coils not to introduce undue strain. Such a wire would possibly be useful in devices requiring about 1 kg magnetic field maxima. The purity and freedom from strain would become particularly important if pulsed, rather than alternating, currents were used.

III. ALTERNATING AND PULSED CURRENTS IN SUPERCONDUCTING ALLOYS AND COMPOUNDS

Emphasis was put in the preceding section on the problem of hysteresis and impurity when using alternating or pulsed currents. It seems likely that these problems would rule out entirely the use of the dramatic high-field superconducting metallic mixtures such as Nb_3Sn, V_3Ga, and Nb_3Zr. These latter are inherently impure and brittle metals. They exhibit strong effects of hysteresis. For example, Boom at the Oak Ridge National Laboratory found that pulsed field critical field measurements on Nb_3Sn were equal to steady field values only when the rise time of the field was ~10 ms, corresponding to a frequency of 100 cps.[3] Other experimenters with Nb_3Zr solenoids have found it necessary to "train" the wire by raising the current gradually in a series of steps, with current off between steps, in order to get optimum field values.[4] All of these effects would be disastrous for a pulsed or a.c. traveling wave line.

---

[3] R. W. Boom, Oak Ridge National Laboratory, personal communication to R. L. Pearson, AGN, September 1961.

[4] M.A.R. LeBlanc, IBM Journal of Research & Development, Vol. 6, No. 1, January 1962, p 122.

As was noted earlier, however, the alloys are ideal for any steady bias fields which may be required. Therefore a digest of their properties is presented in Section IV.

IV. SUPERCONDUCTORS WITH HIGH CRITICAL TEMPERATURES AND HIGH CRITICAL FIELDS

A. FACTORS RESULTING IN A HIGH CRITICAL TEMPERATURE

It has been demonstrated that high critical temperatures (T_c) for superconductivity are achieved for valence electron to atom ratios of 4.4 to 5 and 6.4 to 7. Peaks in the curve relating T_c to the electron-atom ratio appear in these regions. While the valence is the major factor influencing T_c, other factors include the crystal structure, atomic mass, atomic radii, and homogeneity of the material (including vacancy defect structure, impurities, and composition gradients).

T_c tends to increase directly with the thirteenth power of the atomic radius (slightly more than the fourth power of the atomic volume), and inversely with the atomic mass. Some crystal structures are particularly favorable for superconductivity, notably the beta-tungsten and sodium chloride structures. Vacancies and impurities act as alloying elements, and by affecting the local homogeneity of the material, and hence, the valency, they influence T_c. Likewise, composition gradients in alloys also affect the local homogeneity, and hence result in a variable electron to atom ratio, thereby affecting T_c.

In general, a high T_c results in a high critical field (H_c). The relation is not linear. Doubling T_c may increase H_c by a factor of ten.

1. Alloys

Since peaks in T_c are achieved at valences somewhat below 5 and 7, and since the valence of elements consists of whole numbers, alloying makes it possible to achieve valences which produce high T_c values.

For example, the valence of Zr is 4 and that of Nb is 5; a 50-50 alloy would have a valence of 4.5. Two outstanding alloys are listed in Table I.

TABLE I

Element	Valence	T_c	Crystal Structure	H_c
$Nb_{0.7}$-$Zr_{0.3}$	4.7	12°K	Beta Phase (cubic CsCl type)	85,000 gauss
$Technetium_{0.76}$-$Mo_{0.25}$	6.75	16°K	Sigma Phase (Tetragonal, B-U type)	200,000 gauss

Adding Zr to Nb raised T_c from 8° to 12°K, and adding Mo to Technetium raised T_c from 11° to 16°K, with a correspondingly disproportionate gain in H_c.

The optimum T_c for Nb_x-Zr_y is achieved at an approximate valence of 4.7. $Nb_{0.5}$-$Zr_{0.5}$ (valence 4.5) has a lower T_c value of 10.5°K. Similarly, $Technetium_{0.5}$-$Mo_{0.5}$ (valence 6.5) has a lower T_c value of 12°K, compared to 16°K for $Technetium_{0.75}$-$Mo_{0.25}$.

Therefore, there is an optimum composition for each alloy system at which a maximum T_c is achieved for that system. Recent information indicates that there are two T_c peaks in the valency region 4.4 to 5. One of them occurs at around 4.5 and the other at around 4.75. In some crystal systems, T_c peaks at around 4.5 and at around 4.75. The atomic mass and volume, and the material homogeneity determine the exact peak for alloy system.

2. Intermetallic Compounds

These compounds crystallize in structures which are quite different from those of the elements forming the compound. Generally, the crystal structure is complex and quite loose. Bonding tends to be less metallic (free-electron bonding) and far more homopolar (directional bonding). Hence, the compound tends to be quite brittle. Some of the compounds do not have narrow solubility, and therefore, exist over a fairly wide range of composition; they are not limited to their stoichiometric composition.

Examples of compounds with a high T_c are shown in Table II.

TABLE II

Compound	Valence	T_c	Crystal Structure	H_c
NbC	4.5	10°K	Sodium Chloride (cubic, 8 atoms/ unit cell)	?
NbN	5	15°K	" "	?
$(NbN)_{0.85}$-$(NbC)_{0.15}$	4.92	17°K	" "	?
Nb_3Sn	4.75	18°K	Beta-Wolfram (cubic, 8 atoms/ unit cell)	300,000?
V_3Si	4.75	17°K	" "	250,000?
$V_{2.95}Ga$	4.44	17°K	" "	500,000?

The sodium chloride structure is a fairly compact interstitial structure. Nevertheless, it is favorable for a high T_c. C and N tend to lower the atomic mass while expanding the Nb lattice. In addition, it is not common for the interstitial C or N atoms to be ideally distributed in the lattice. Inhomogeneity is therefore the rule, rather than the exception. It is also probable that regions such as $Nb_1N_{0.9}$ vacancies$_{0.1}$(valence 4.75) are the superconducting regions, since NbN has a valence of 5. Hence, a slight deficiency in N is advantageous.

Mixed crystals of the nitride and carbide result in a higher T_c. It is probable that a ternary compound, such as $Nb_1N_{0.85}C_{0.15}$ (valence 4.92) has been formed, or more probably, an

imperfect compound such as $Nb_1N_{0.8}C_{0.1}$ vacancies$_{0.1}$ (valence 4.7). Deviation from stoichiometric values can occur, since compounds often exist over a fairly wide range of composition. In evidence is the general rule that, when a compound is made more complex, the optimum properties are enhanced. An example of this is the raising of the melting point, when TaC and WC are combined. So it is not surprising that T_c is enhanced by combining NbN and NbC.

The X_1Y_1 compounds above are seen to crystallize in the sodium chloride structure. Likewise, many X_3Y compounds crystallize in the beta-wolfram structure. A notable example is Nb_3Sn with a T_c of 18°K. V_3Si and V_3Ga also crystallize in the beta-wolfram structure and have T_c values of about 17°K. This structure seems to be particularly favorable to superconductivity. The structure is quite loose with six X atoms and two Y atoms per unit cell, on average. It can be quite inhomogeneous, as shown by the $V_{2.95}Ga$ composition actually tested. Nb_3Sn and V_3Si have a valence of 4.75, $V_{2.95}Ga$ has a valence of 4.44. Both the 4.75 and 4.44 values are believed to be near the peak T_c valences for each respective compound system.

B. FACTORS RESULTING IN A HIGH CRITICAL FIELD

1. Nature of the Superconducting Channels

Theory requires that the superconducting channels be quite narrow, if a high critical field is to be achieved. This requirement is met in thin films, but it is also met in some of the bulk superconductors (those based on a transition element as the primary element). It must be postulated that the current flows through filaments. Hauser has shown that these filaments are associated with dislocations. The higher the dislocation density, the more filaments there are active, and the higher is H_c. The superconducting fiber network bears a direct relationship to the dislocation pattern. An analogous relationship exists between the two geometries. The dislocation structure determines the superconducting filament structure. By controlling the dislocation geometry, the ability of the superconductor to withstand a high field is enhanced. A high dislocation density enhances the superconducting current density by furnishing more paths for this current. The magnitude of the current flowing through a path is a function of the geometry of this path; it is restricted by the weakest link in the chain which forms this path.

When the magnetic field is raised, the number of paths capable of sustaining a superconducting current diminishes. The flow is blocked in the weaker paths; only the strongest paths are capable of sustaining a superconducting current.

The strongest paths are the most highly strained paths. All dislocations create a strain field which surrounds them. Those with the highest strain fields are the ones which resist the magnetic field penetration the least, and hence are affected least by the field. The superconducting current keeps flowing through the paths of highest strain. The weakest section in the path is that which is insufficiently strained and is therefore destroyed by a sufficiently high magnetic field. The magnetic field thus counteracts the strain field. As soon as there is an insufficient number of channels left open to carry the superconducting current, the current turns normal, and with the help of the magnetic field, moves through normal channels.

When the temperature is raised, the superconducting current density that a path can carry is restricted. As T_c is approached, the current density drops to zero. Each path has its individual H_c and T_c. The maximum H_c and T_c which are experimentally measured are those of the single filament whose geometry is most resistant to the impeding effect of magnetic field and temperature. Such a filament has a preferred geometry.

Single crystal work has demonstrated that orientation of the crystal lattice in the magnetic field influences the superconducting characteristics. Since dislocations occur in preferred crystallographic directions, the direction of the dislocations influences the superconducting characteristics. It is desirable to orient as many dislocations as possible in the desired direction of current flow.

2. Strain Variables Influencing Superconductive Channels

It has been shown that a high dislocation density is desirable, and that furthermore, the strain field surrounding the dislocations should be high. Experimental work with niobium and with rhenium has shown that cold working enhances superconductivity by generating a high dislocation density and a high strain field. High elastic moduli are desirable, since this results in a high strain field around the dislocations. A high work hardening index is also desirable since this results in a high dislocation density. Therefore, metals, alloys, and compounds which have crystal structures which promote work hardening are desirable for superconductors. Unfortunately, materials which work harden most readily are also very brittle as a result of the work hardening.

Cold working is only one means of producing the desired dislocation density and surrounding strain fields. When stress is applied to a metal, dislocations form in an attempt to relieve the resultant strain field. The strain field then localizes itself around the dislocations. Alloying produces inhomogeneity and thus promotes strain fields which the dislocations try to relieve. Thus any initial inhomogeneity, with its accompanying strain field, promotes a condition favorable to a high density of dislocations with their surrounding strain field. Strain fields help nucleate dislocations. Thus, grain boundaries, which are regions of inhomogeneity, promote the desired conditions. Precipitates, impurities, dispersions, all tend to promote the desired conditions, since they are regions of inhomogeneity. Inhomogeneity in composition in alloys and compounds also produces strain fields. Atomic disorder is desirable, since ordering promotes homogeneity. However, a limited amount of short range ordering has been shown to create maximum strain conditions, and therefore is desirable.

It can be understood why $Nb_{0.7}$-$Zr_{0.3}$ is an outstanding superconducting alloy. When properly heat treated, a very fine precipitate forms which creates a very large number of points of strain which serve as dislocation sources. Likewise, by their nature, the compounds mentioned readily form a great density of dislocations when stressed. All impurity atoms in such compounds tend to nucleate dislocations. Because of the directional bonding, strain fields in these compounds attain a large magnitude with very little stressing.

It can be said that the nature and magnitude of the strain fields surrounding dislocations in metals, to a large extent, governs the ability of the metal to remain superconducting in a large magnetic field. The elastic properties of the material are a determining factor in its resistance to penetration by the magnetic field.

APPENDIX B

TIME DEVELOPMENT OF MAGNETIC FIELDS ALONG AXIS WITH AND WITHOUT PLASMA

The figures on the following pages show the time sequential development of B_z, B_r, B_θ, and plasma density in the traveling field accelerator. For the magnetic field distributions, each page is for a different instant of time in the accelerator and shows the distribution of density or magnetic field along the length of the accelerator at that particular time. The magnetic field distributions are shown as they appear both with, and without, plasma in the accelerator. The vertical lines (dashed lines in the density distributions) indicate the positions of the low-speed and high-speed ends of the transmission line.

AXIAL MAGNETIC FIELD DISTRIBUTIONS

(Figures B-1 through B-16)

Upper Curve: B_z, axial component of the magnetic field at the axis of the transmission line in the absence of plasma. Obtained from the integrated signal of an induction probe at two-inch intervals in the line. The abscissa shows the distance from the plasma source, and the ordinate gives the magnetic induction (1 tesla = 10,000 gauss). The line was energized by a 15 μf capacitor charged to 6 kV.

Lower Curve: B_z, as in the upper curve, except the plasma source (0.6 μf charged to 18 kV) was triggered simultaneously with the line.

TIME: 6 MICROSECONDS

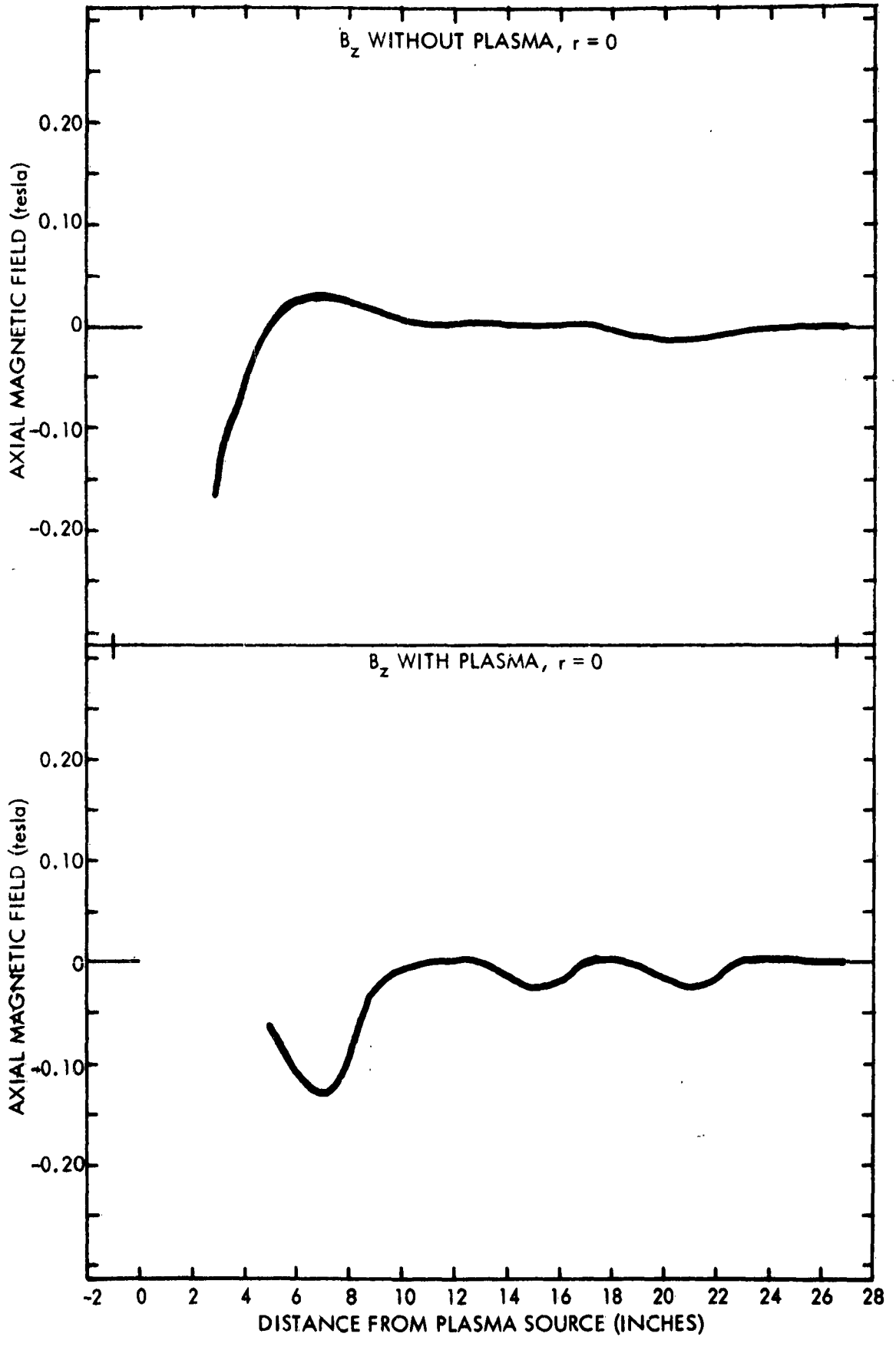

FIGURE B-1

TIME: 8 MICROSECONDS

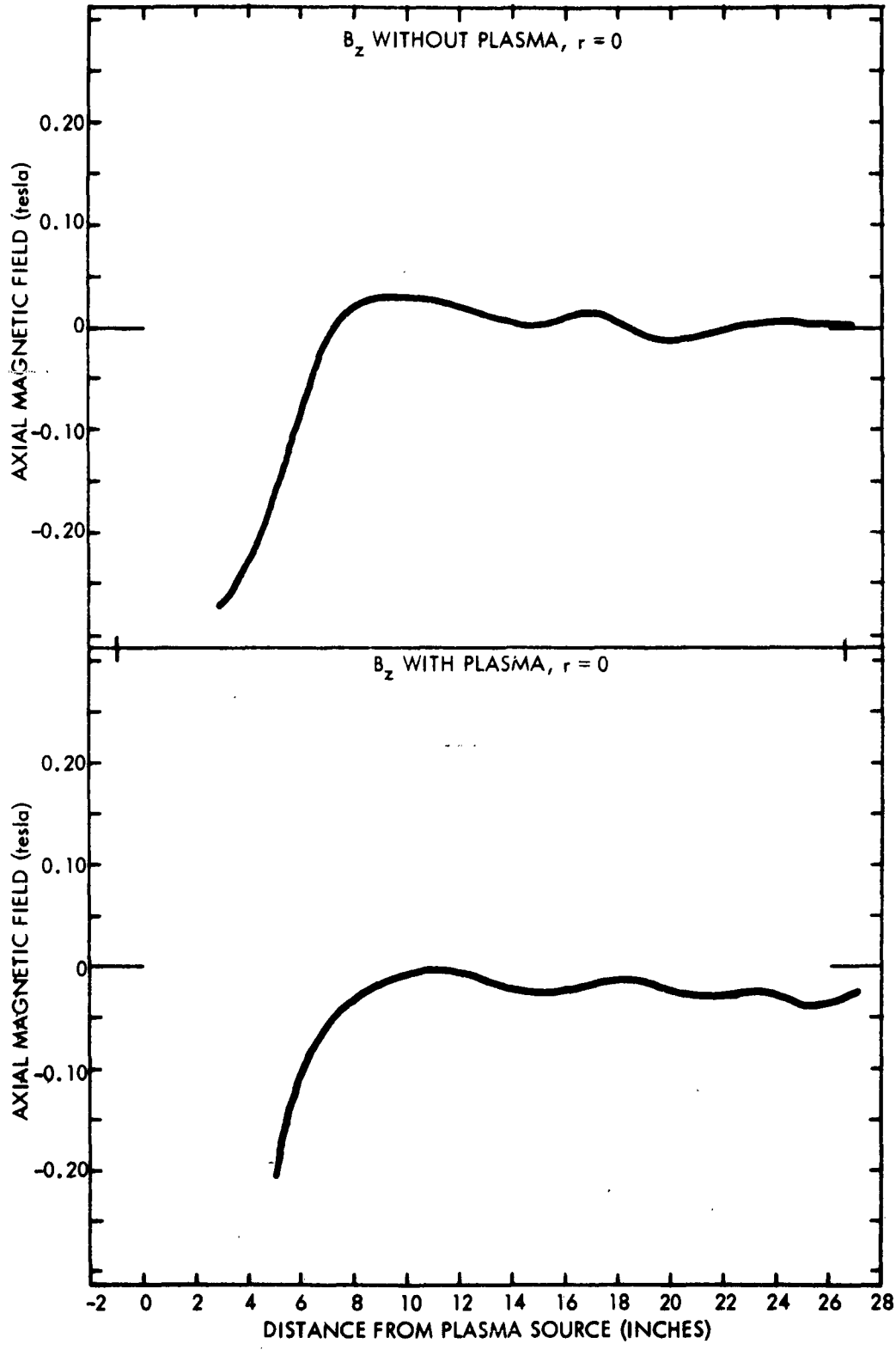

FIGURE B-2

TIME: 10 MICROSECONDS

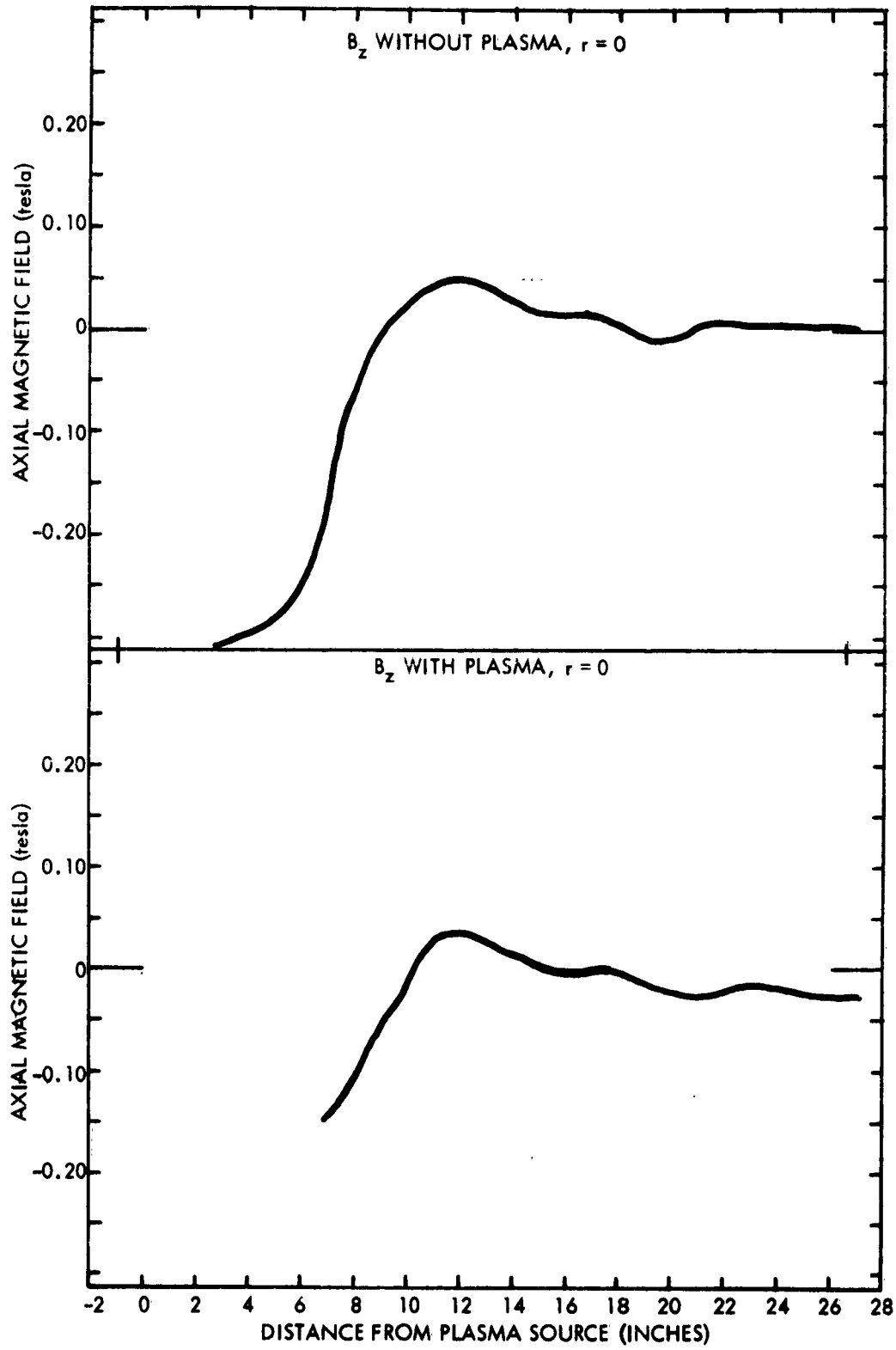

FIGURE B-3

TIME: 12 MICROSECONDS

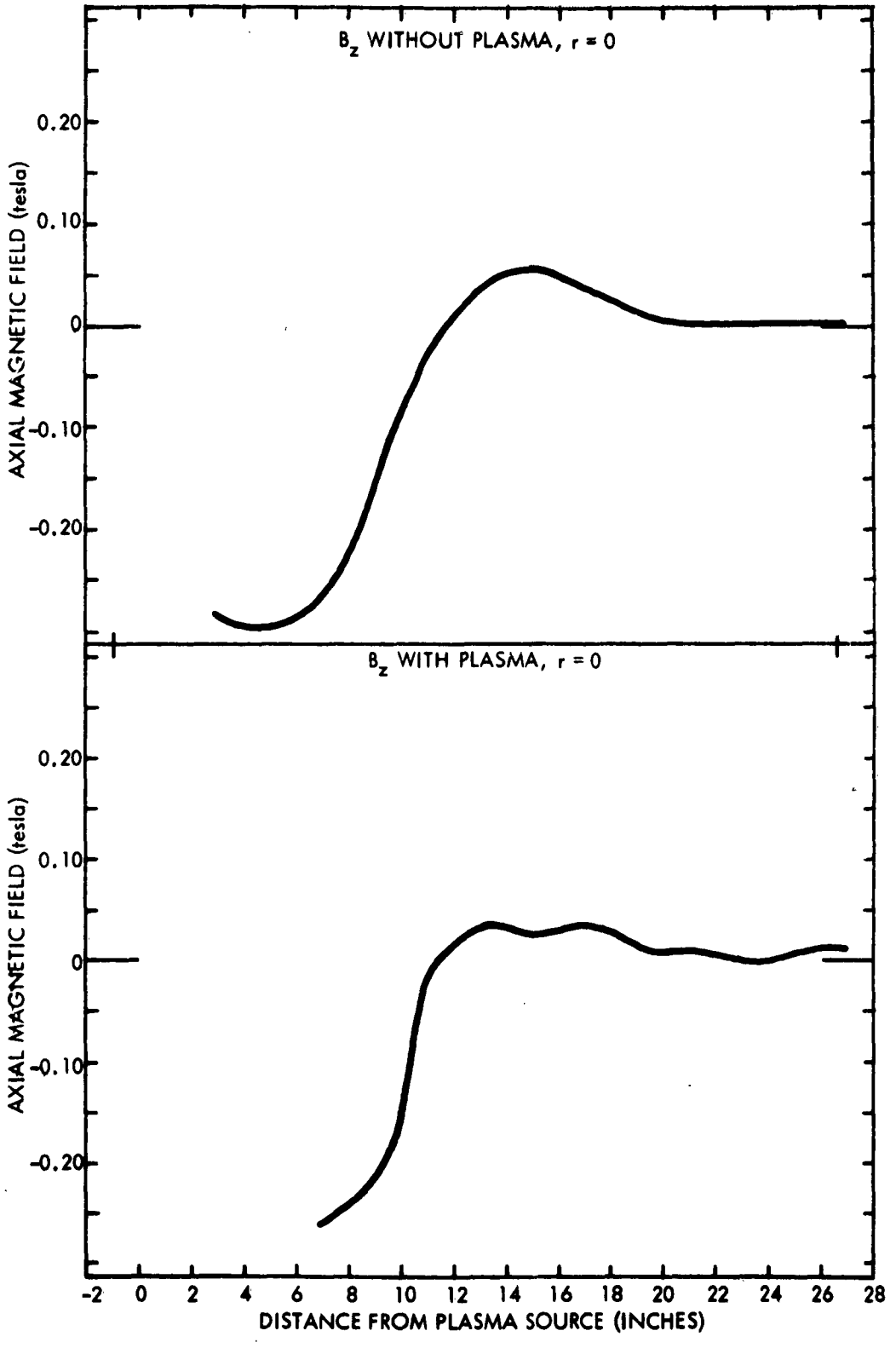

FIGURE B-4

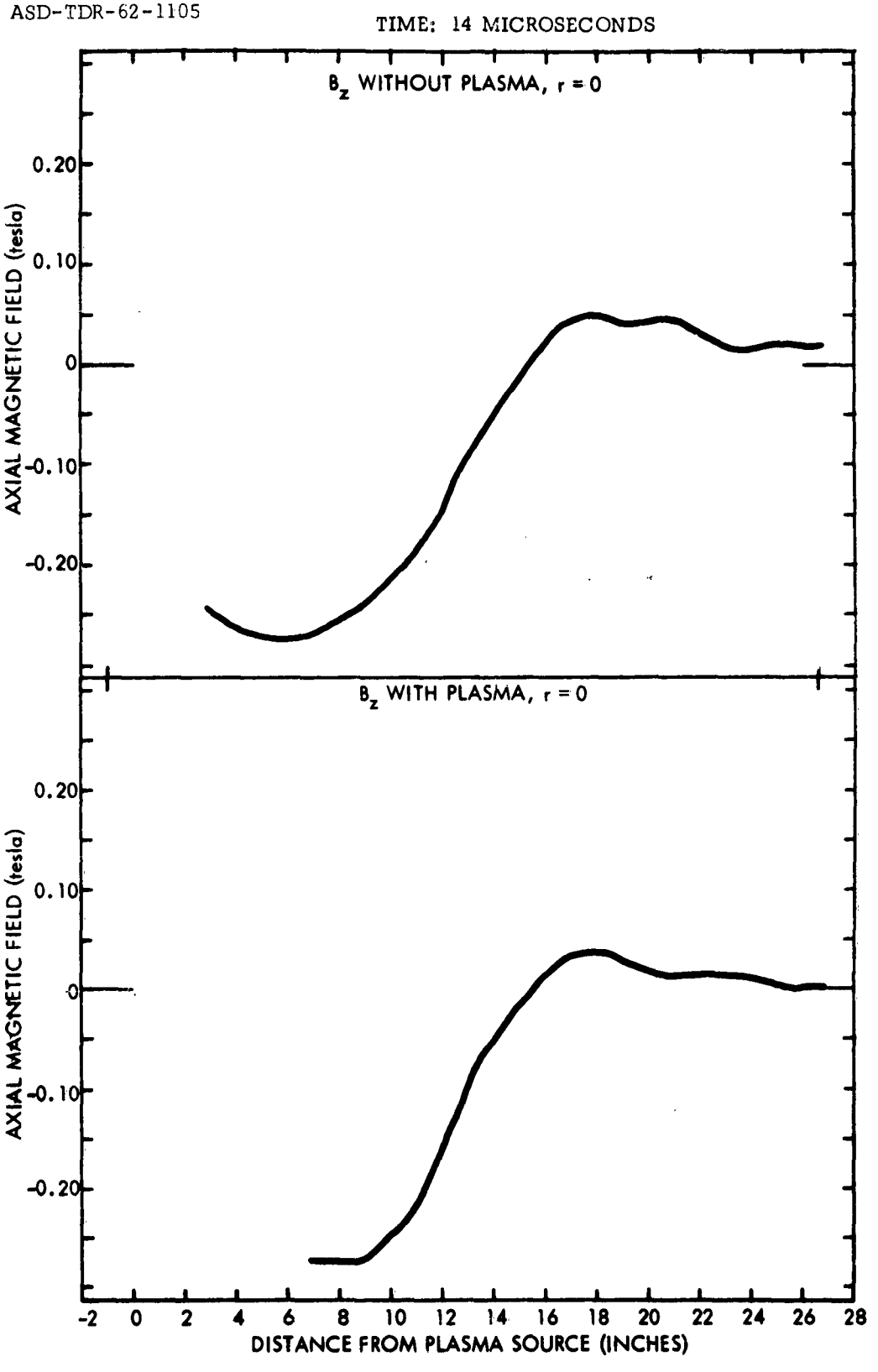
TIME: 14 MICROSECONDS
B_z WITHOUT PLASMA, r = 0
AXIAL MAGNETIC FIELD (tesla)
0.20
0.10
0
-0.10
-0.20
B_z WITH PLASMA, r = 0
AXIAL MAGNETIC FIELD (tesla)
0.20
0.10
0
-0.10
-0.20
-2 0 2 4 6 8 10 12 14 16 18 20 22 24 26 28
DISTANCE FROM PLASMA SOURCE (INCHES)

FIGURE B-5

TIME: 16 MICROSECONDS

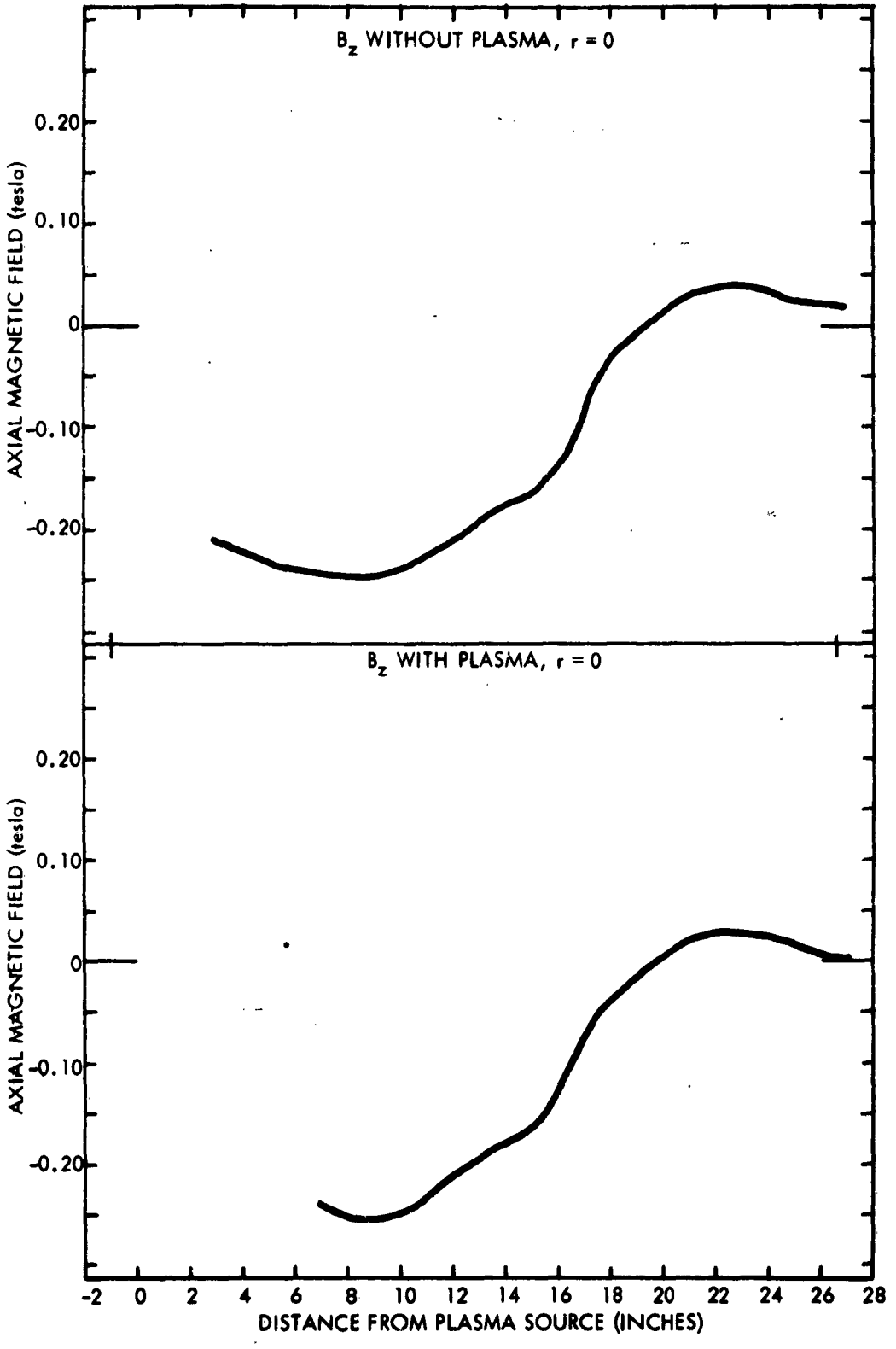

FIGURE B-6

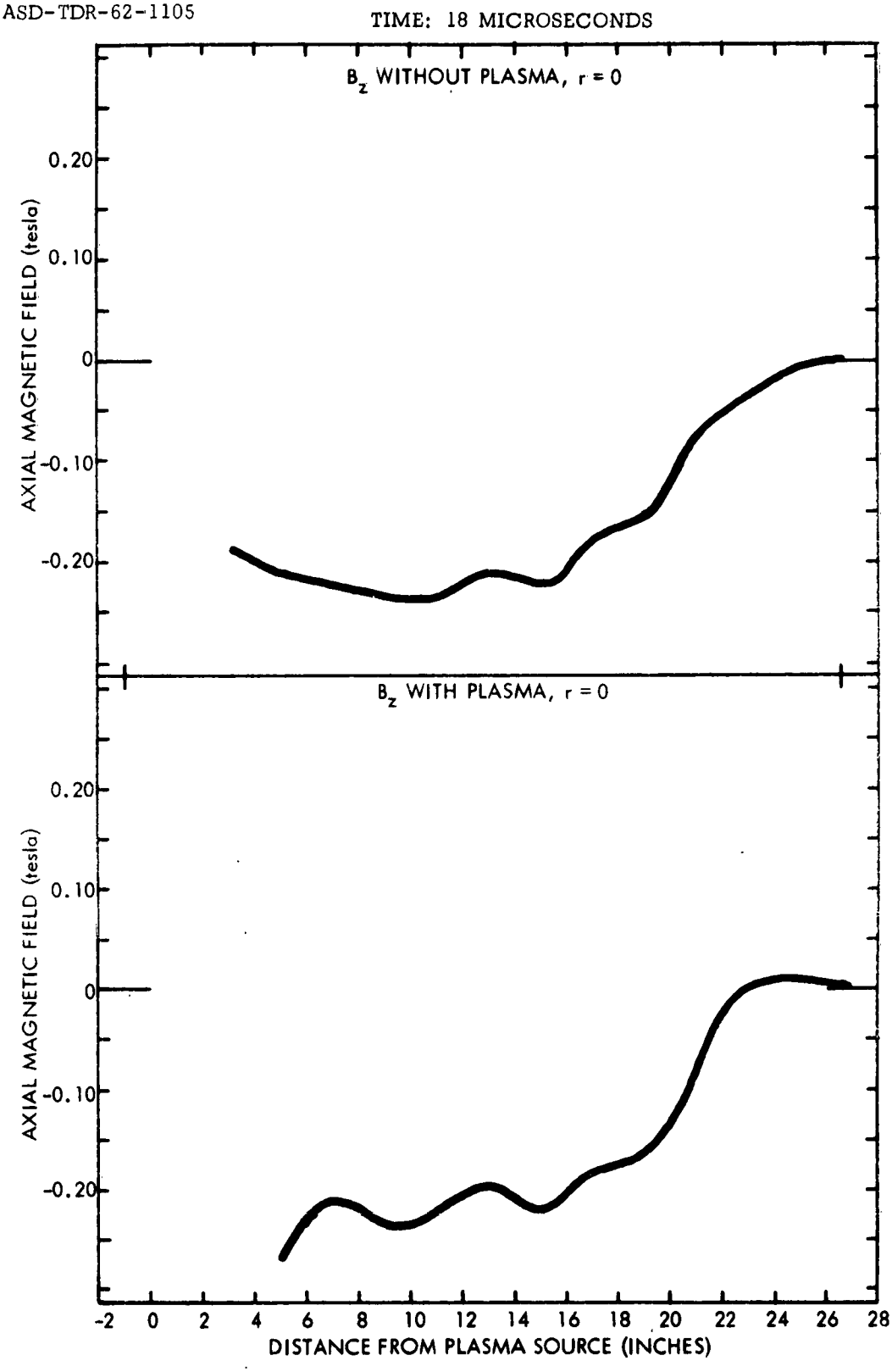
TIME: 18 MICROSECONDS
B_z WITHOUT PLASMA, r = 0
AXIAL MAGNETIC FIELD (tesla)
0.20
0.10
0
-0.10
-0.20
B_z WITH PLASMA, r = 0
AXIAL MAGNETIC FIELD (tesla)
0.20
0.10
0
-0.10
-0.20
-2 0 2 4 6 8 10 12 14 16 18 20 22 24 26 28
DISTANCE FROM PLASMA SOURCE (INCHES)

FIGURE B-7

TIME: 20 MICROSECONDS

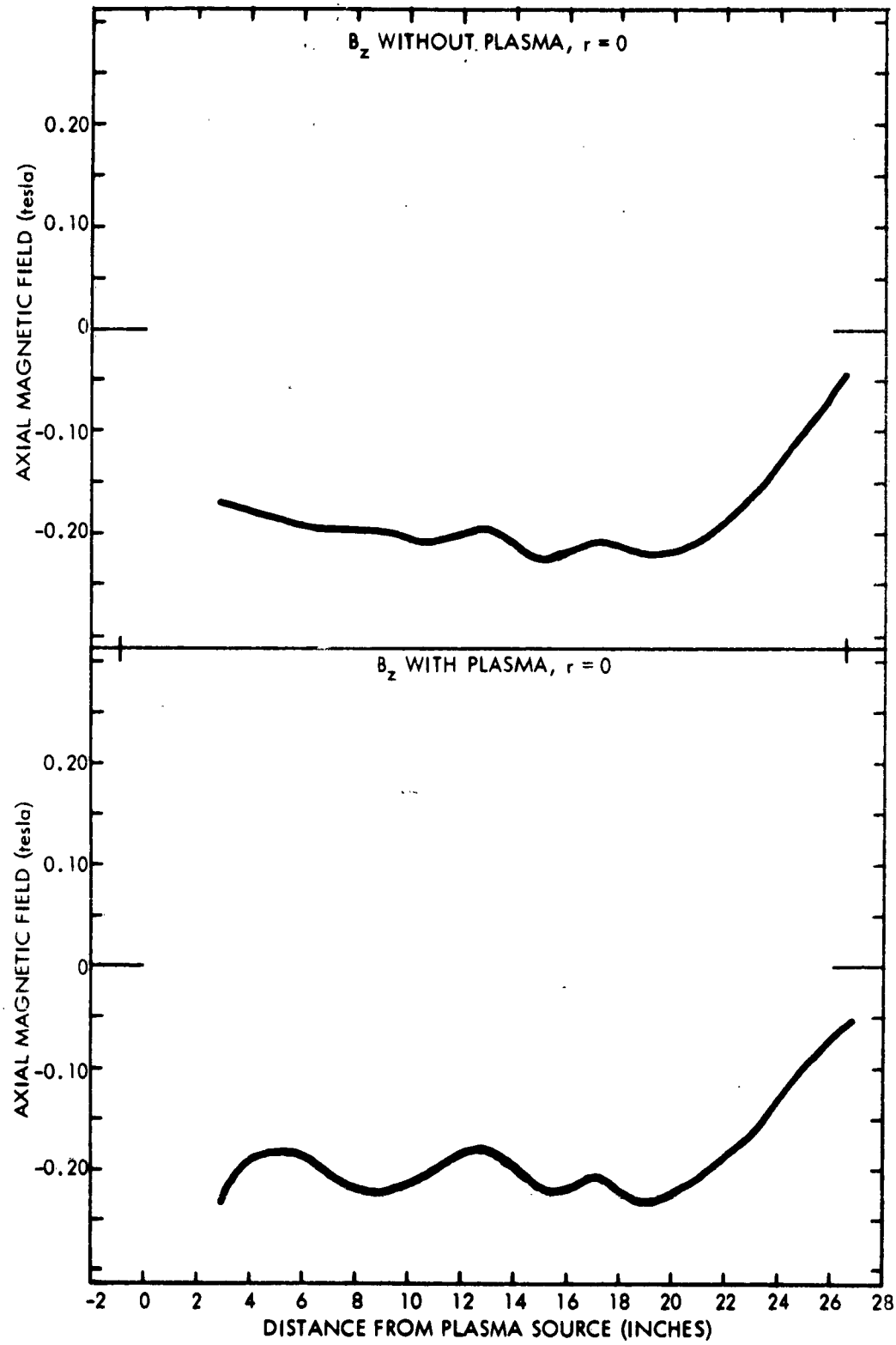

FIGURE B-8

TIME: 22 MICROSECONDS

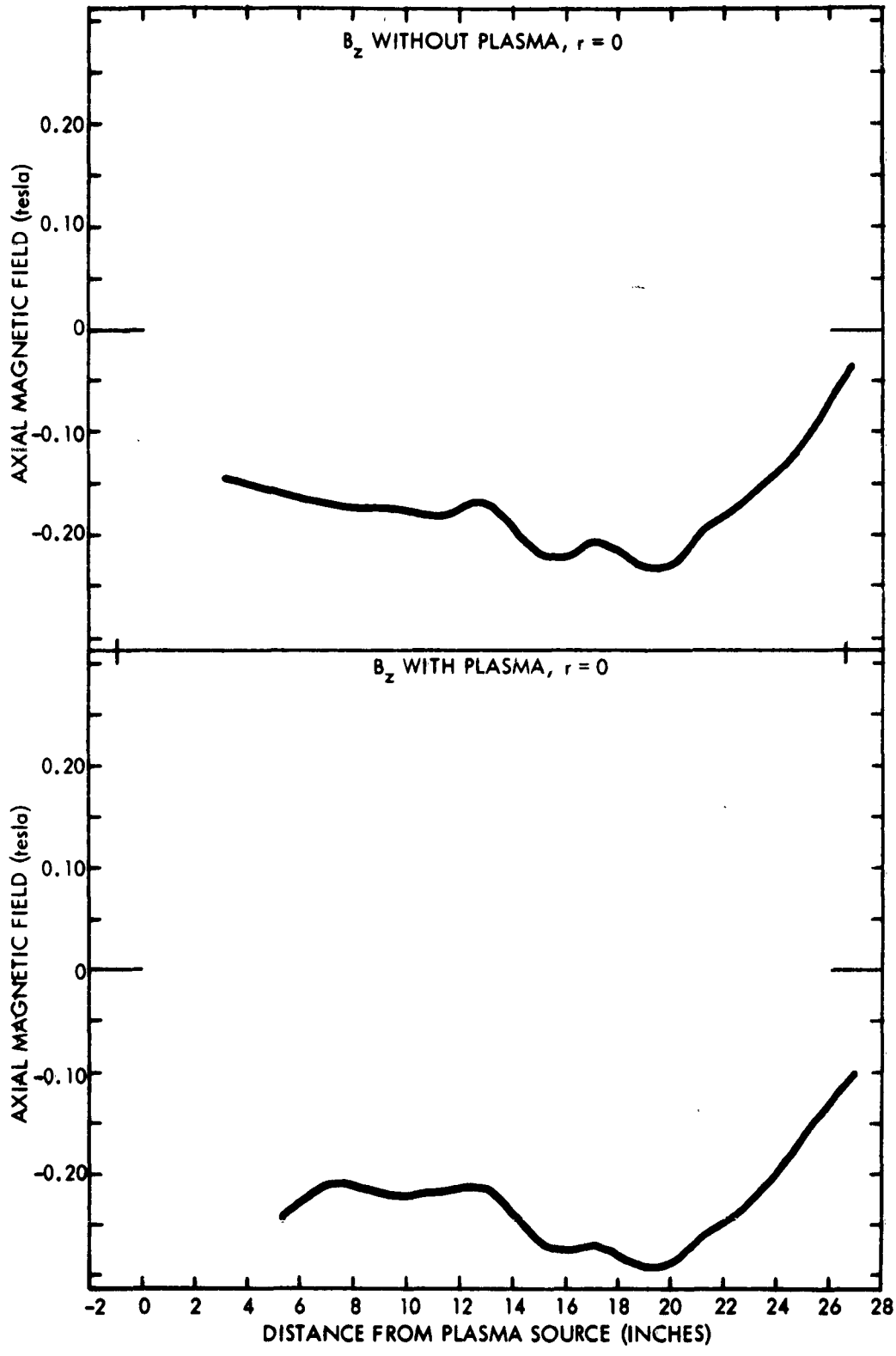

FIGURE B-9

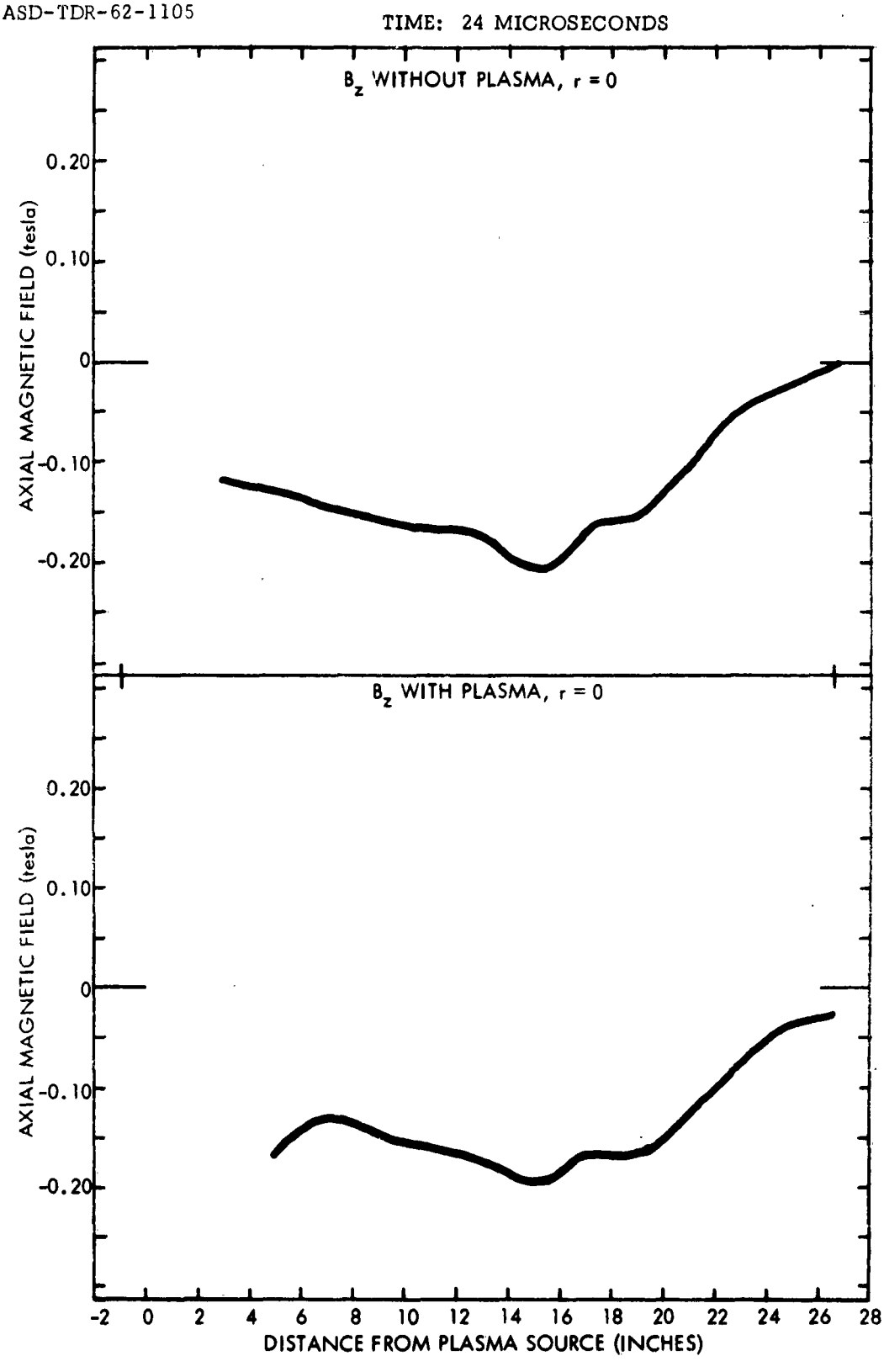
TIME: 24 MICROSECONDS
B_z WITHOUT PLASMA, r = 0
AXIAL MAGNETIC FIELD (tesla)
0.20
0.10
0
-0.10
-0.20
B_z WITH PLASMA, r = 0
AXIAL MAGNETIC FIELD (tesla)
0.20
0.10
0
-0.10
-0.20
-2 0 2 4 6 8 10 12 14 16 18 20 22 24 26 28
DISTANCE FROM PLASMA SOURCE (INCHES)

FIGURE B-10

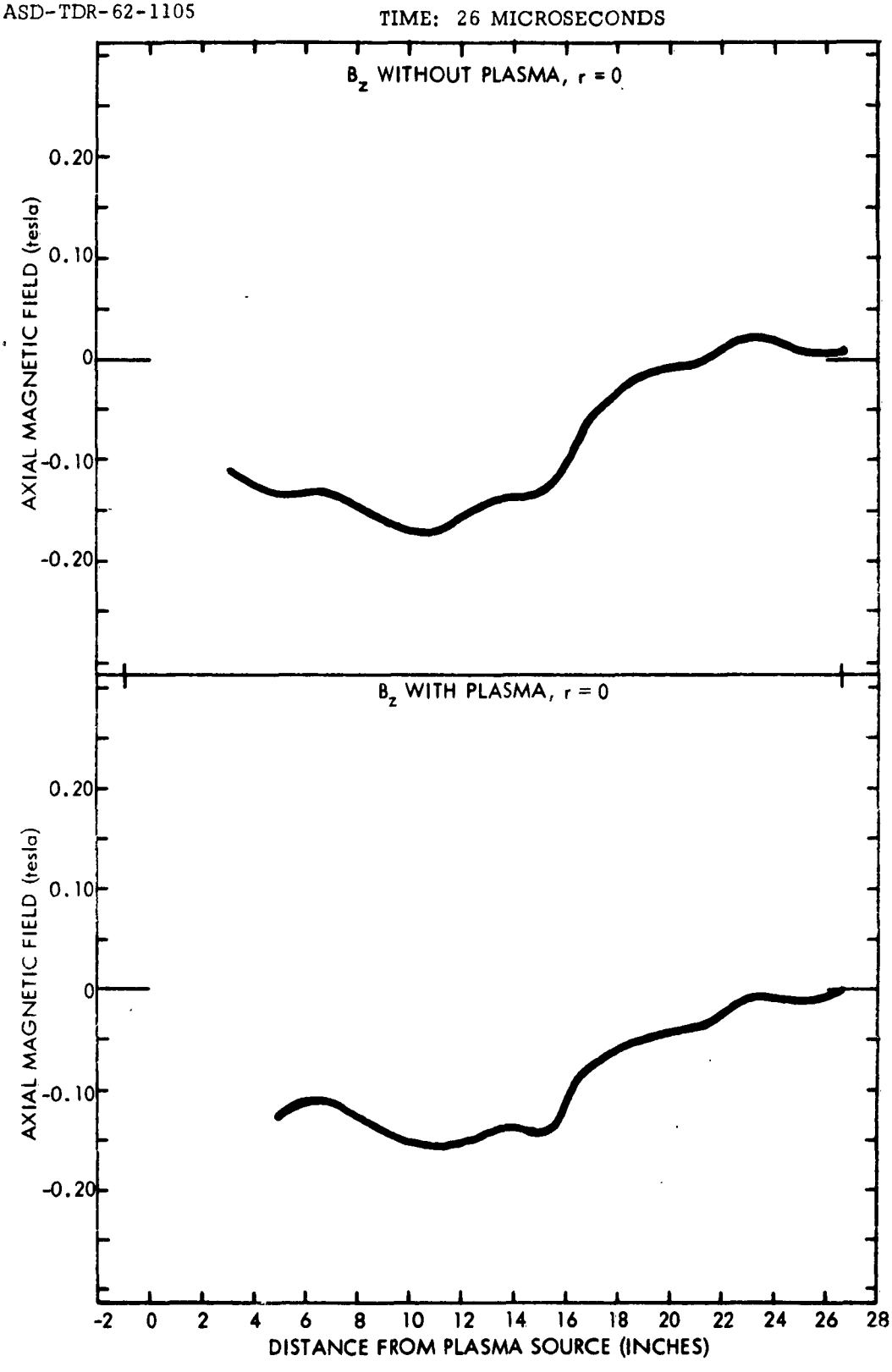
TIME: 26 MICROSECONDS
B_z WITHOUT PLASMA, r = 0
AXIAL MAGNETIC FIELD (tesla)
0.20
0.10
0
-0.10
-0.20
B_z WITH PLASMA, r = 0
AXIAL MAGNETIC FIELD (tesla)
0.20
0.10
0
-0.10
-0.20
-2 0 2 4 6 8 10 12 14 16 18 20 22 24 26 28
DISTANCE FROM PLASMA SOURCE (INCHES)

FIGURE B-11

TIME: 28 MICROSECONDS

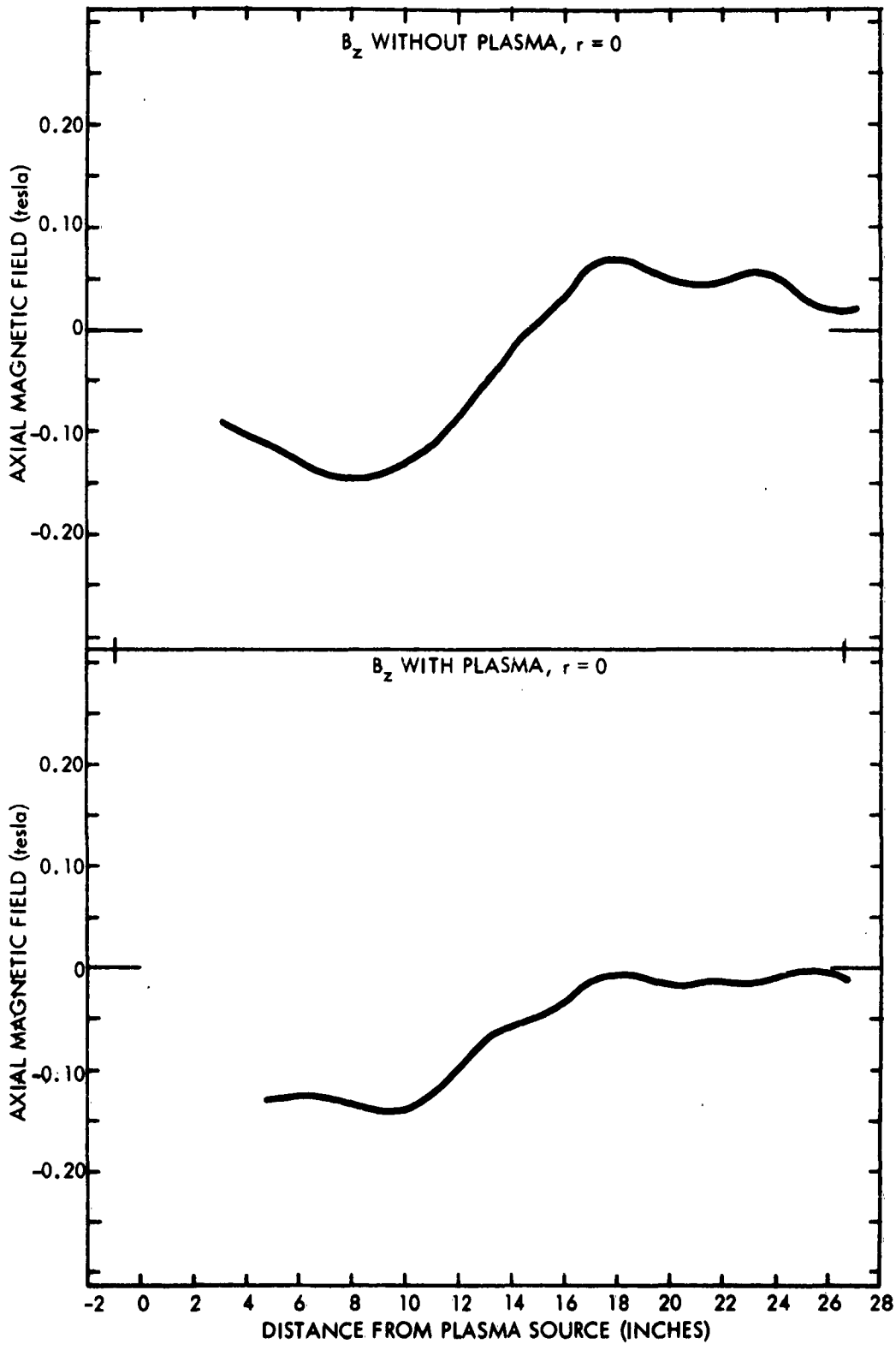

FIGURE B-12

TIME: 30 MICROSECONDS

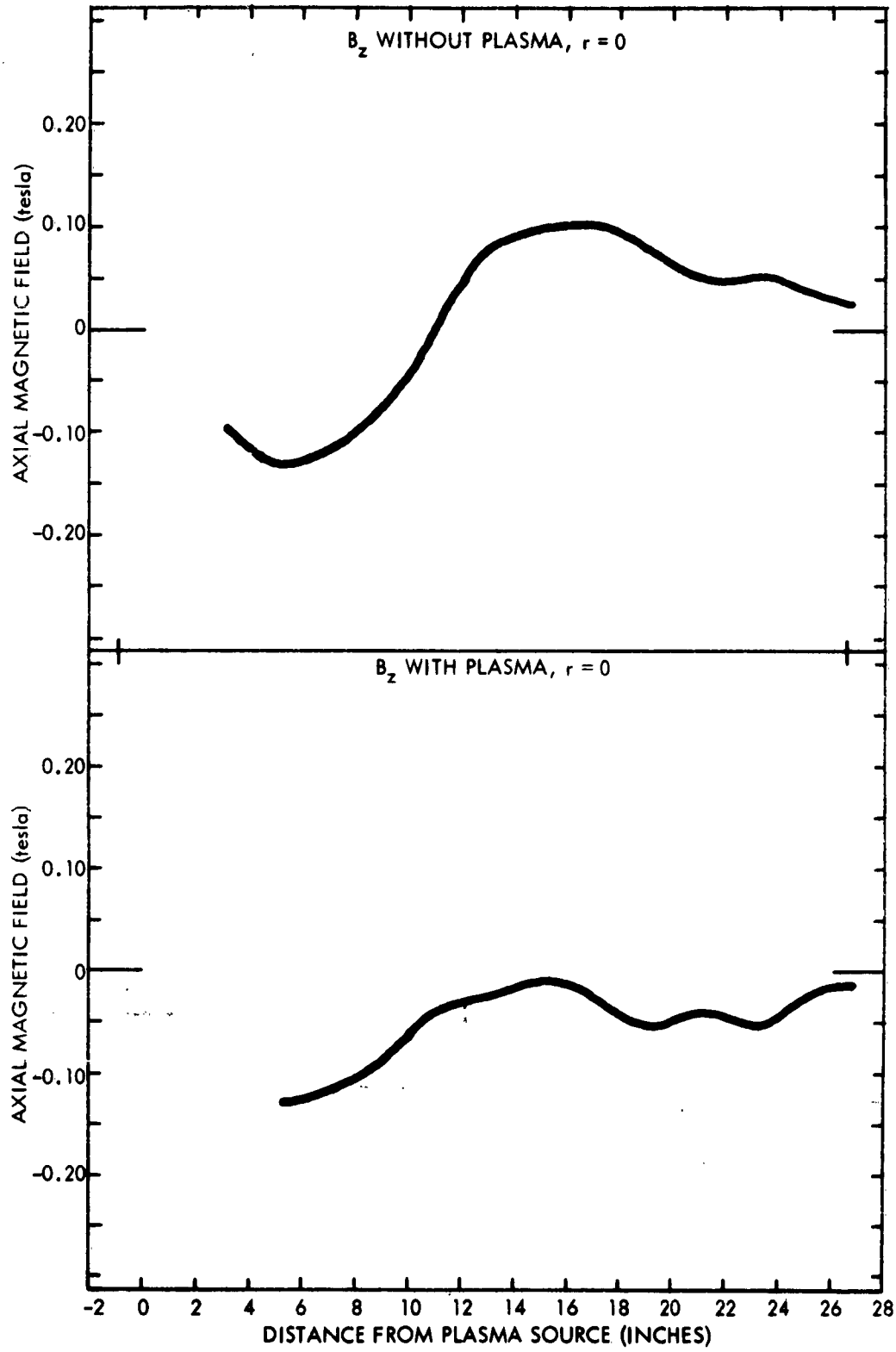

FIGURE B-13

TIME: 32 MICROSECONDS

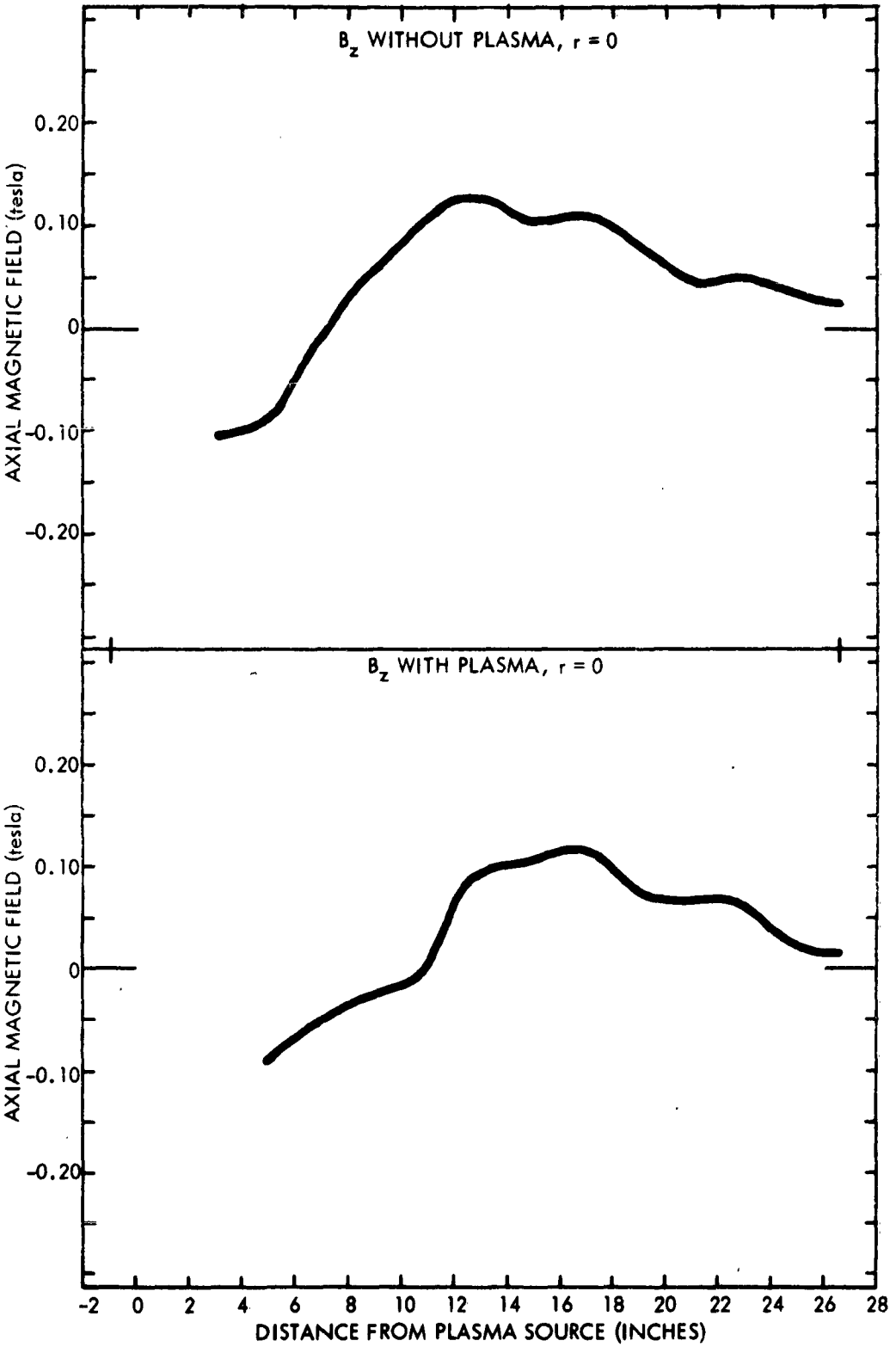

FIGURE B-14

TIME: 34 MICROSECONDS

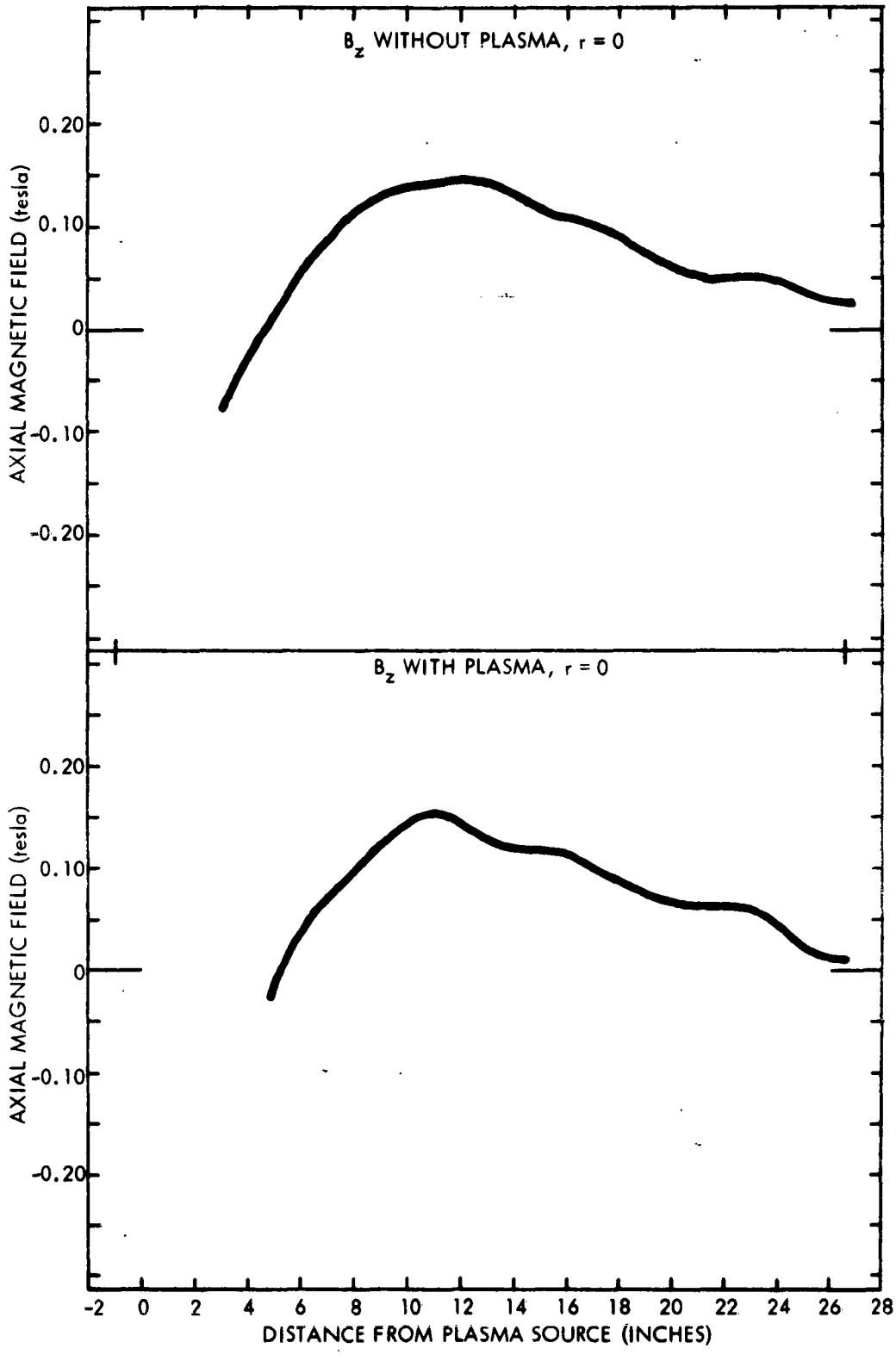

FIGURE B-15

TIME: 36 MICROSECONDS

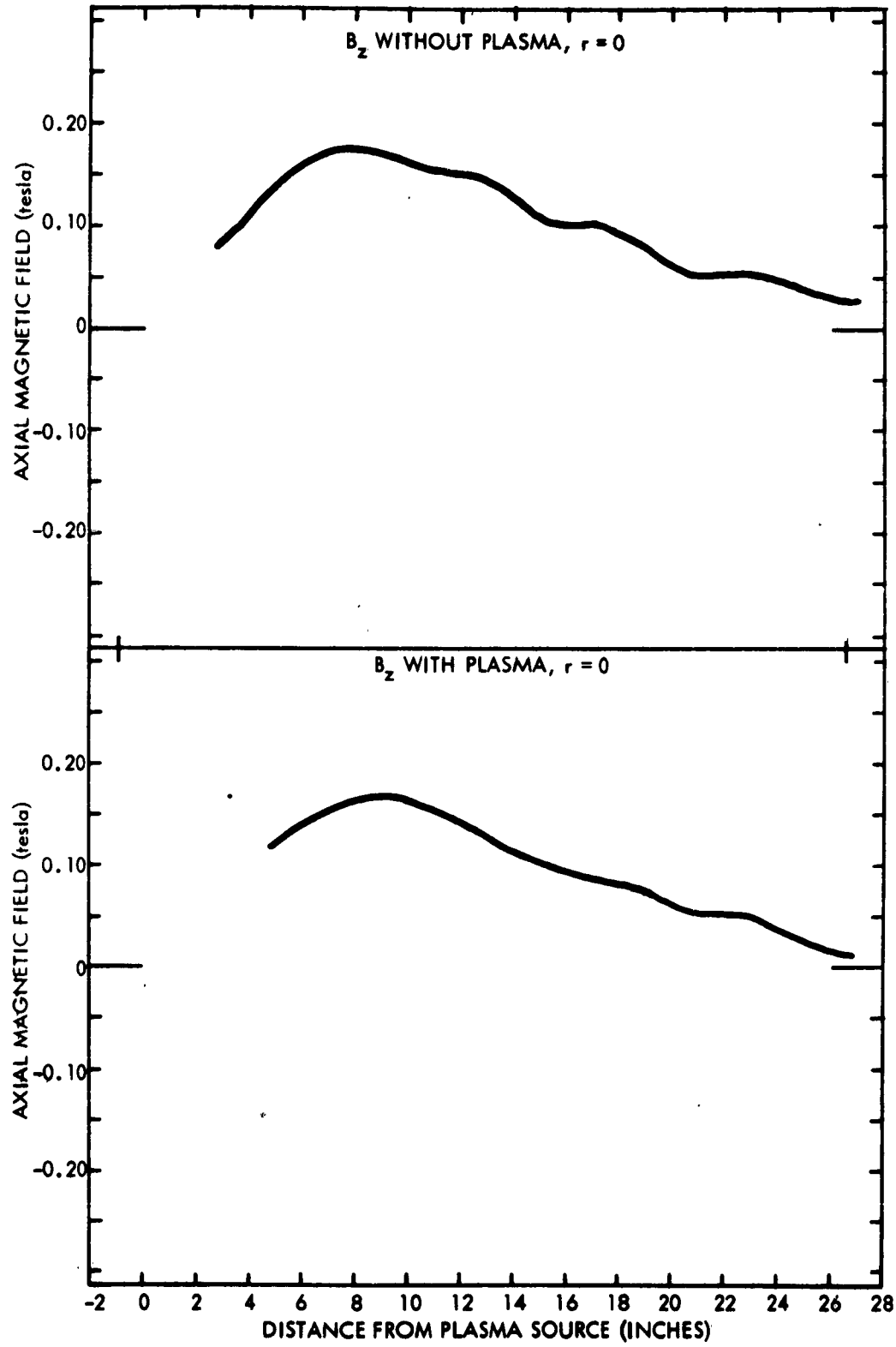

FIGURE B-16

RADIAL MAGNETIC FIELD DISTRIBUTIONS

(Figures B-17 through B-32)

Upper Curve: B_r, radial component of the magnetic field, 2 cm from the axis of the transmission line in the absence of plasma. Obtained from the integrated signal of an induction probe at two-inch intervals in the line. The abscissa shows the distance from the plasma source, and the ordinate gives the magnetic induction. The line was energized by a 15 μf capacitor charged to 6 kV.

Lower Curve: B_r, as in the upper curve, except the plasma source (0.6 μf charged to 18 kV) was triggered simultaneously with the line.

TIME: 6 MICROSECONDS

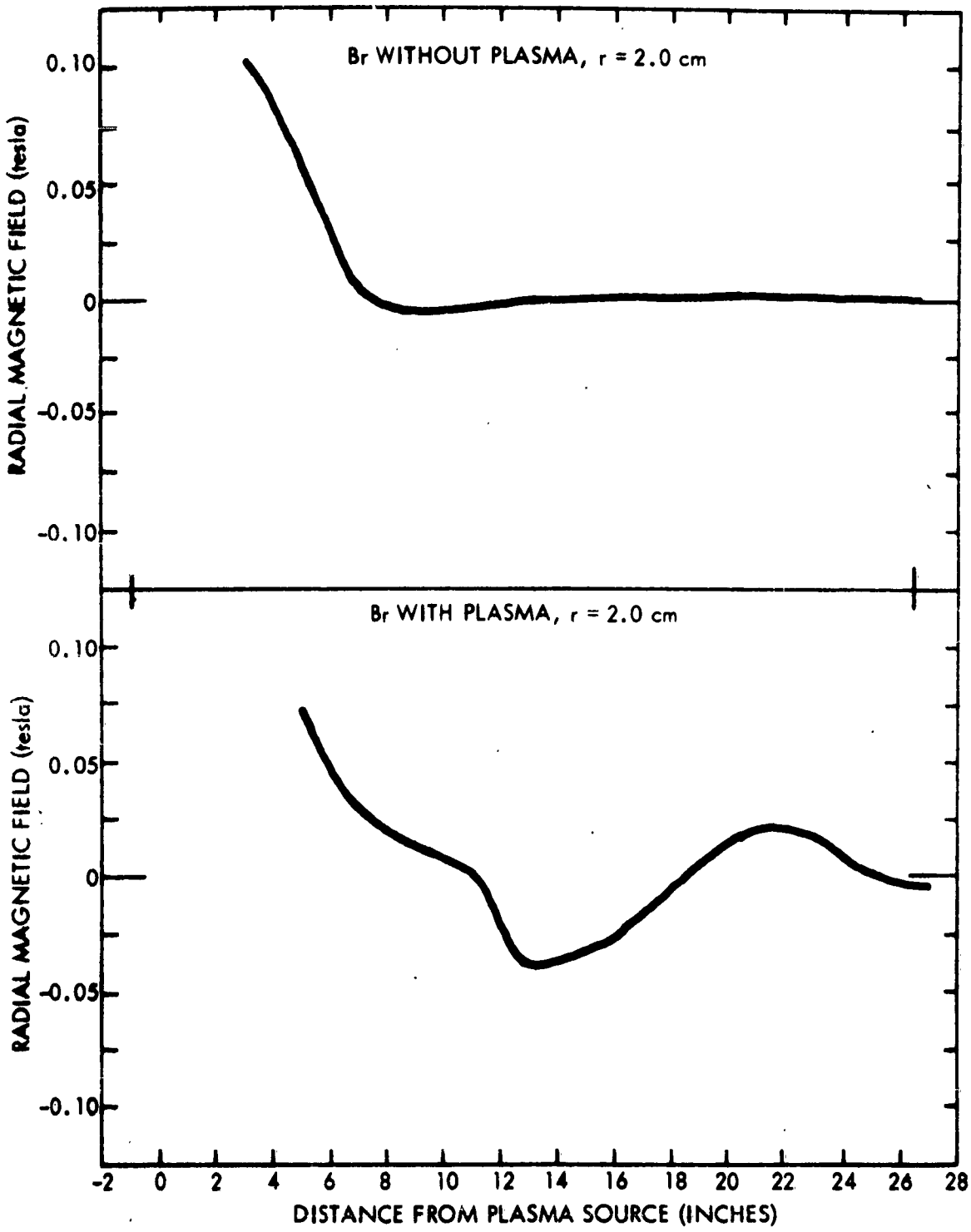

FIGURE B-17

TIME: 8 MICROSECONDS

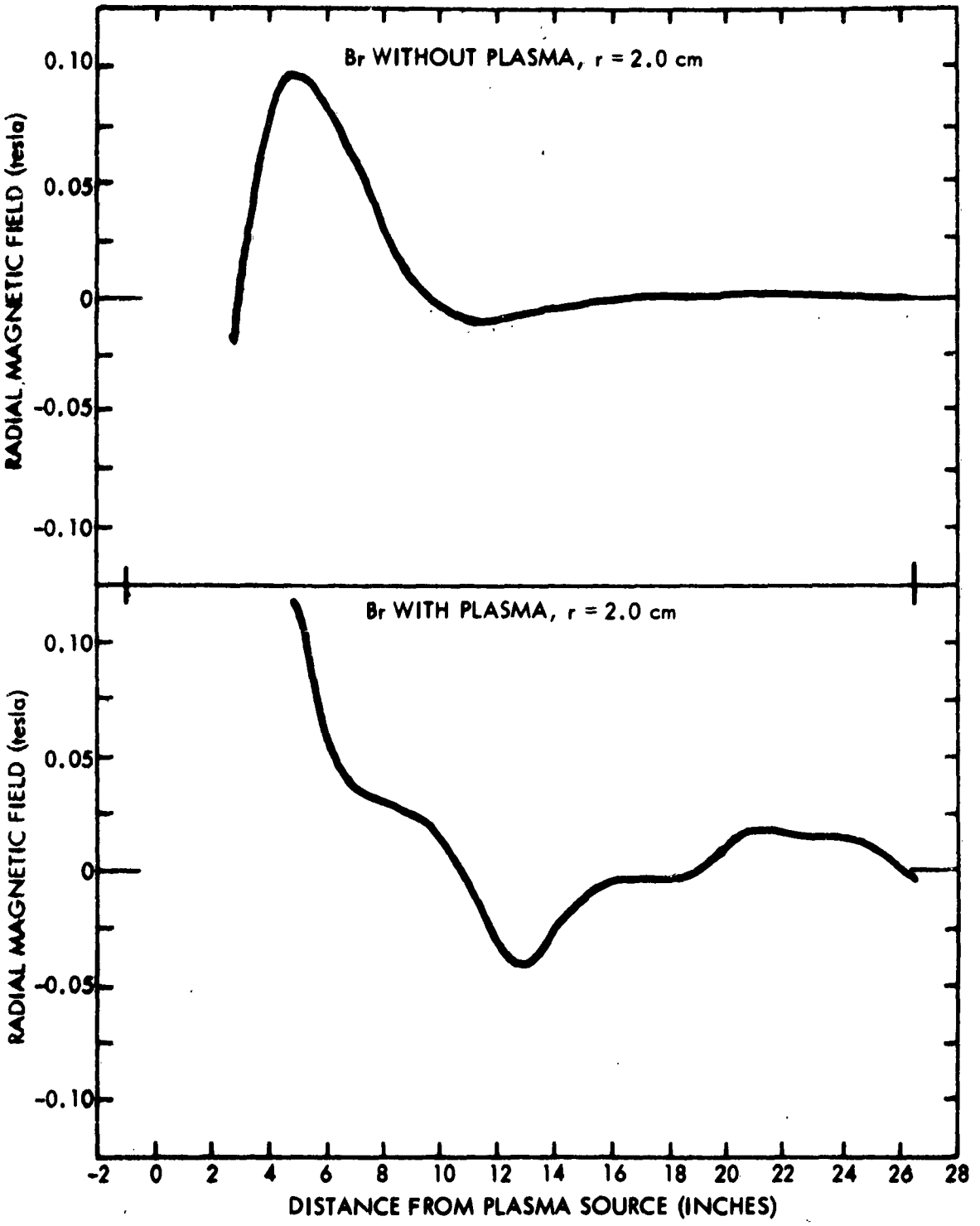

FIGURE B-18

TIME: 10 MICROSECONDS

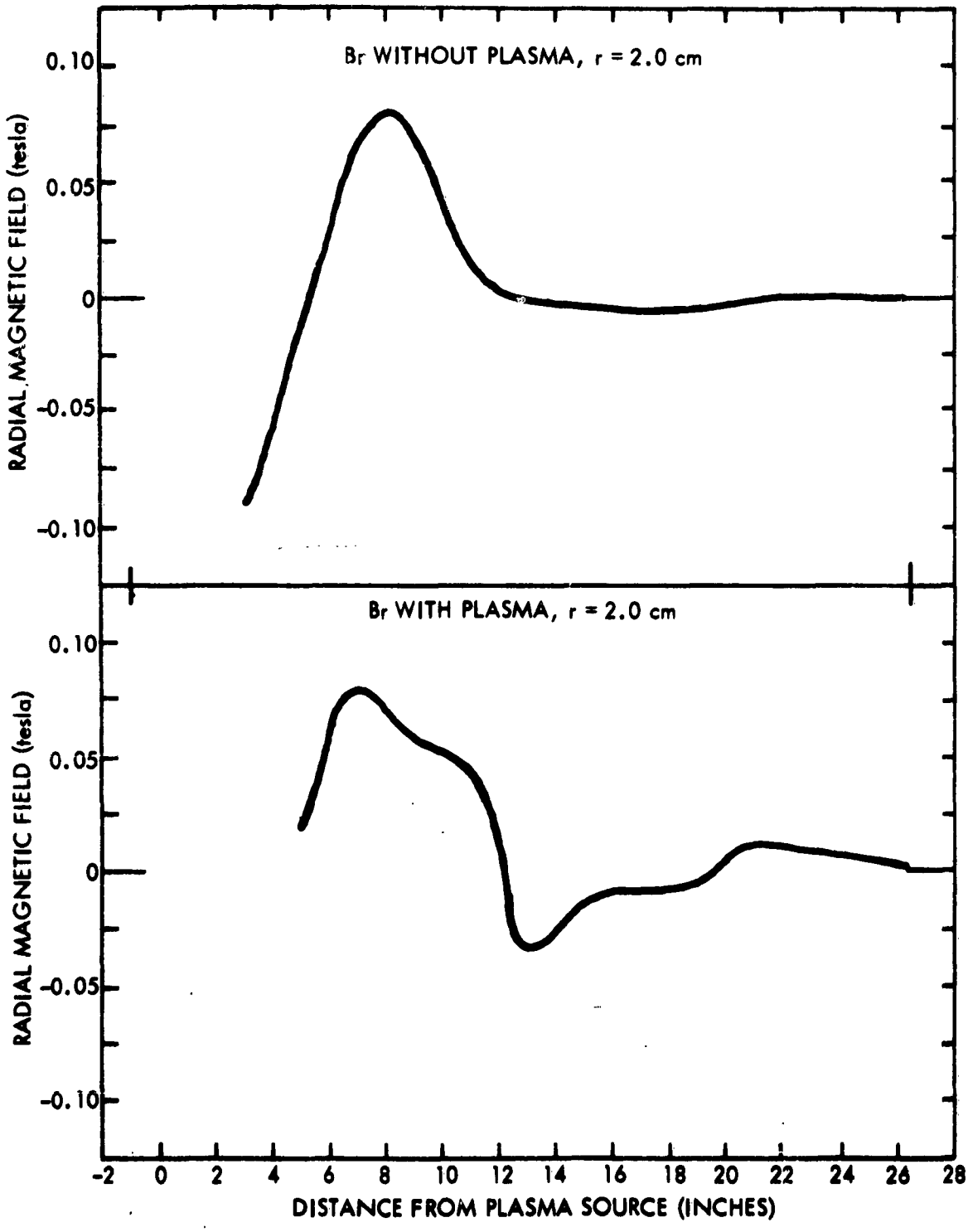

FIGURE B-19

TIME: 12 MICROSECONDS

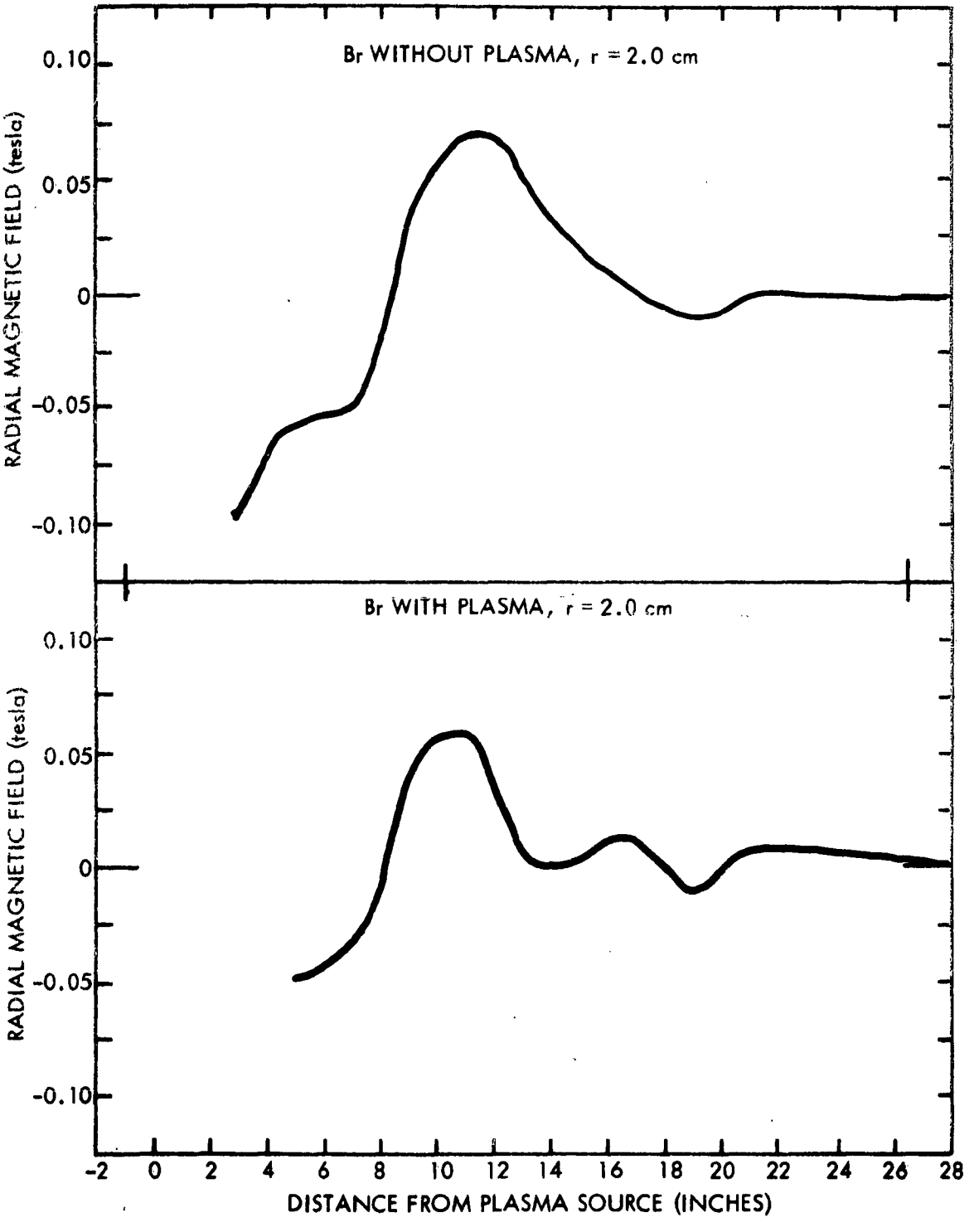

FIGURE B-20

TIME: 14 MICROSECONDS

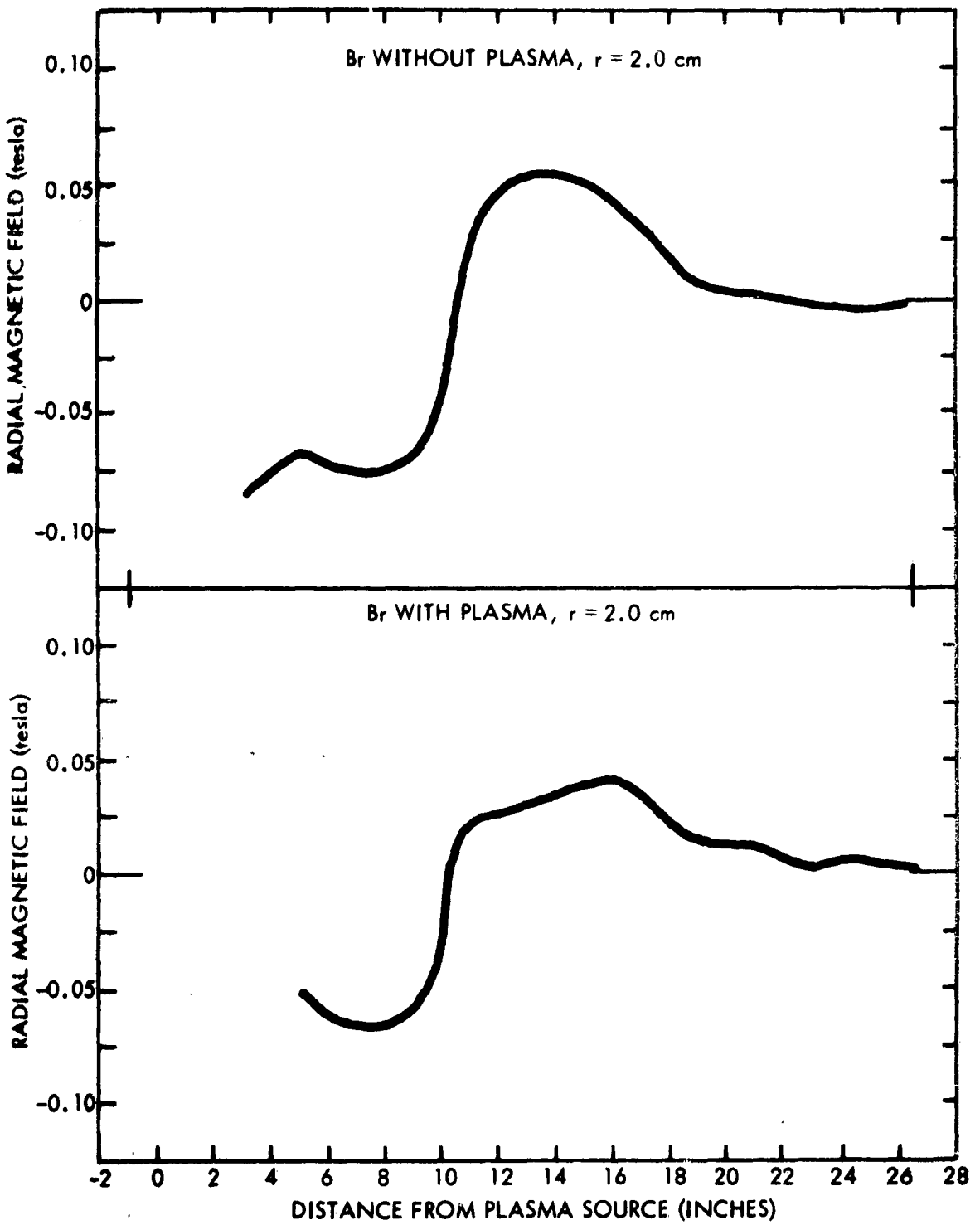

FIGURE B-21

TIME: 16 MICROSECONDS

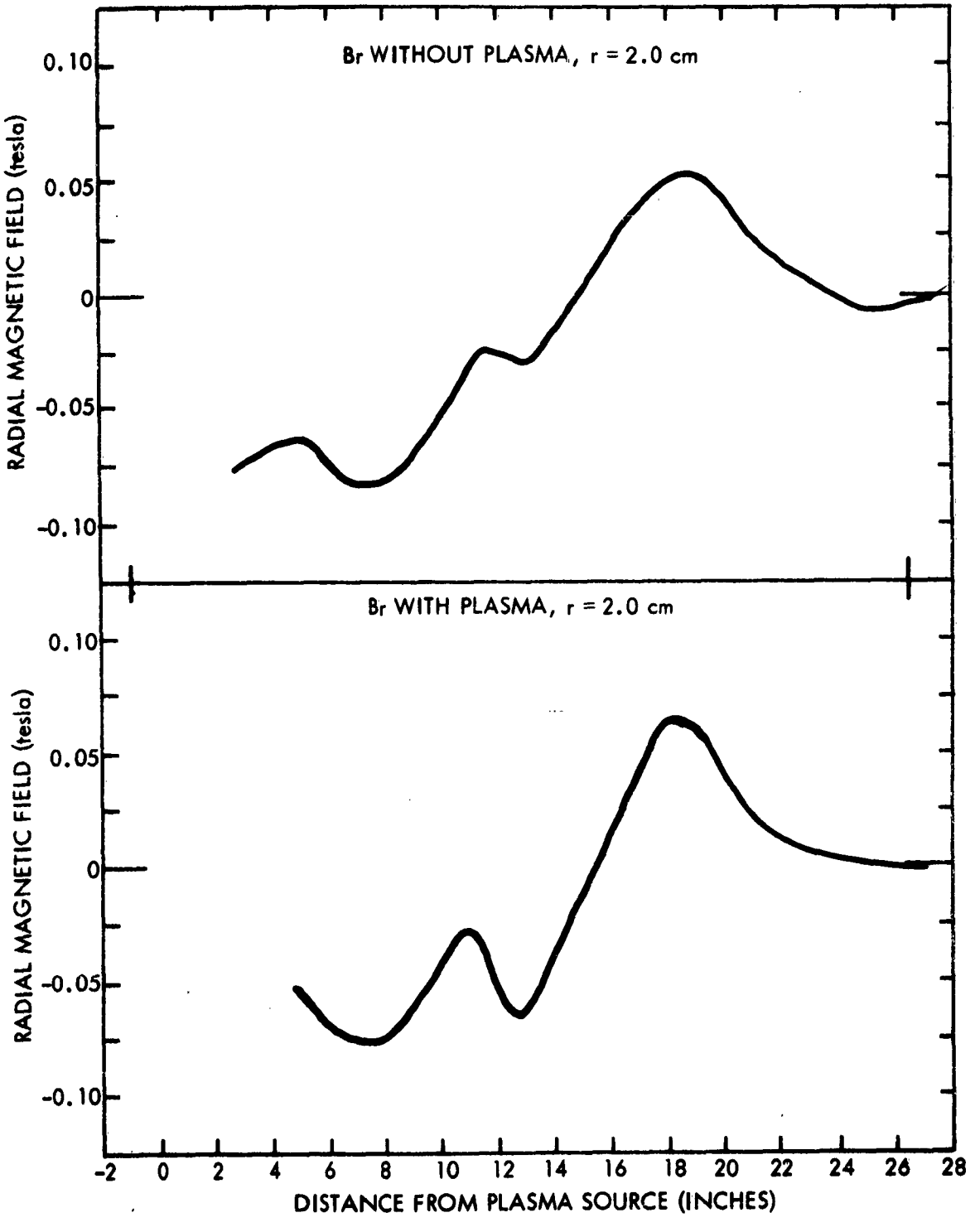

FIGURE B-22

TIME: 18 MICROSECONDS

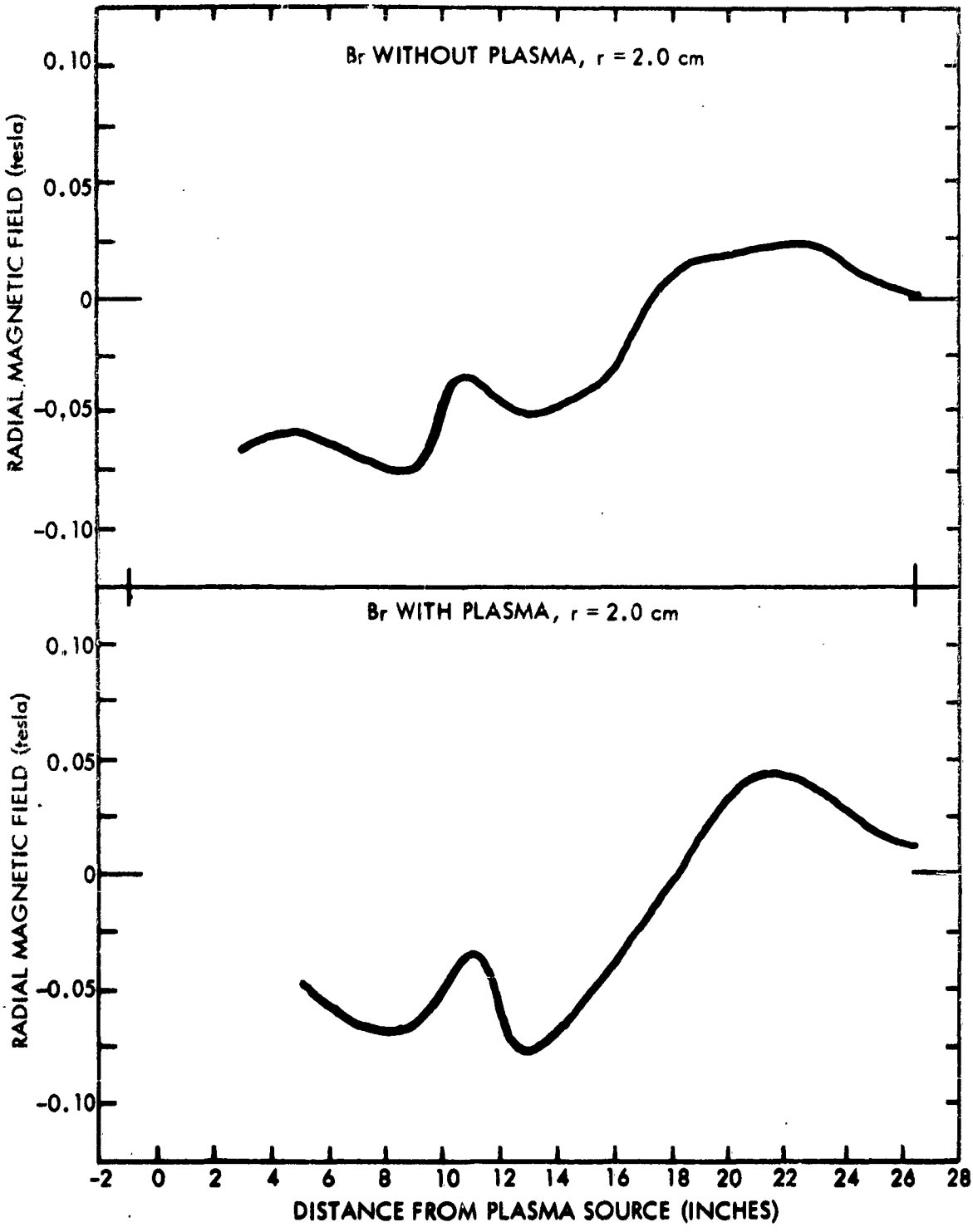

FIGURE B-23

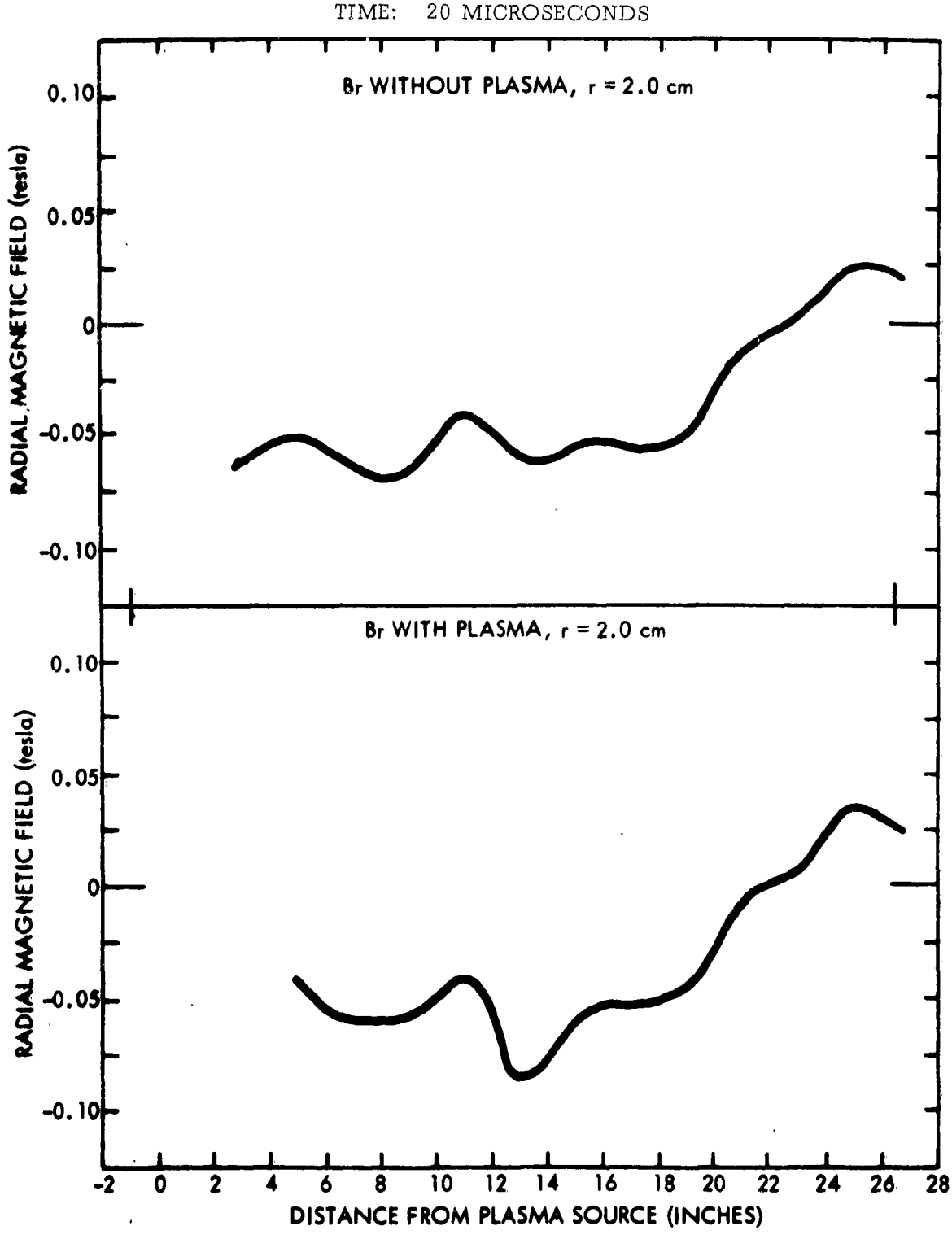
TIME: 20 MICROSECONDS
Br WITHOUT PLASMA, r = 2.0 cm
RADIAL MAGNETIC FIELD (tesla)
0.10
0.05
0
-0.05
-0.10
Br WITH PLASMA, r = 2.0 cm
RADIAL MAGNETIC FIELD (tesla)
0.10
0.05
0
-0.05
-0.10
-2 0 2 4 6 8 10 12 14 16 18 20 22 24 26 28
DISTANCE FROM PLASMA SOURCE (INCHES)

FIGURE B-24

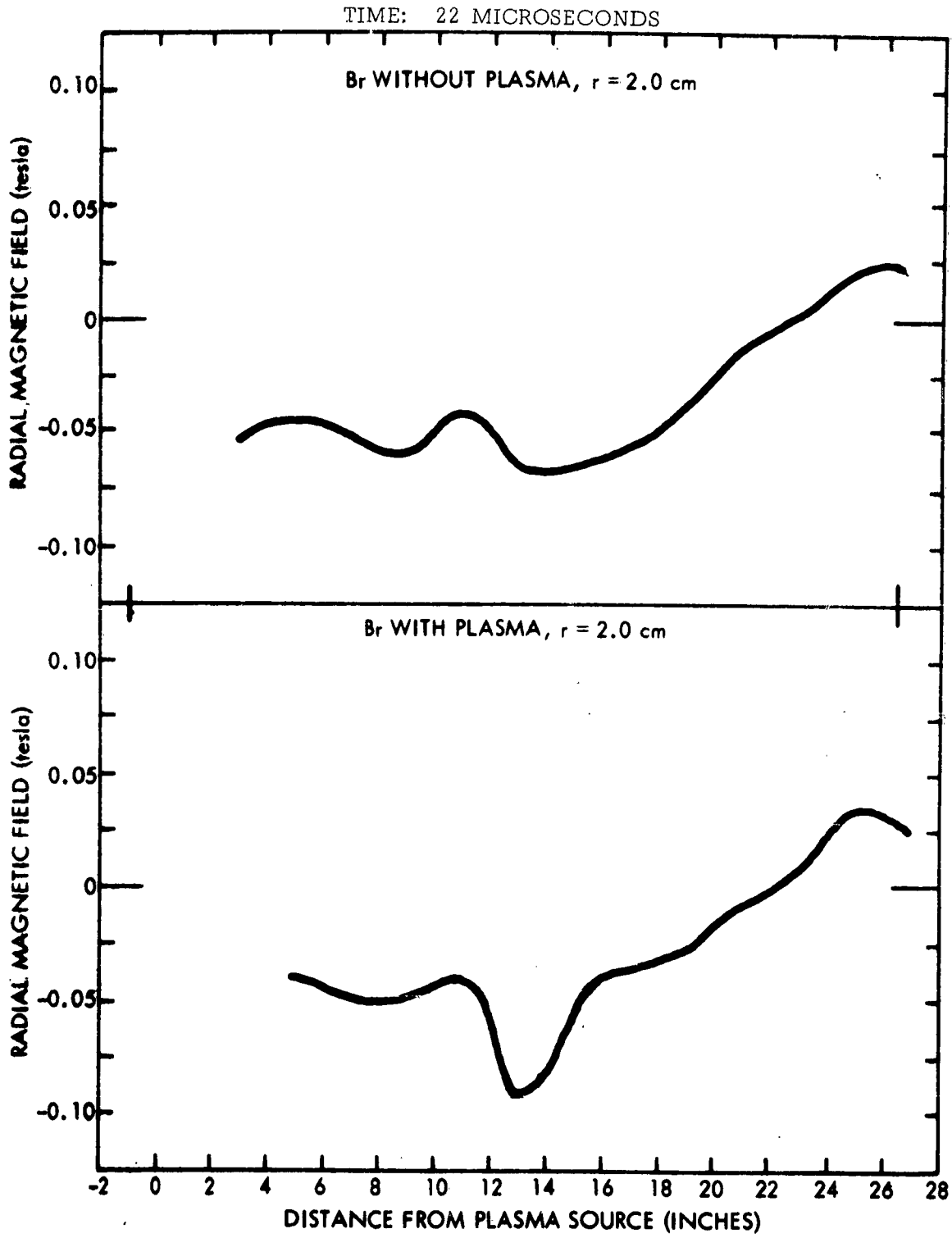
TIME: 22 MICROSECONDS
Br WITHOUT PLASMA, r = 2.0 cm
Br WITH PLASMA, r = 2.0 cm
RADIAL MAGNETIC FIELD (tesla)
0.10
0.05
0
-0.05
-0.10
-2
0
2
4
6
8
10
12
14
16
18
20
22
24
26
28
DISTANCE FROM PLASMA SOURCE (INCHES)

FIGURE B-25

TIME: 24 MICROSECONDS

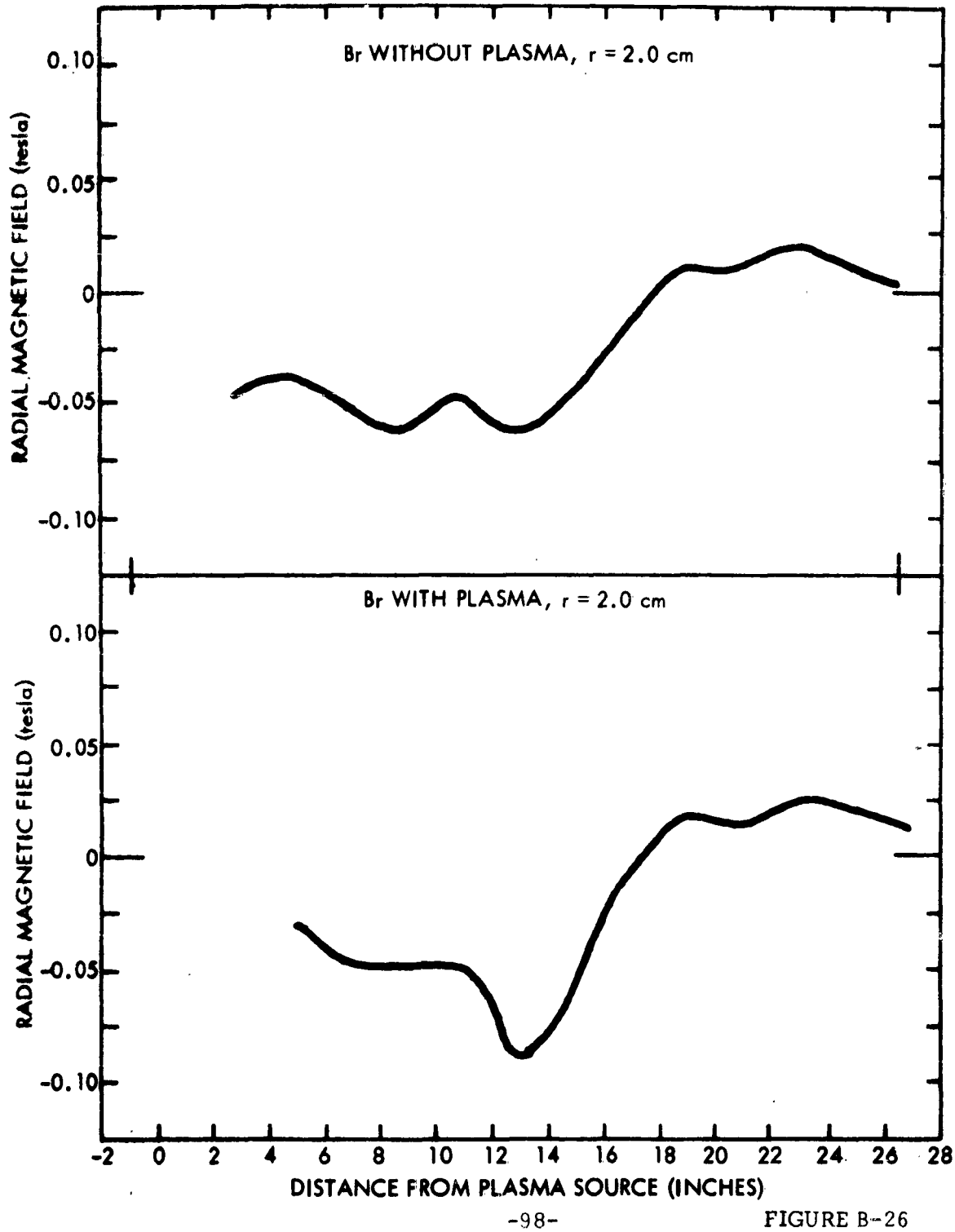

FIGURE B-26

TIME: 26 MICROSECONDS

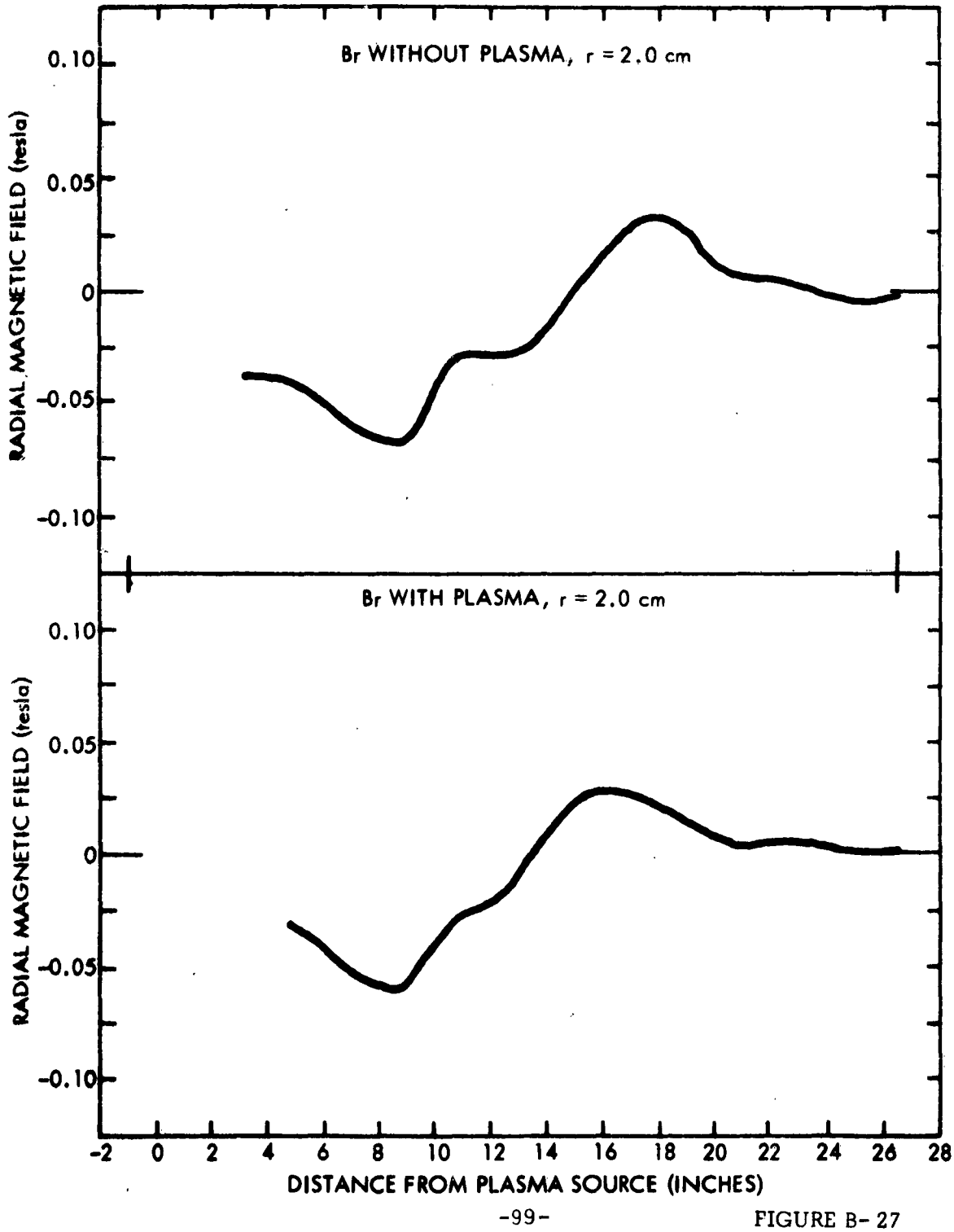

FIGURE B-27

TIME: 28 MICROSECONDS

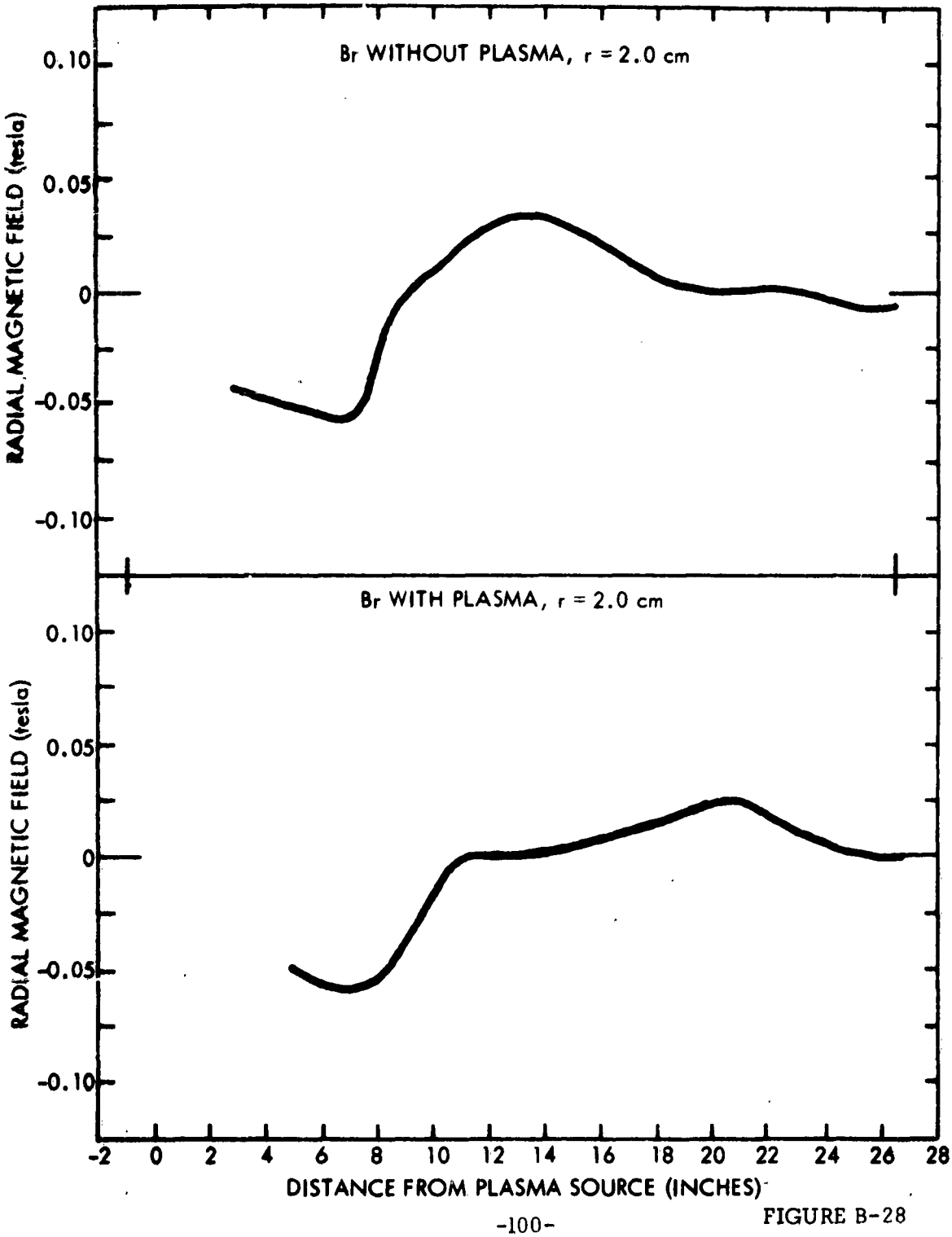

FIGURE B-28

TIME: 30 MICROSECONDS

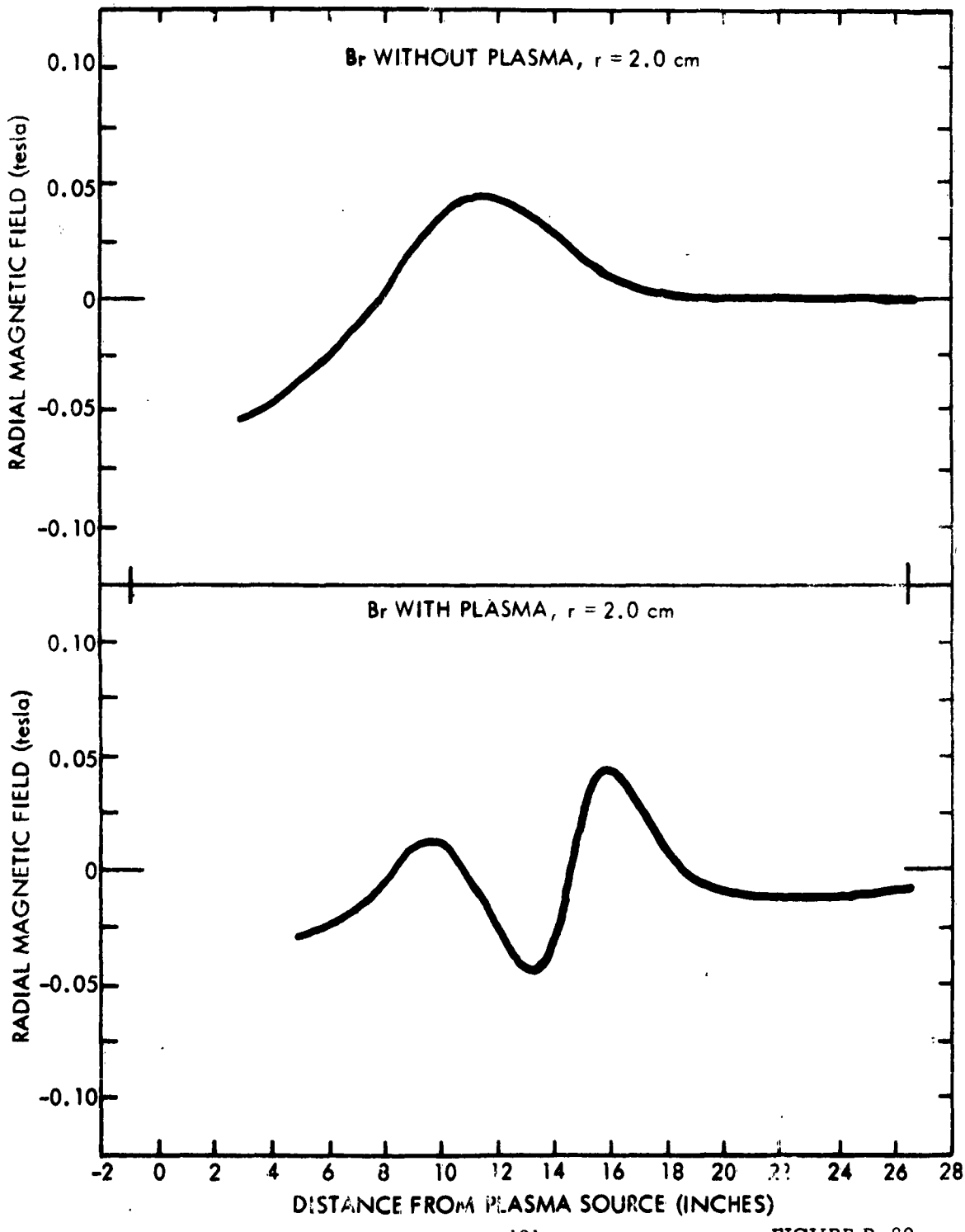

FIGURE B-29

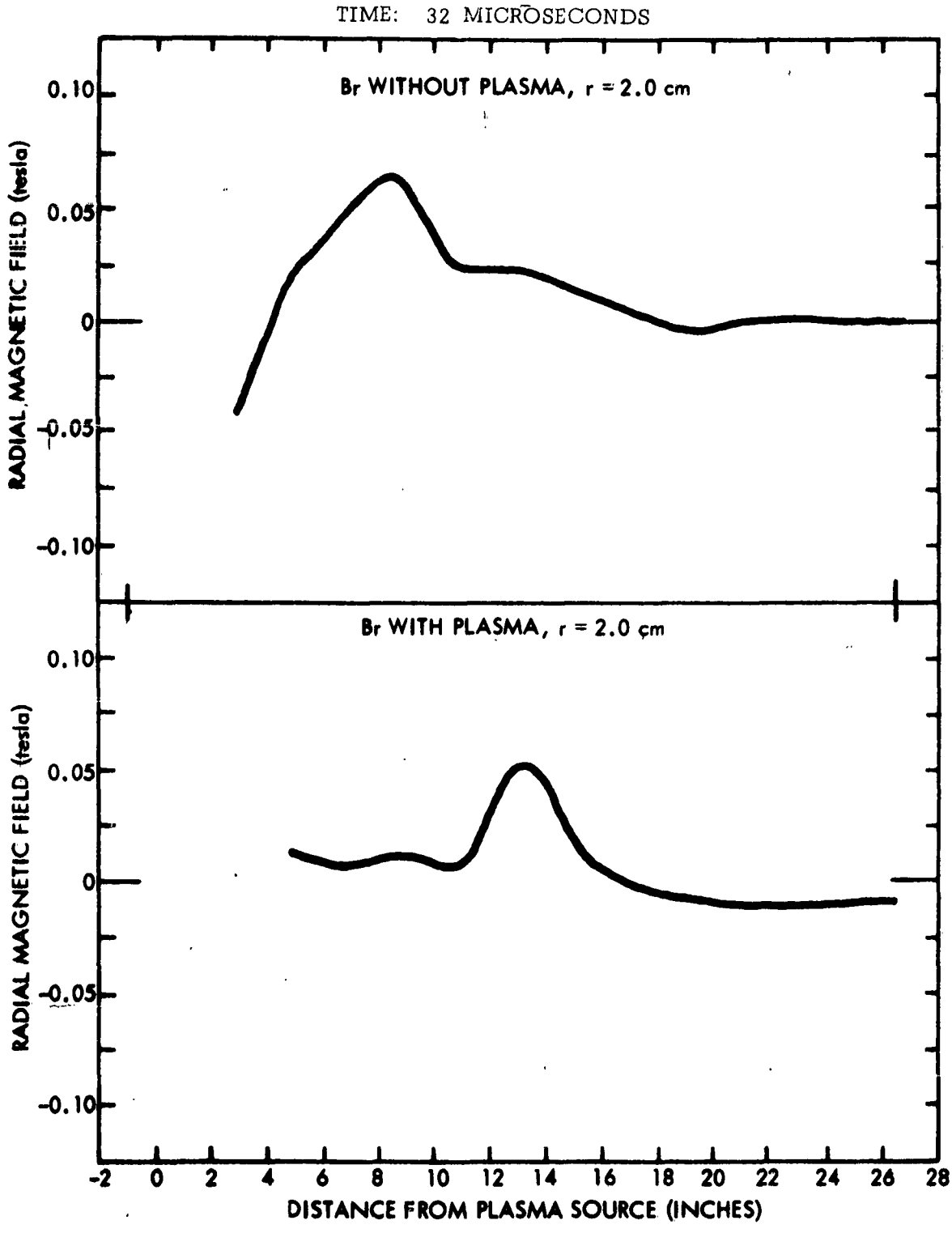
TIME: 32 MICROSECONDS
Br WITHOUT PLASMA, r = 2.0 cm
Br WITH PLASMA, r = 2.0 cm
RADIAL MAGNETIC FIELD (tesla)
0.10
0.05
0
-0.05
-0.10
-2
0
2
4
6
8
10
12
14
16
18
20
22
24
26
28
DISTANCE FROM PLASMA SOURCE (INCHES)

FIGURE B-30

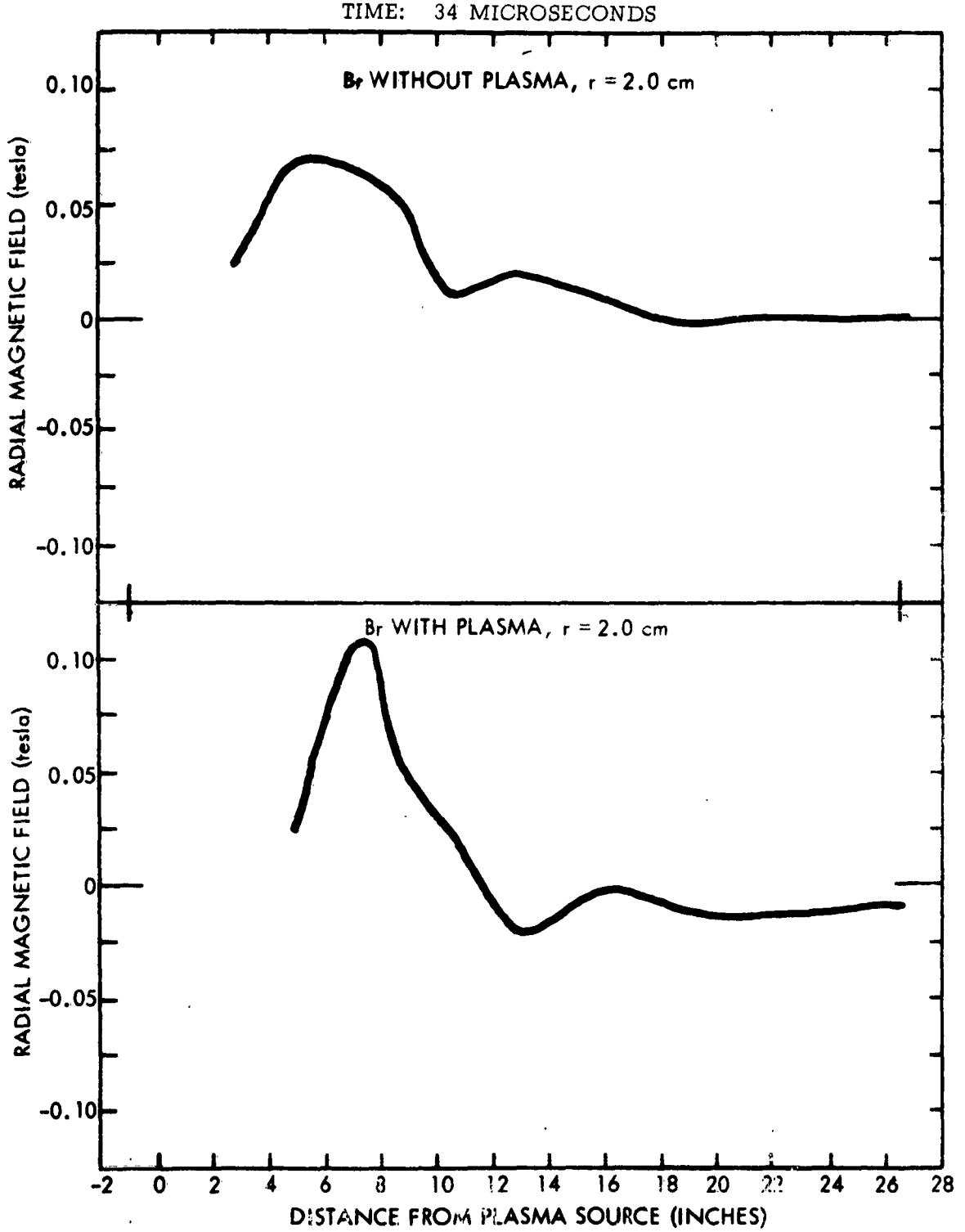
TIME: 34 MICROSECONDS
Br WITHOUT PLASMA, r = 2.0 cm
RADIAL MAGNETIC FIELD (tesla)
0.10
0.05
0
-0.05
-0.10
Br WITH PLASMA, r = 2.0 cm
RADIAL MAGNETIC FIELD (tesla)
0.10
0.05
0
-0.05
-0.10
-2 0 2 4 6 8 10 12 14 16 18 20 22 24 26 28
DISTANCE FROM PLASMA SOURCE (INCHES)

FIGURE B-31

TIME: 36 MICROSECONDS

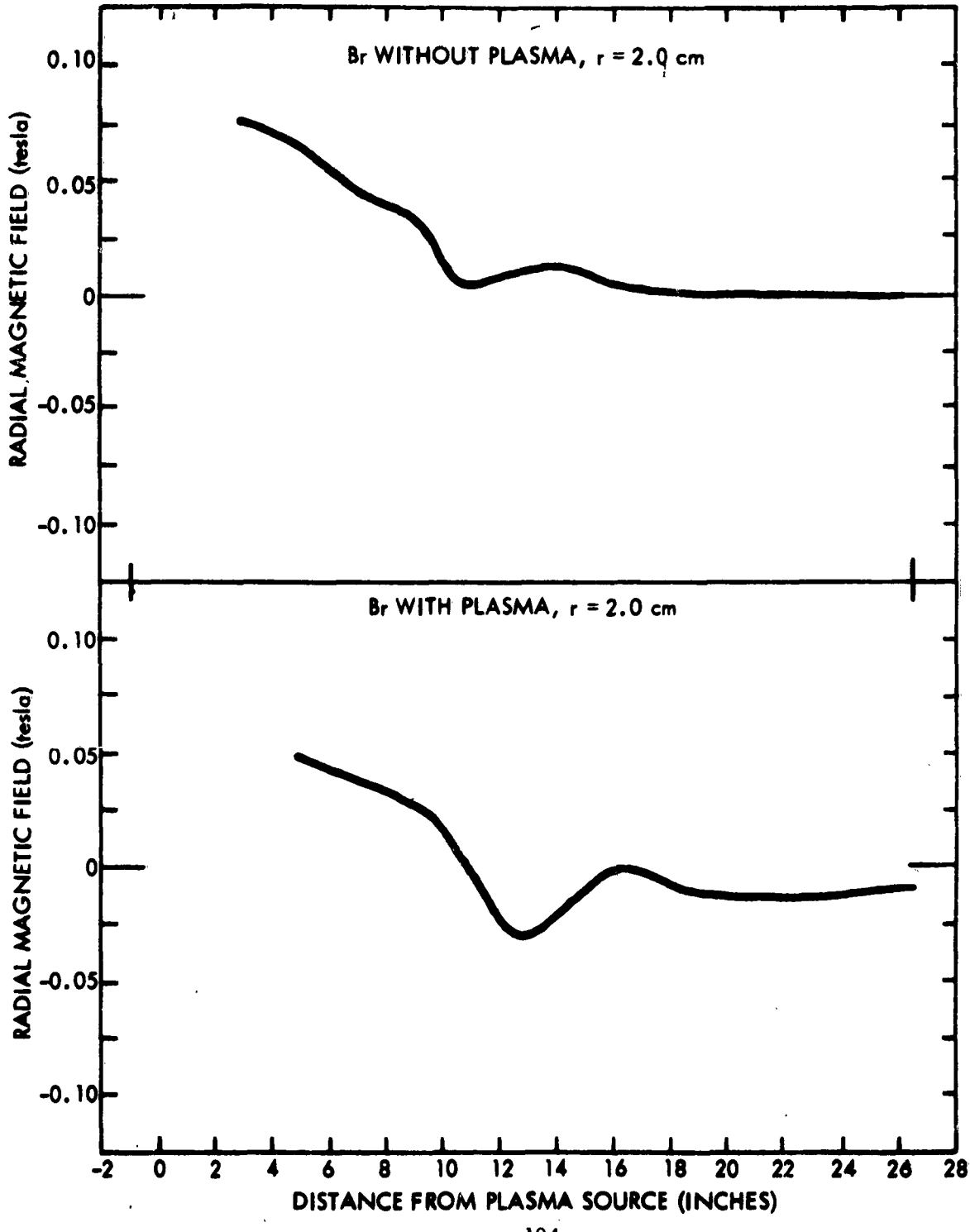

FIGURE B-32

AZIMUTHAL MAGNETIC FIELD DISTRIBUTIONS

(Figures B-33 through B-44)

Upper Curve: B_θ, azimuthal component of the magnetic field, 2 cm from the axis of the transmission line in the absence of plasma. Obtained from the integrated signal of an induction probe at two-inch intervals in the line. The abscissa shows the distance from the plasma source, and the ordinate gives the magnetic induction. The line was energized by a 15 μf capacitor charged to 6 kV.

Lower Curve: B_θ, as in the upper curve, except the plasma source (0.6 μf charged to 18 kV) was triggered simultaneously with the line.

TIME: 14 MICROSECONDS

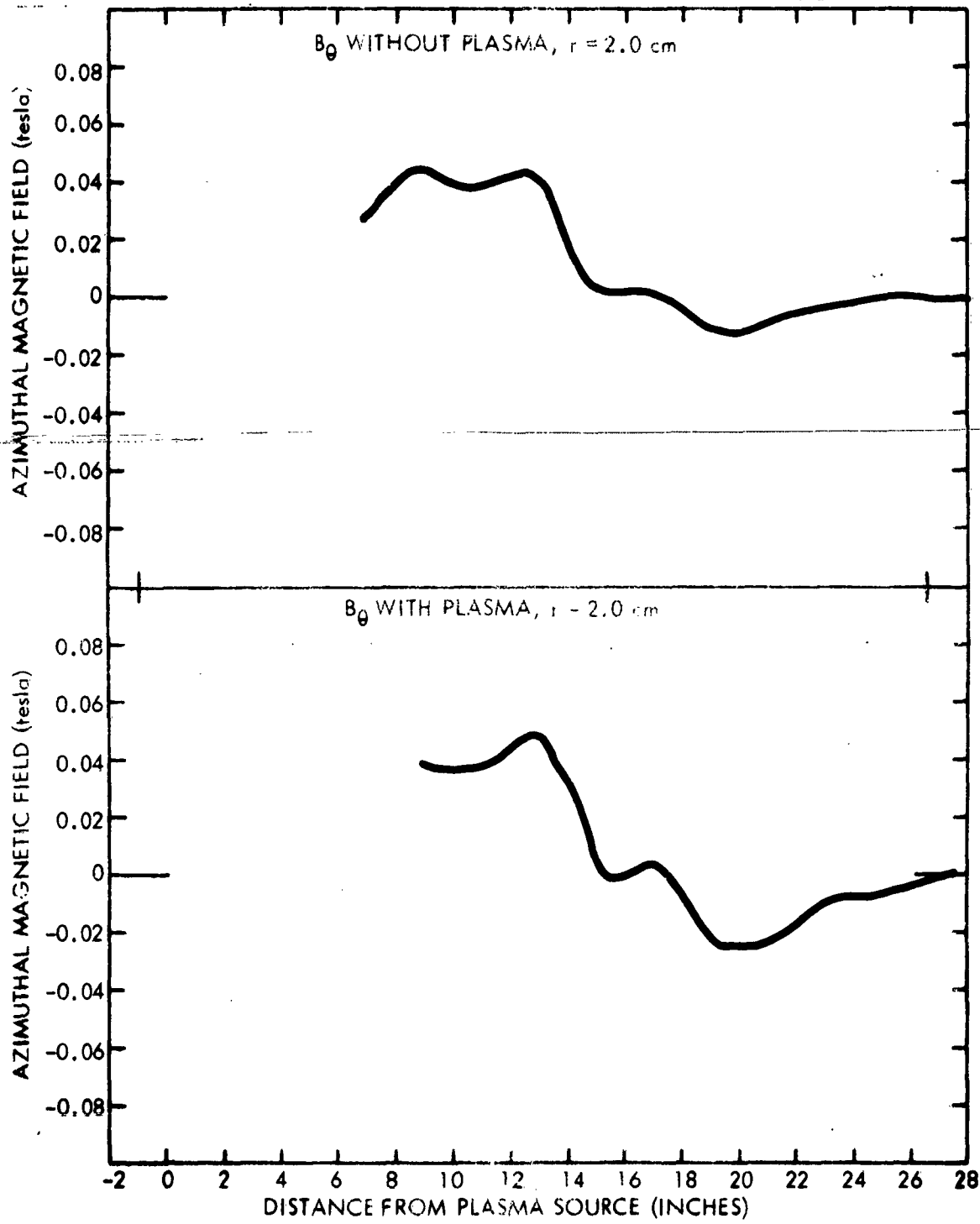

FIGURE B-33

TIME: 16 MICROSECONDS

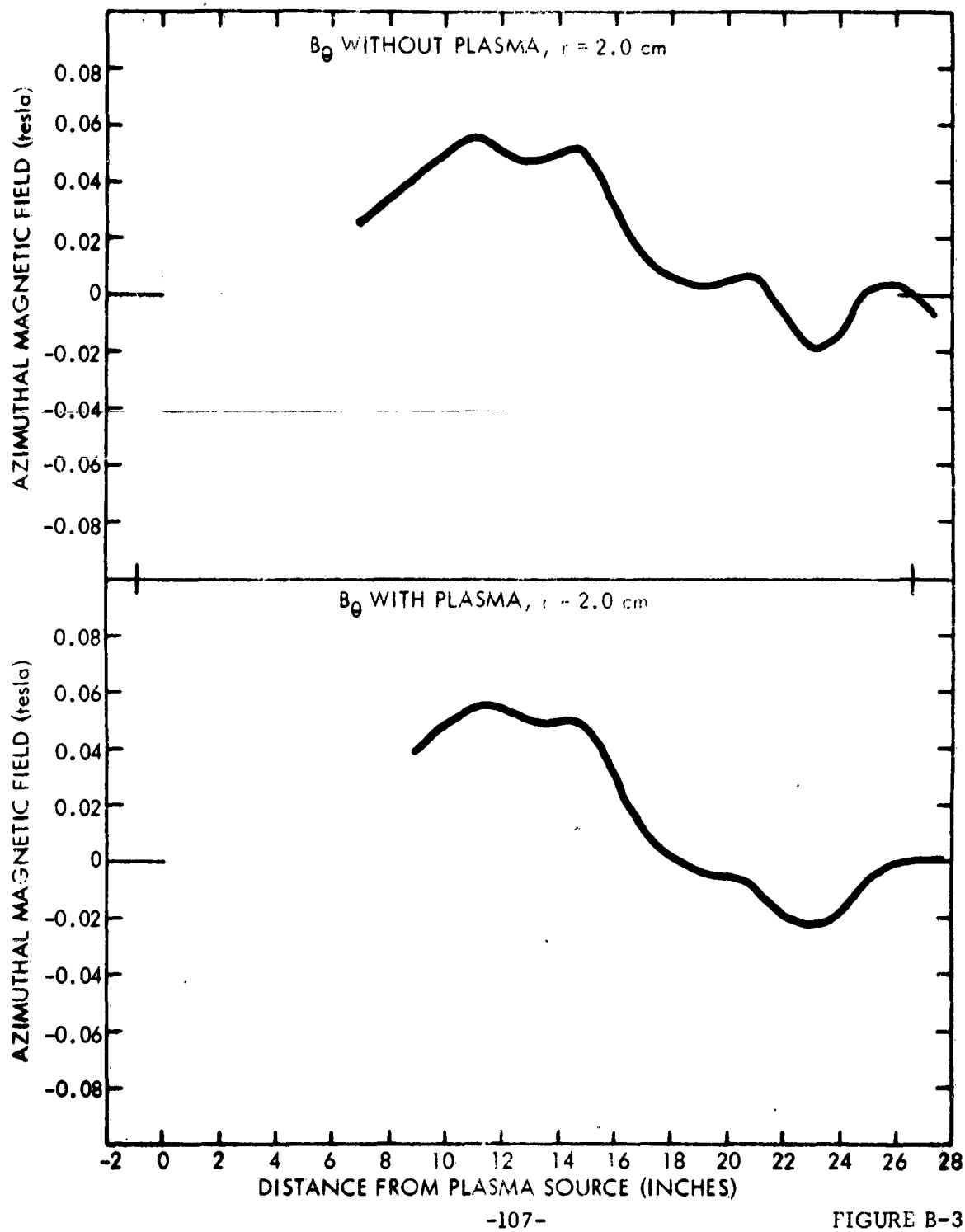

FIGURE B-34

TIME: 18 MICROSECONDS

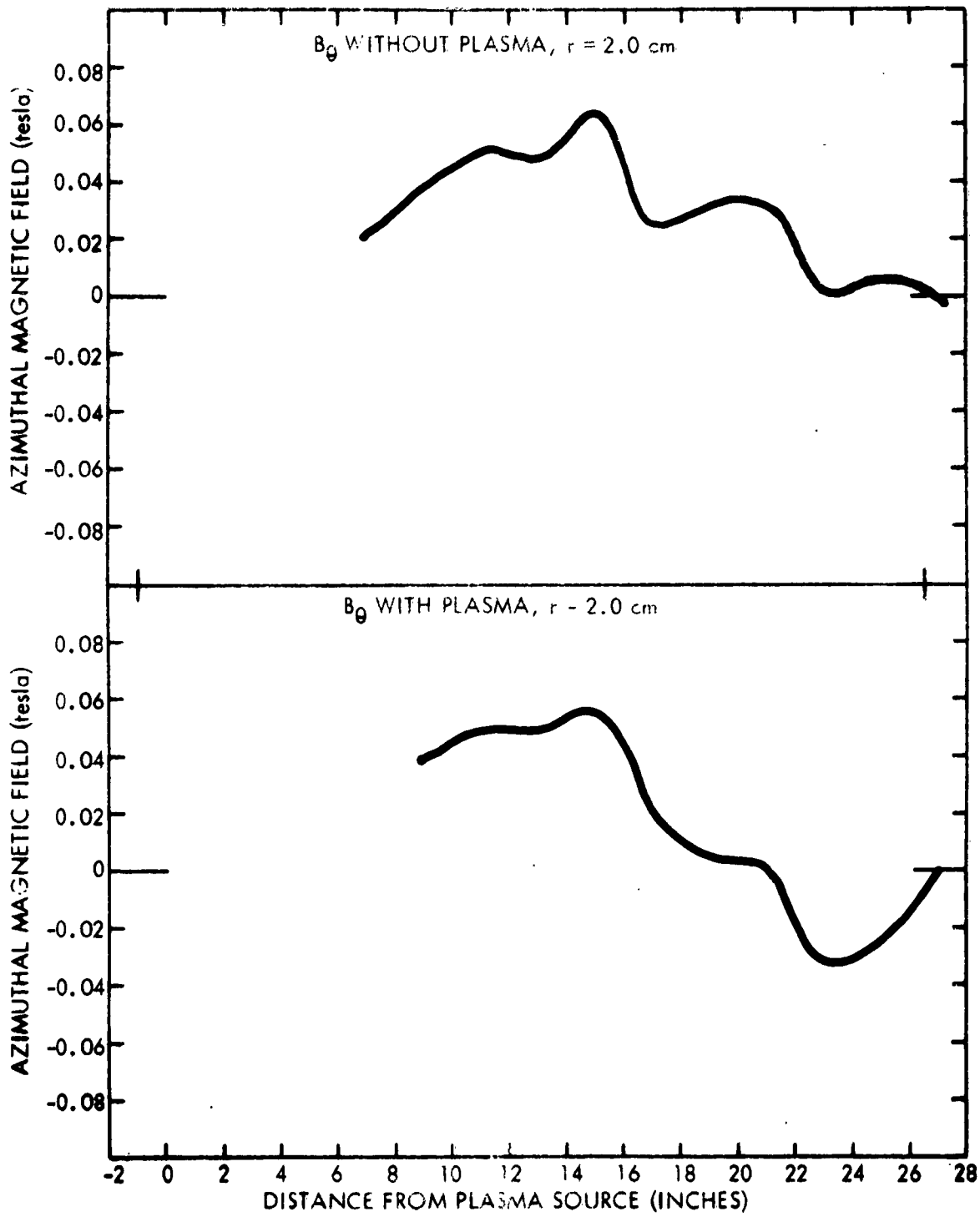

FIGURE B-35

TIME: 20 MICROSECONDS

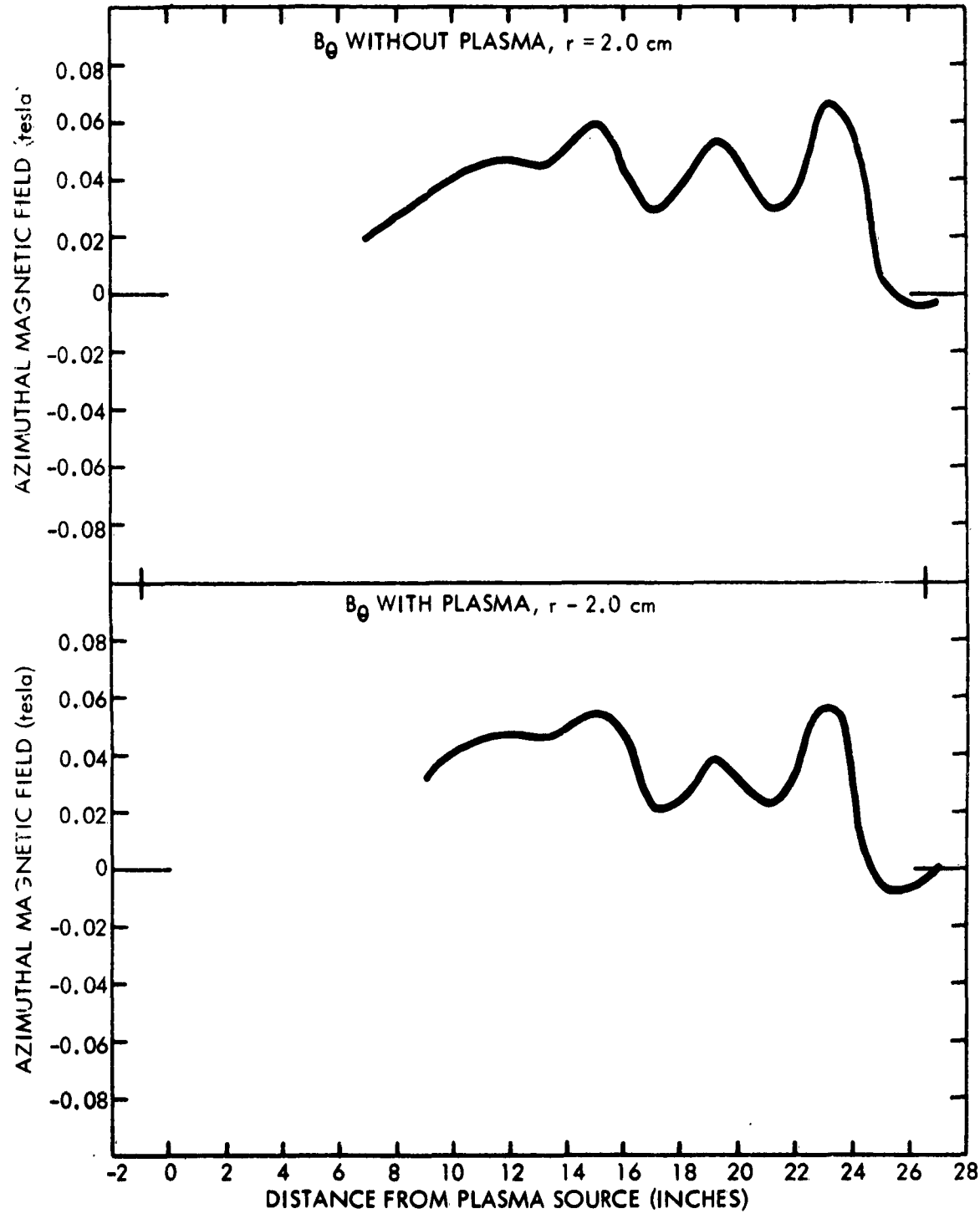

FIGURE B-36

TIME: 22 MICROSECONDS

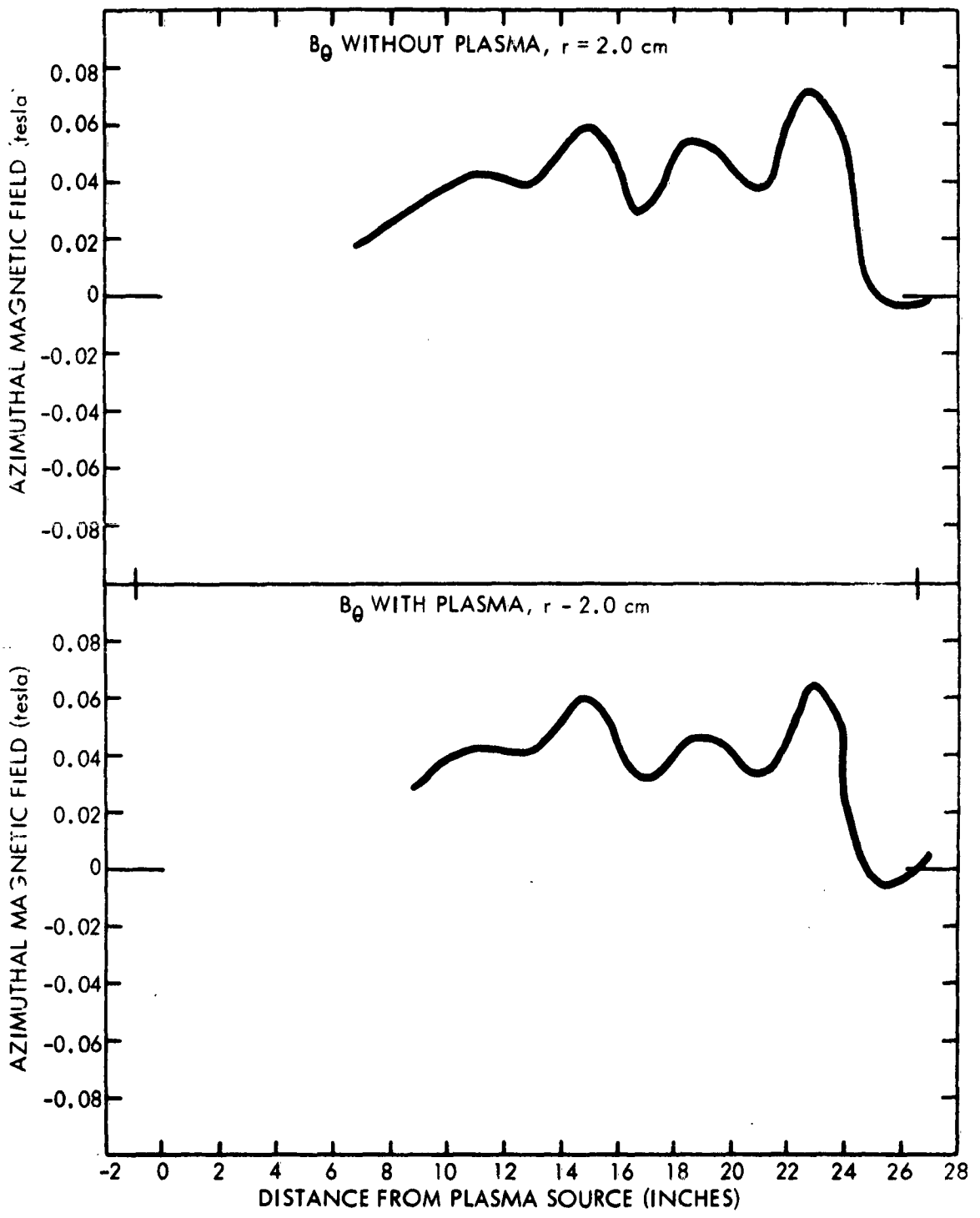

FIGURE B-37

TIME: 24 MICROSECONDS

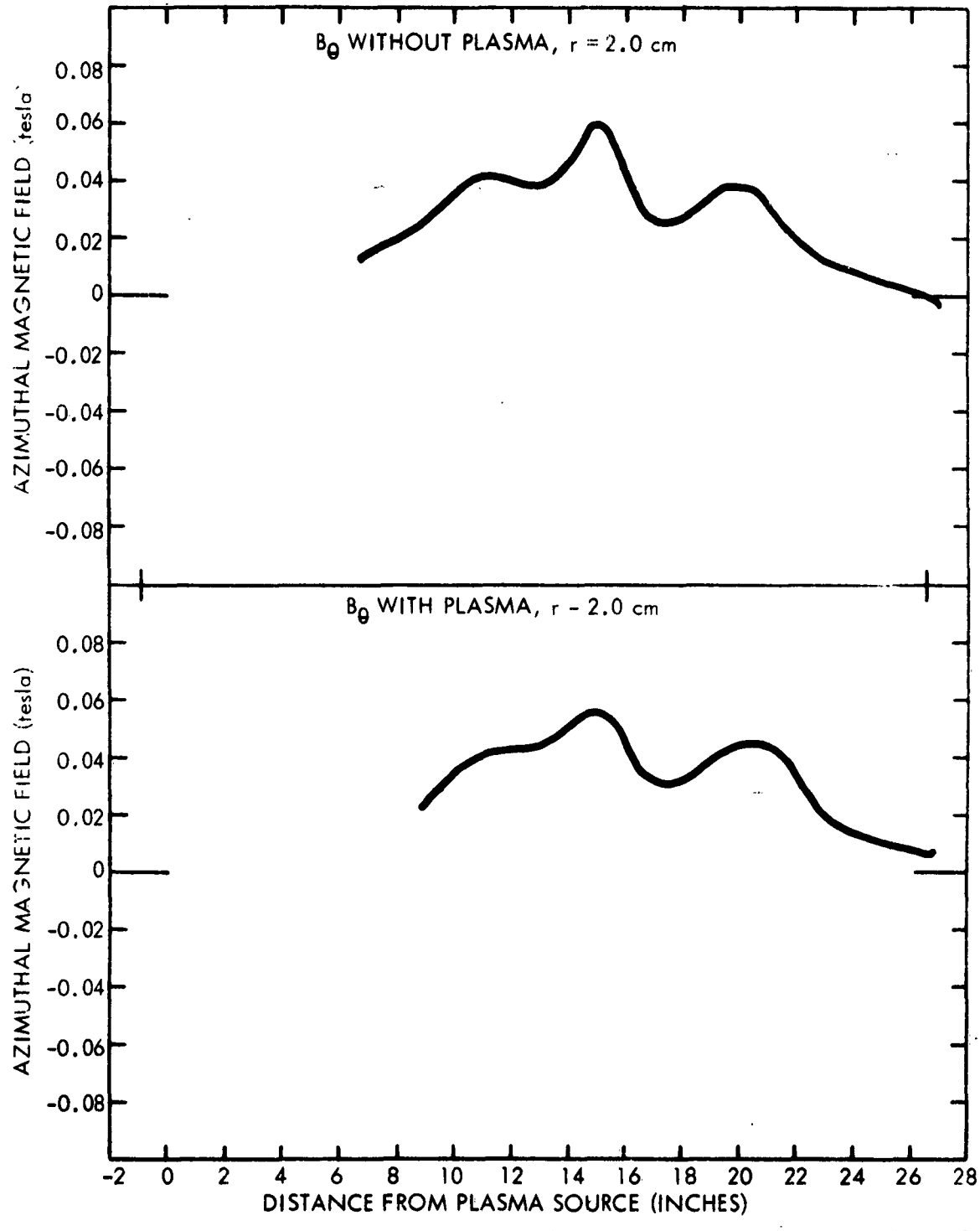

FIGURE B-38

TIME: 26 MICROSECONDS

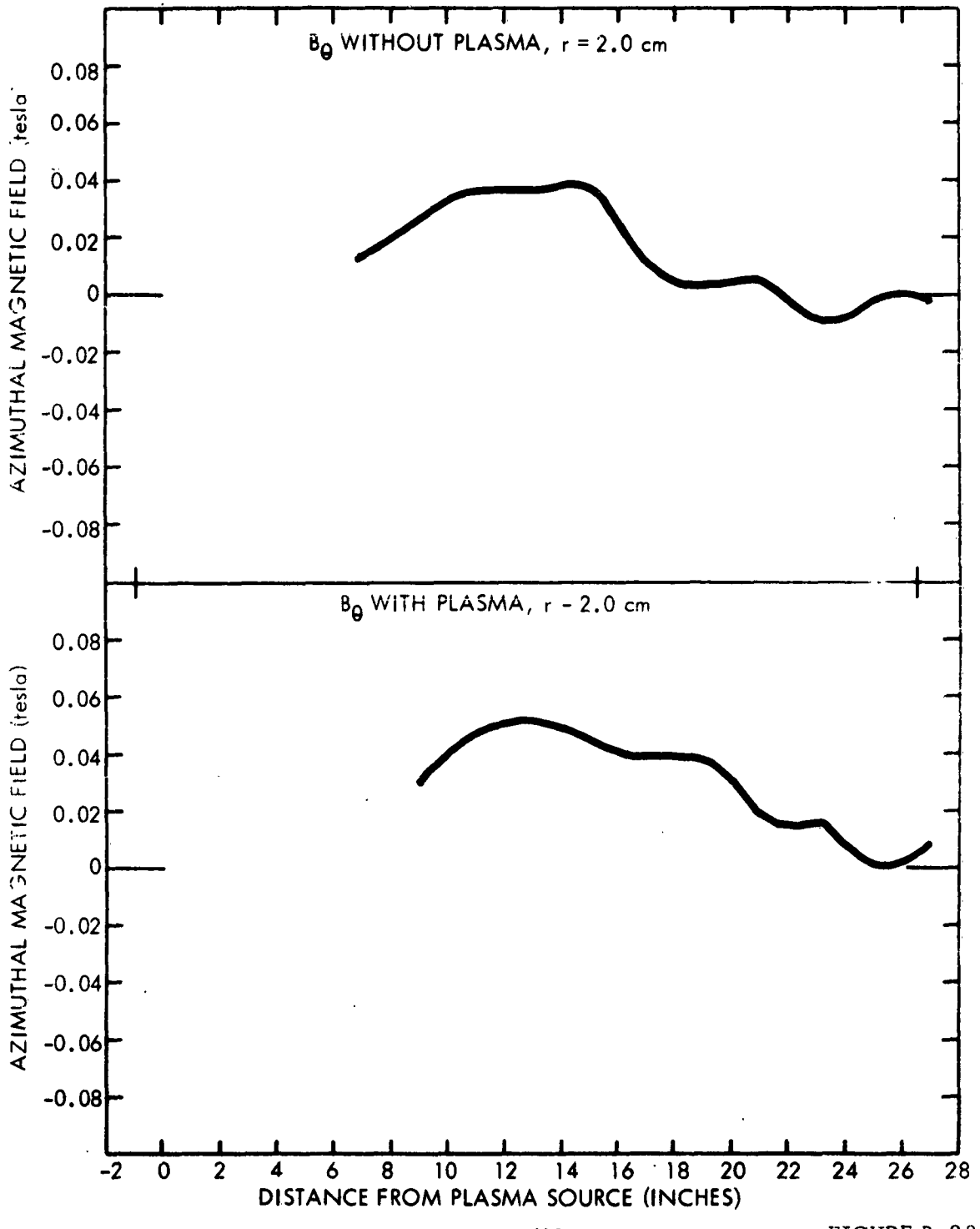

FIGURE B-39

TIME: 28 MICROSECONDS

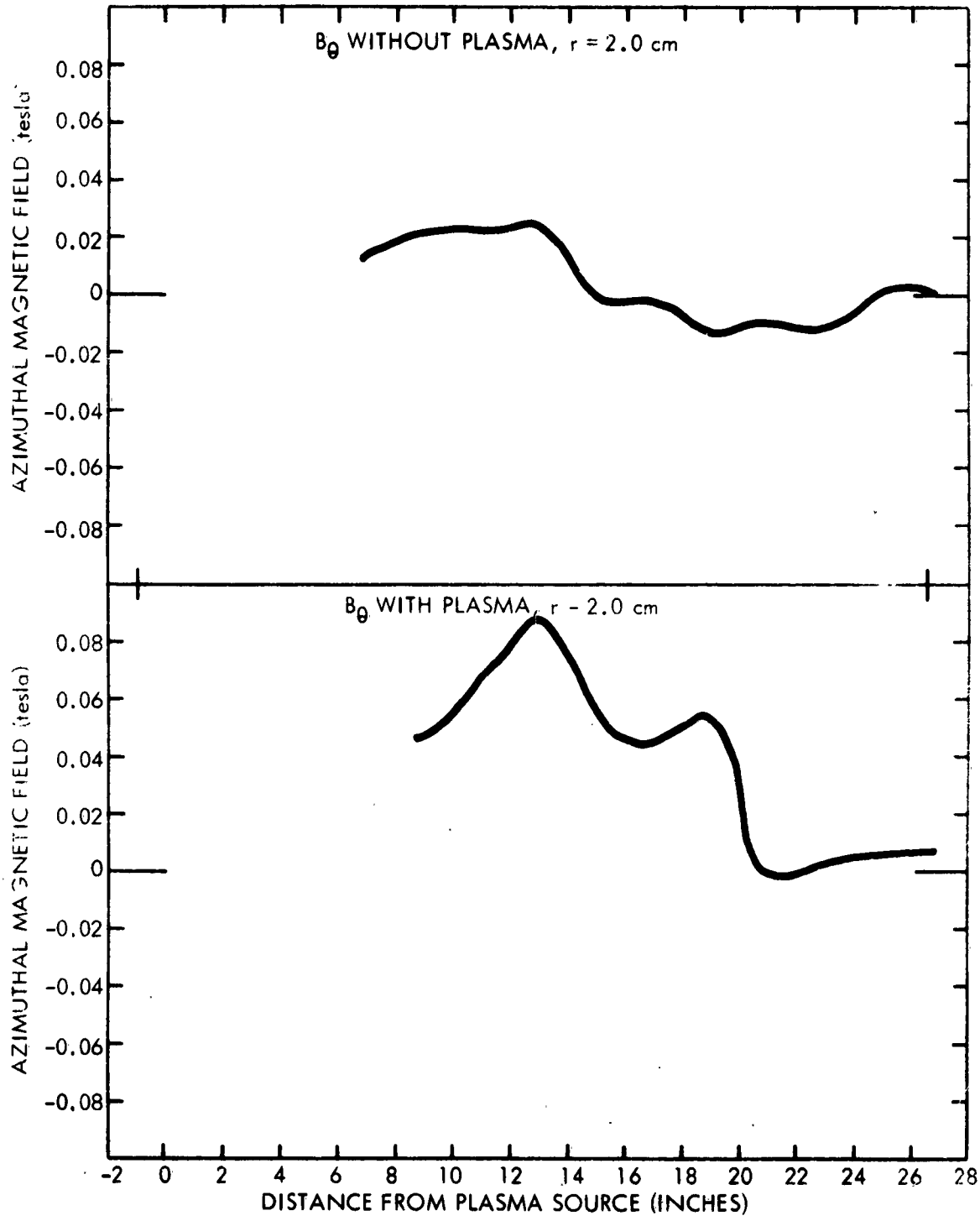

FIGURE B-40

TIME: 30 MICROSECONDS

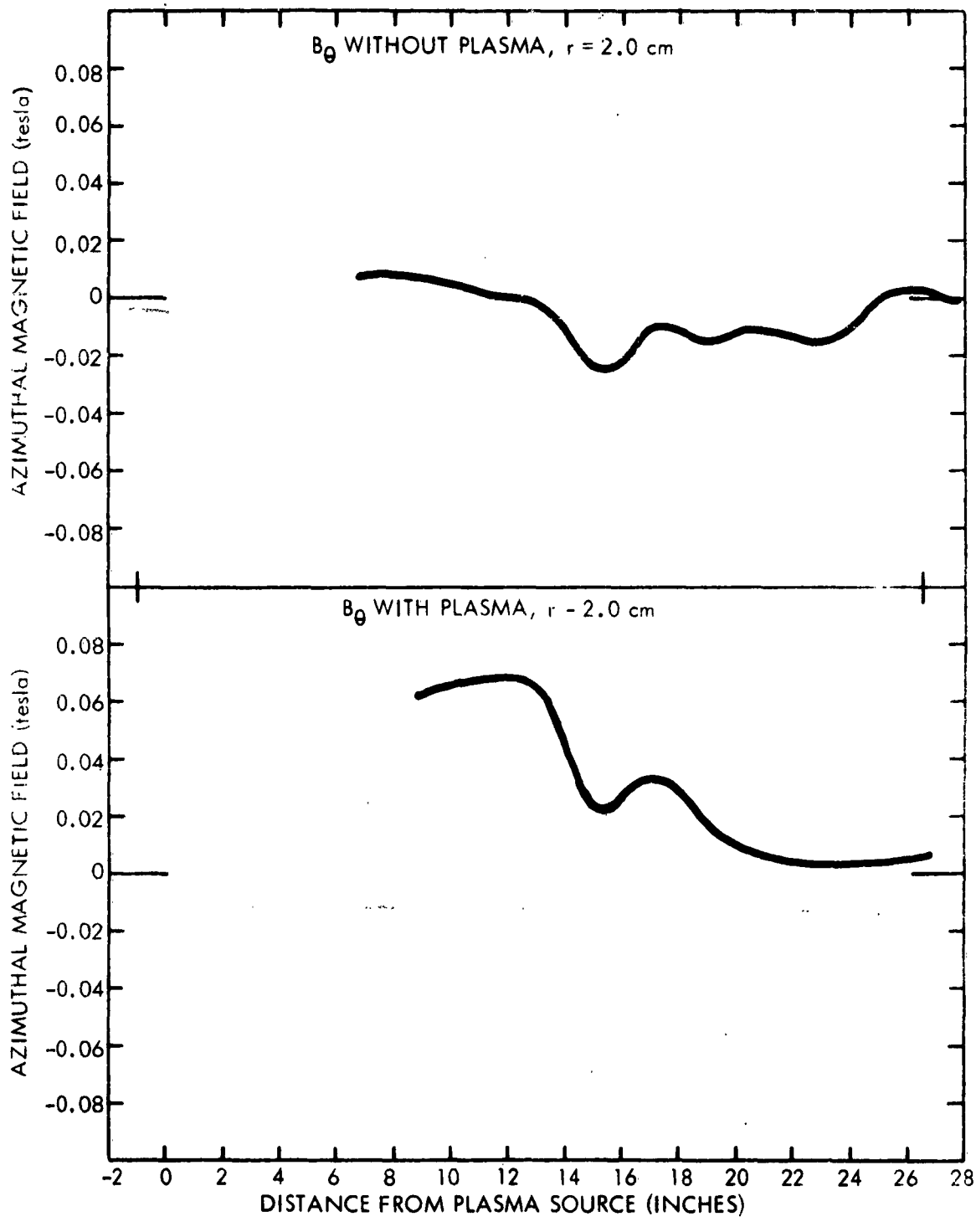

FIGURE B-41

TIME: 32 MICROSECONDS

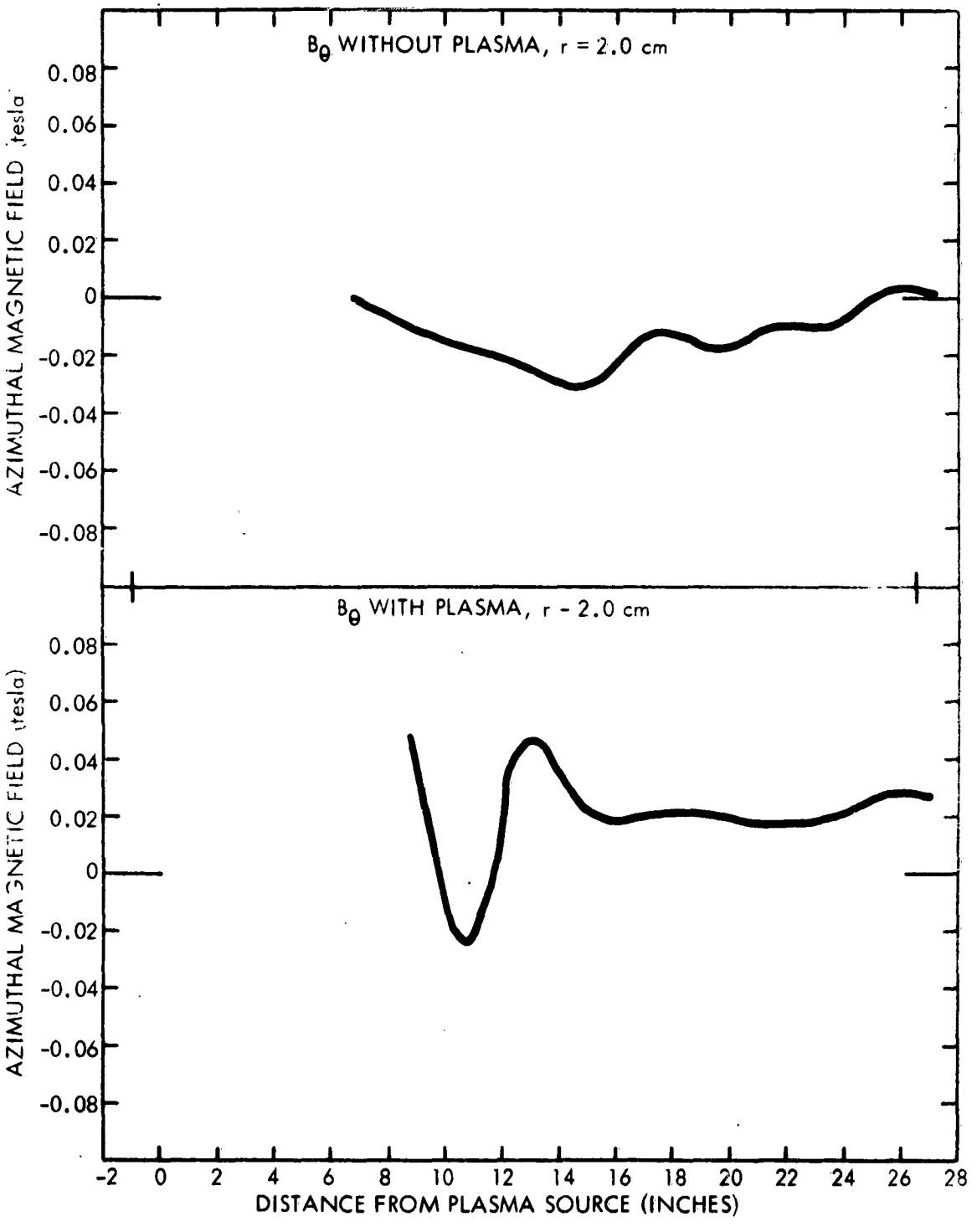

FIGURES B-42

TIME: 34 MICROSECONDS

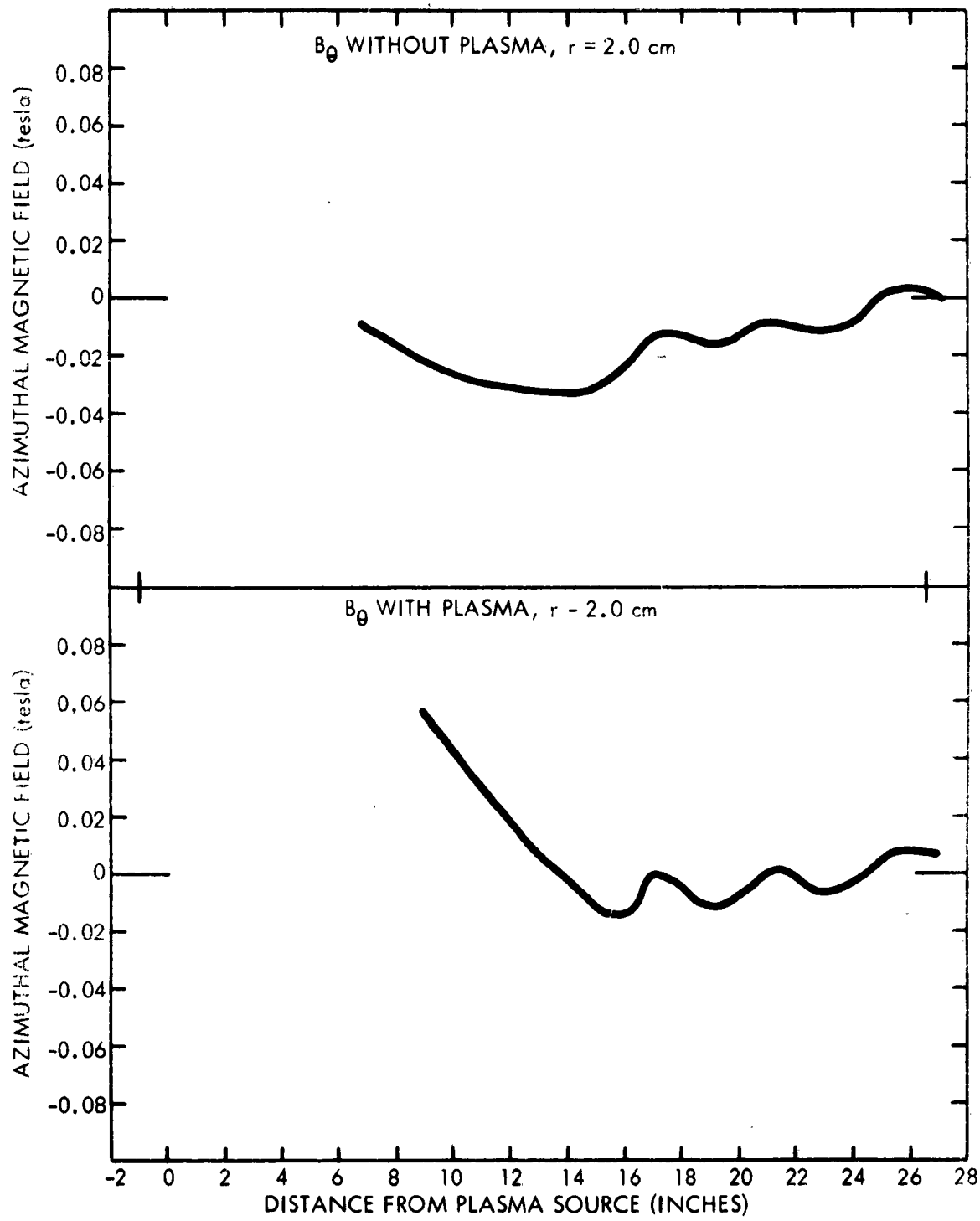

FIGURE B-43

TIME: 36 MICROSECONDS

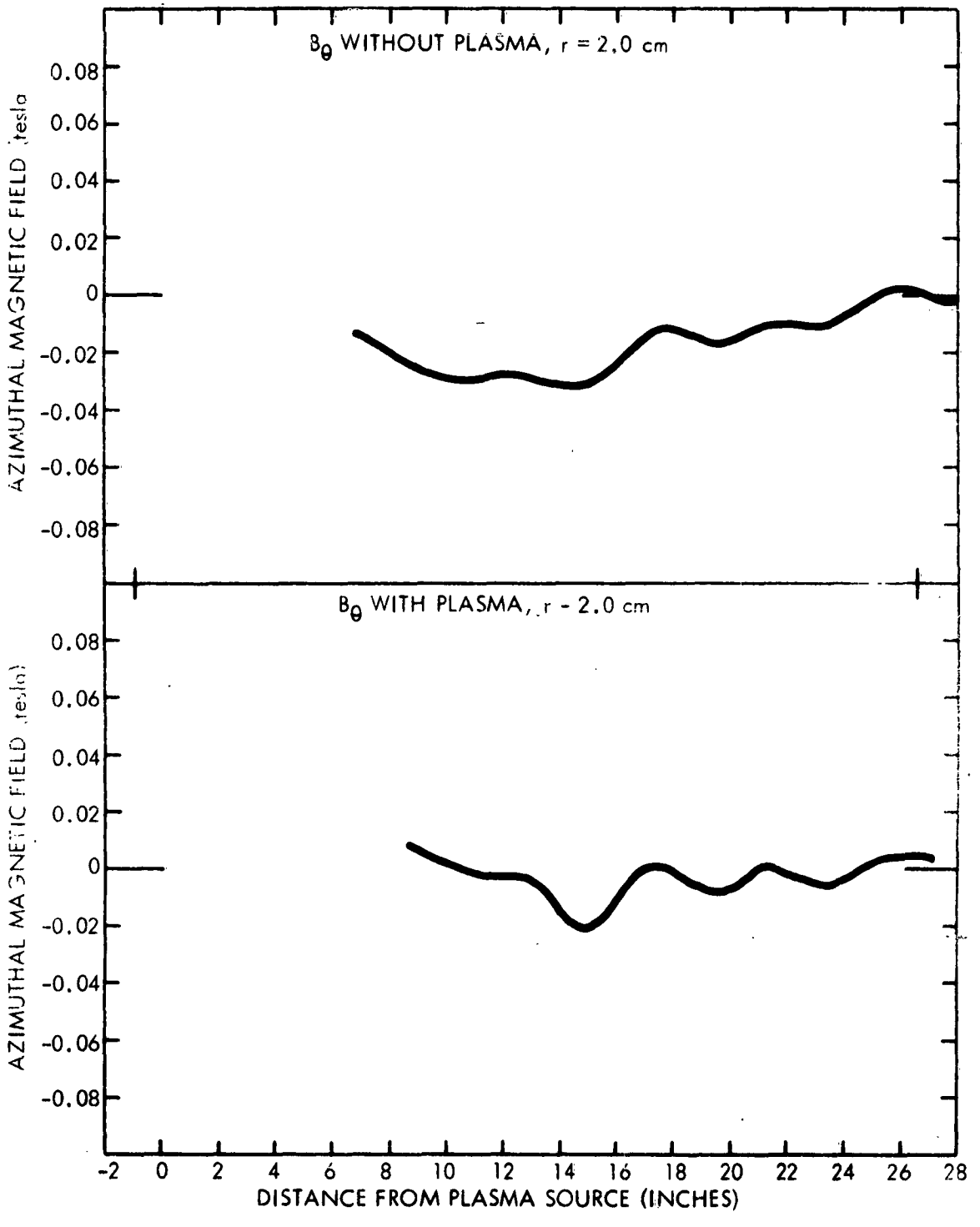

FIGURE B-44

PLASMA DENSITY DISTRIBUTIONS

(Figures B-45 through B-51)

Plasma density distribution, 0.5 cm from transmission line axis measured with a floating double probe at two-inch intervals from the plasma source. The source was energized by a 0.6 μf capacitor charged to 18 kV and was triggered simultaneously with the transmission line, which was energized by a 15 μf capacitor charged to 6 kV. The abscissa shows distance from the plasma source, and the ordinate is in arbitrary units with a nominal calibration of 6×10^{13} ions/cc/unit.

TIME: 12 MICROSECONDS

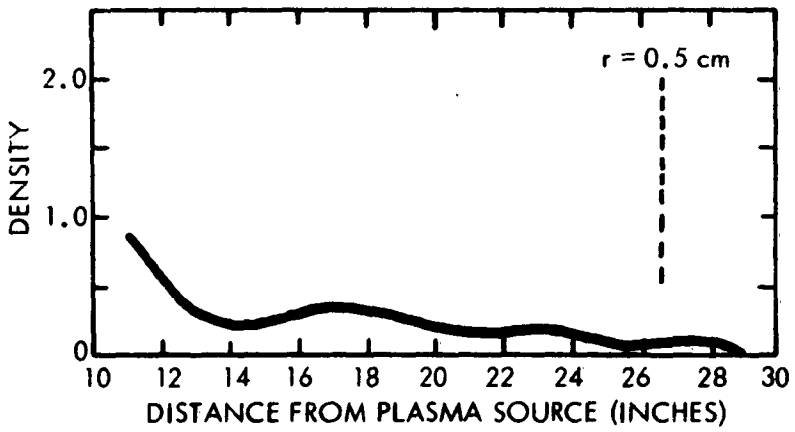

TIME: 14 MICROSECONDS

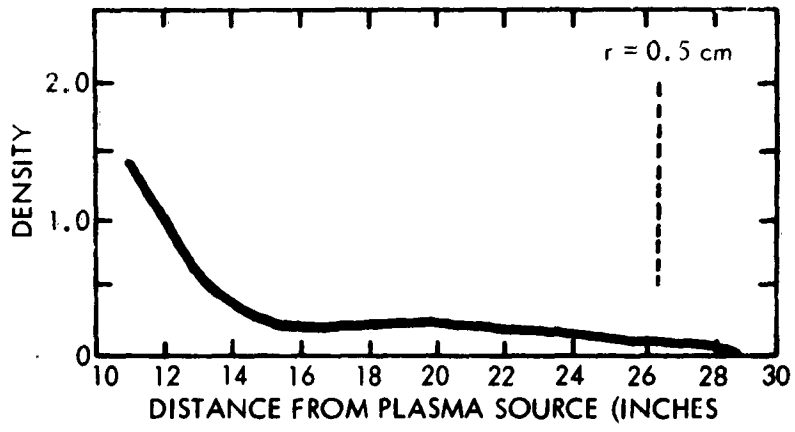

FIGURE B-45

TIME: 16 MICROSECONDS

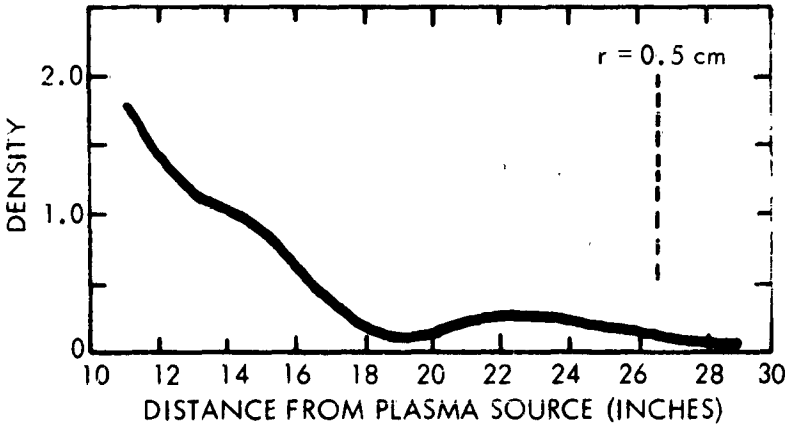

TIME: 18 MICROSECONDS

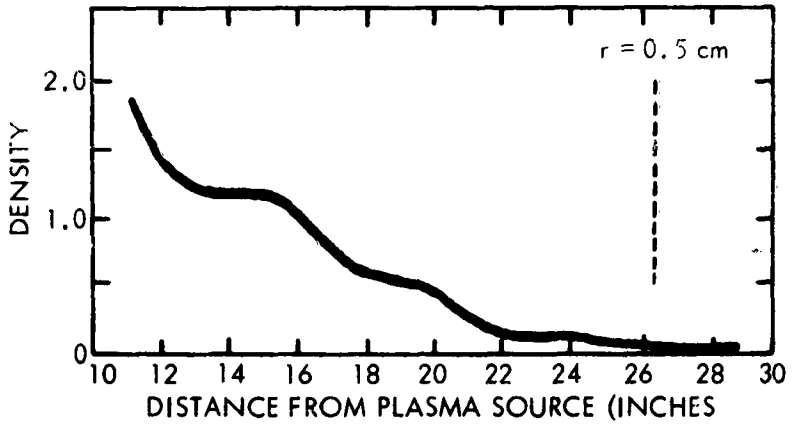

FIGURE B-46

TIME: 20 MICROSECONDS

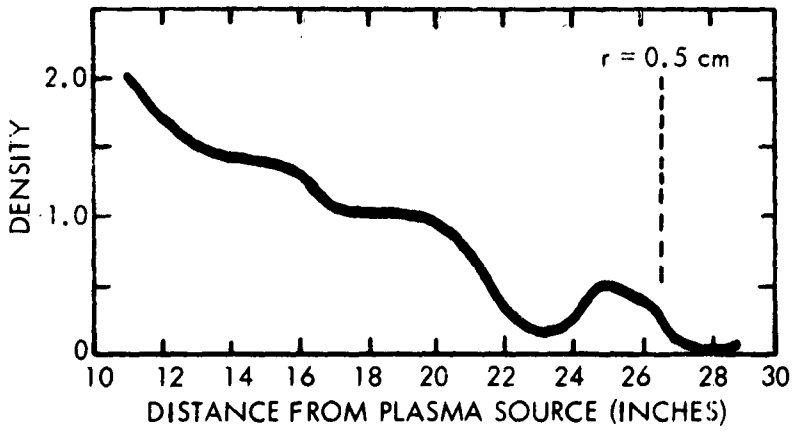

TIME: 22 MICROSECONDS

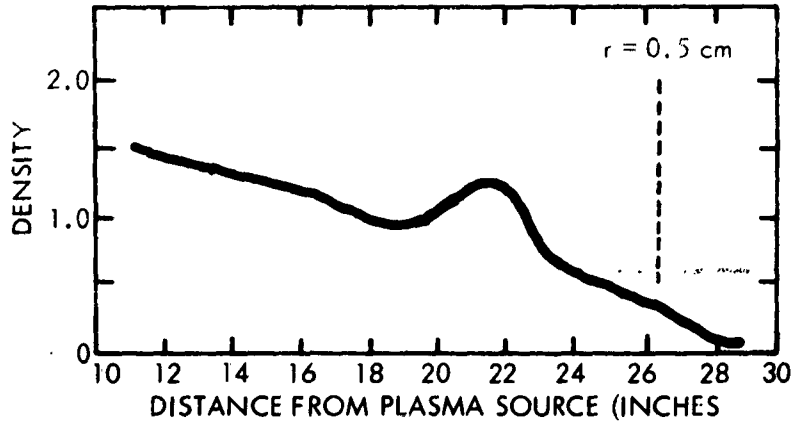

FIGURE B-47

TIME: 24 MICROSECONDS

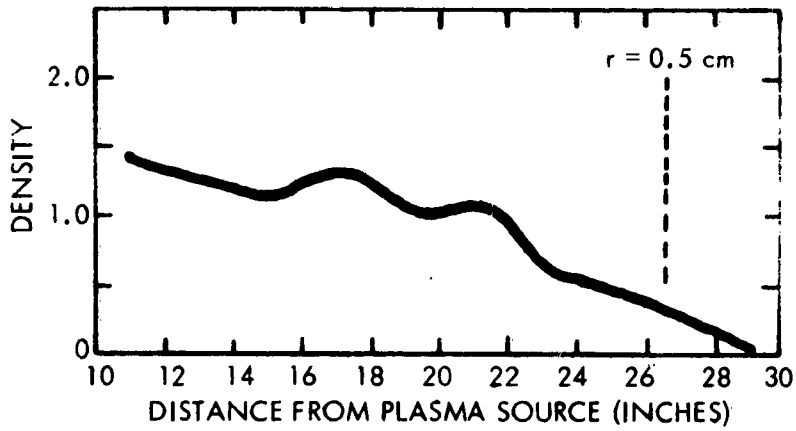

TIME: 26 MICROSECONDS

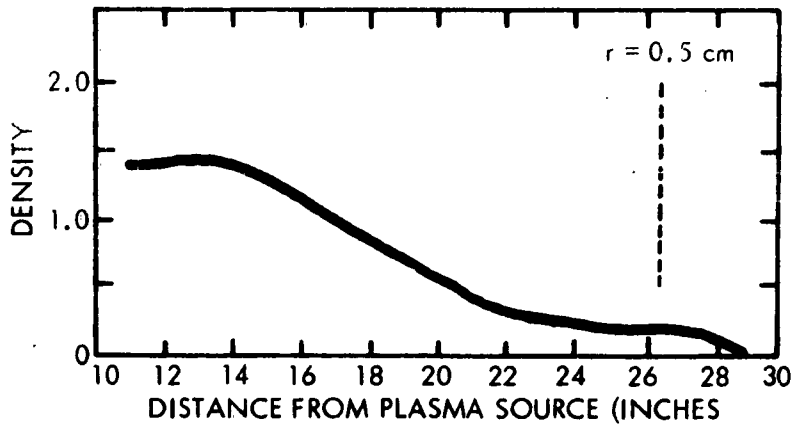

FIGURE B-48

TIME: 28 MICROSECONDS

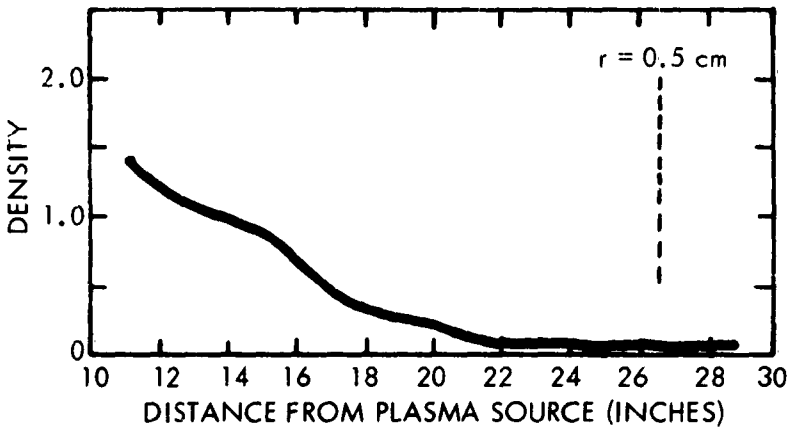

TIME: 30 MICROSECONDS

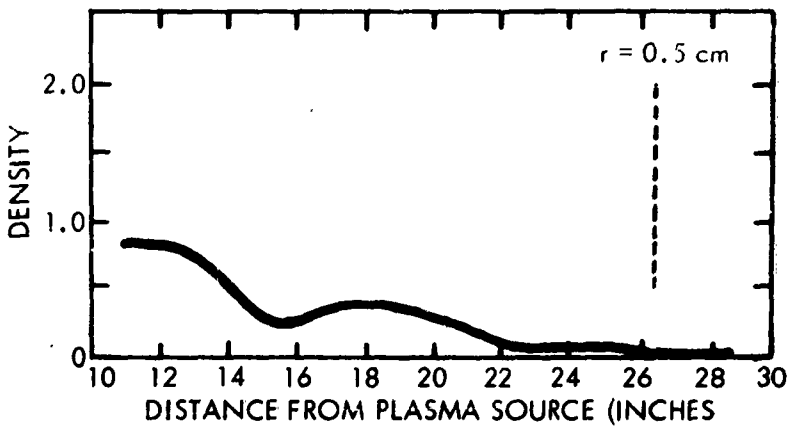

FIGURE B-49

TIME: 32 MICROSECONDS

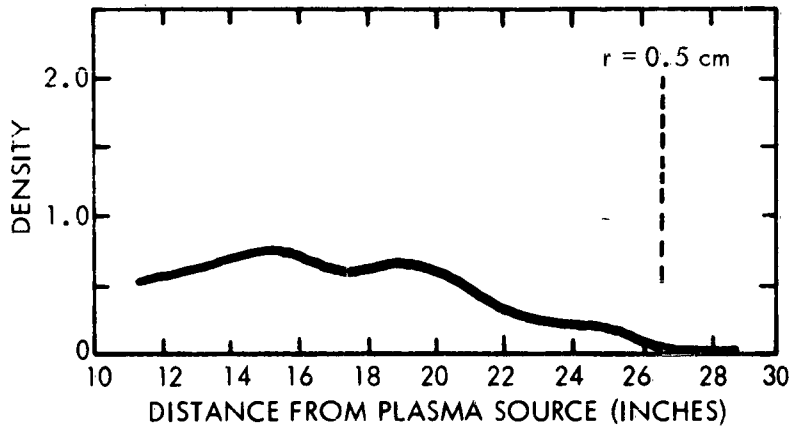

TIME: 34 MICROSECONDS

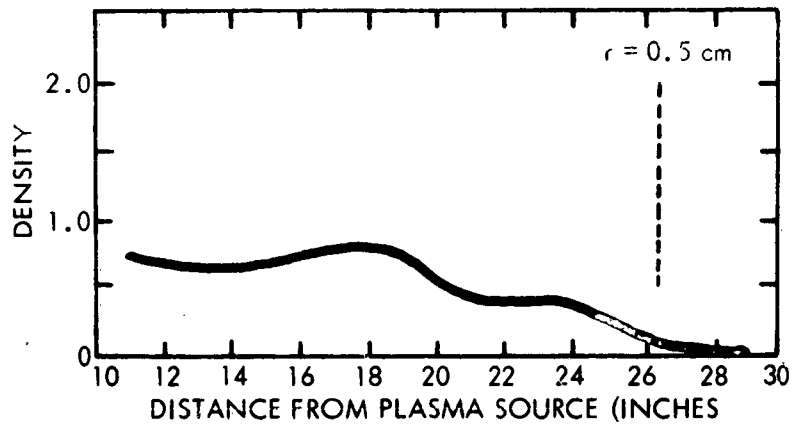

FIGURE B-50

TIME: 36 MICROSECONDS

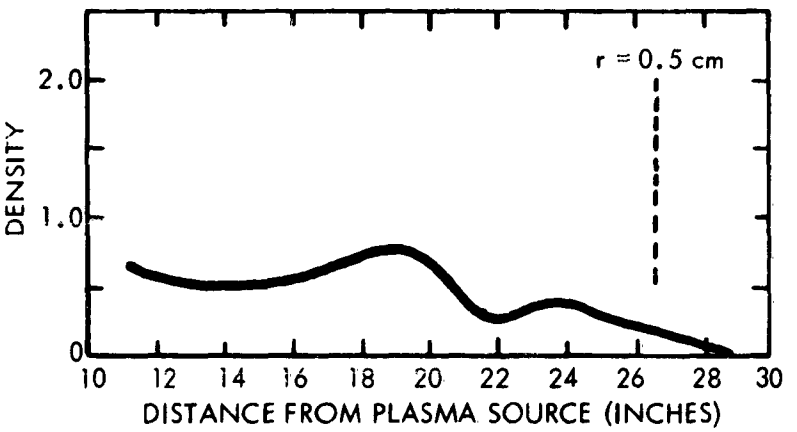

TIME: 38 MICROSECONDS

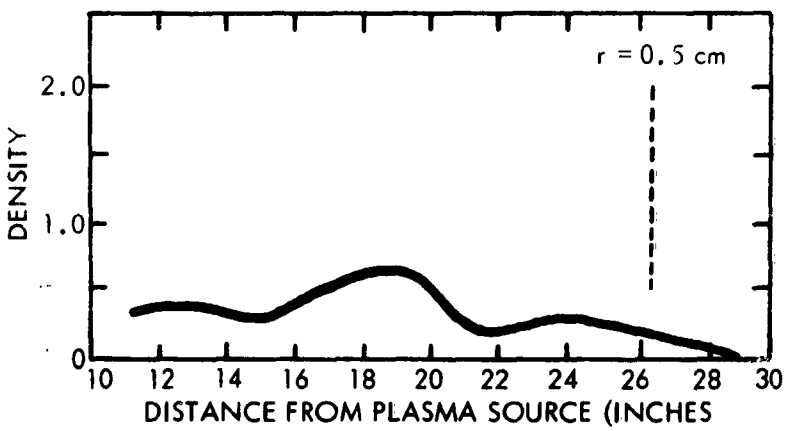

FIGURE B-51

DISTRIBUTION LIST

CONTRACT AF 33(616)-8331

1. AEDC (AEGP)
Arnold AFS, Tennessee

2. AFOSR
Attn: Dr. M. Slawsky
Building T-D
Washington 25, D.C.

3. AFSC (SCG)
Andrews AFB
Washington 25, D.C.

4. AFSWC (Library)
Kirtland AFB
Albuquerque, New Mexico

5. - 14. ASTIA (TIPDR)
Arlington Hall Station
Arlington 12, Virginia

15. ATIC (AFCIN-4E3c)
Wright-Patterson AFB, Ohio

16. National Aeronautics & Space Administration
George C. Marshall Space Flight Center
Attn: Dr. E. Stuhlinger
Huntsville, Alabama

17. National Aeronautics & Space Administration
Goddard Space Flight Center
Advanced Project Group
Attn: Mr. Eugene Dangle
Greenbelt, Maryland

18. National Aeronautics & Space Administration
Attn: Dr. H. Finger
1520 H Street, N.W.
Washington 25, D.C.

DISTRIBUTION LIST
(Continued)

19. National Aeronautics & Space Administration
Attn: Mr. I. R. Schwartz
1520 H Street, N.W.
Washington 25, D.C.

20. National Aeronautics & Space Administration (BIL)
Technical Library
1520 H Street, N.W.
Washington 25, D.C.

21. - 22. National Aeronautics & Space Administration
Lewis Research Center
Attn: Mr. H. Childs
21000 Brookpark Road
Cleveland 35, Ohio

23. Naval Bureau of Weapons
Attn: Library
Washington 25, D.C.

24. SSD
Attn: Maj. Frances E. Baker
Air Force Systems Command
A. F. Unit Post Office
Los Angeles 45, Calif.

25. U. S. Naval Research Laboratory Library
Washington 25, D.C.

26. U. S. Atomic Energy Commission
Technical Information Service
1901 Constitution Avenue
Washington 25, D.C.

27. Cornell University
Ithica, New York

28. Massachusetts Institute of Technology
Attn: Library
Cambridge 39, Mass.

DISTRIBUTION LIST
(Continued)

29. University of Michigan
Ann Arbor, Michigan

30. Northwestern University
Evanston, Illinois

31. Purdue University
West Lafayette, Indiana

32. Stevens Institute of Technology
Hoboken, New Jersey

33. University of Southern California
Los Angeles 7, California

34. Advanced Kinetics, Inc.
Attn: Mr. R. L. Gradishar
1231 Victoria Street
Costa Mesa, California

35. Aerojet-General Nucleonics
Attn: Mr. John Luce
San Ramon, California

36. Aeronutronics
Division of Ford Motor Co.
Attn: Library
Newport Beach, California

37. Technical Data Center
Aerospace Corporation
Attn: D. H. Loughridge
Director of Applied Research Management
USAF Unit Post Office
Los Angeles 45, California

38. Allison Division
General Motors Corporation
Attn: Mr. T. L. Rosebrock
Indianapolis 6, Indiana

DISTRIBUTION LIST
(Continued)

39. Armour Research Foundation
10 W. 35th Street
Chicago 16, Illinois

40. Astropower, Inc.
3801 Lakewood Blvd.
Long Beach, California

41. AVCO-Everett Research Laboratory
2385 Revere Beach Parkway
Everett 49, Massachusetts

42. AVCO Research and Development
201 Lowell Street
Wilmington, Massachusetts

43. Clauser Technology
3510 Torrance Blvd.
Torrance, California

44. Electro-Optical Systems, Inc.
125 N. Vinedo Avenue
Pasadena, California

45. General Electric Company
Aerosciences Laboratory
3750 D Street
Philadelphia 24, Pennsylvania

46. General Electric Company
Space Power and Propulsion Section
Cincinnati 15, Ohio

47. General Dynamics/Astronautics
5001 Kearny Villa Road
San Diego 12, California

48. Giannini Controls Corporation
Attn: Mr. A. J. Mancrieff-Yeates
1600 S. Mountain Avenue
Duarte, California

DISTRIBUTION LIST
(Continued)

49. Jet Propulsion Laboratory
Attn: Mr. J. J. Paulson
California Institute of Technology
4800 Oak Grove Drive
Pasadena, California

50. Litton Industries
Attn: Mr. E. L. DeGraeve
336 N. Foothill Road
Beverly Hills, California

51. Lockheed Aircraft Corporation
Missiles and Space Division
Technical Information Center
3256 Hanover Street
Palo Alto, California

52. Marquardt Corporation
Attn: Mr. A. Thomas
16555 Saticoy Street
Van Nuys, California

53. MHD Inc.
Attn: Dr. V. Blackman
Box 1815
Newport Beach, California

54. Norair Division
Northrop Corporation
1000 E. Broadway
Hawthorne, California

55. Plasmadyne Corporation
3839 S. Main Street
Santa Ana, California

56. Radio Corporation of America
Princeton, New Jersey

DISTRIBUTION LIST
(Continued)

57. Rand Corporation
1700 Main Street
Santa Monica, California

58. Republic Aviation Corporation
Attn: Mr. A. Kunen
Conklin Street
Farmingdale, Long Island, New York

59. Rocketdyne
A Division of North American Aviation
Attn: Dr. McDole
6633 Canoga Avenue
Canoga Park, California

60. Space Craft General
777 Flower Street
Glendale 1, California

61. Space Dynamics Laboratory
2215 Florence Avenue
Cincinnati 6, Ohio

62. Space Sciences
2 Mercer Road
Nantucket, Massachusetts

63. Space Technology Laboratories, Inc.
1 Space Park
Redondo Beach, California

64. Thermal Dynamics
Hanover, New Hampshire

65. Thompson Ramo Wooldridge
New Devices Laboratory
7209 Platt Avenue
Cleveland, Ohio

DISTRIBUTION LIST
(Continued)

66. Thiokol Chemical Corporation
Reaction Motors Division
Attn: Mr. M. Levoy
Denville, New Jersey

67. Unified Science Associates, Inc.
826 South Arroyo Parkway
Pasadena, California

68. United Aircraft Corporation
(Research Laboratory)
400 Main Street
East Hartford, Connecticut

69. Vidya, Inc.
2626 Hanover Street
Palo Alto, California

70. Vitro Laboratories
Div. of Vitro Corporation
200 Pleasant Valley Way
West Orange, New Jersey

71. Aero-Chem Research Laboratories
Attn: Dr. H. F. Colcote
Princeton, New Jersey

72. - 75. ASD (ASRMPE-1)
Wright-Patterson AFB, Ohio

Aeronautical Systems Div., Dir/Aeromechanics, Propulsion Laboratory, Wright-Patterson AFB, Ohio Rept. Nr. ASD-TDR-62-1105, INVESTIGATION OF ELECTRODELESS PULSED PLASMA PROPULSION. Final report, Feb. 1963. 132 p. incl. illus., tables, 10 refs. Unclassified report

The investigation was directed toward the determination of the nature of the field-plasma interaction and the over-all performance characteristics of electrodeless accelerators. The button-type sources studied proved suitable for injecting into the lumped-parameter helical transmission line and capable of producing a copper plasma with densities up to 10^{15}/cc and velocities in the neighborhood of 2×10^4 m/sec. Conductivities were in the range

(over)

of 1000 to 1500 mho/m. Among the principal results of the studies of the interaction of this plasma with the transmission line was the preferential trapping of plasma on the leading portion of the traveling cusp. This result was in sharp contrast to the ineffectiveness of the trailing half of the cusp to retain and accelerate the plasma. Also, there was found direct evidence for the presence of circulating Hall currents in the accelerator. Finally, there is strong evidence for the occurrence of a large-scale instability which developed in the reflected wave.

UNCLASSIFIED

1. Accelerators
2. Propulsion devices
3. Acceleration
4. Plasma sources
5. Inductive plasma accelerators

I. AFSC Project 3141, Task 314103

II. Contract AF 33(616)-8331

III. Aerojet-General Nucleonics, San Ramon, California

IV. Luce, J. S., Gates, D.C., et al.

V. AGN Report No. AN-759

VI. In ASTIA collection

UNCLASSIFIED

Aeronautical Systems Div., Dir/Aeromechanics, Propulsion Laboratory, Wright-Patterson AFB, Ohio Rept. Nr. ASD-TDR-62-1105, INVESTIGATION OF ELECTRODELESS PULSED PLASMA PROPULSION. Final report, Feb. 1963. 132 p. incl. illus., tables, 10 refs. Unclassified report

The investigation was directed toward the determination of the nature of the field-plasma interaction and the over-all performance characteristics of electrodeless accelerators. The button-type sources studied proved suitable for injecting into the lumped-parameter helical transmission line and capable of producing a copper plasma with densities up to 10^{15}/cc and velocities in the neighborhood of 2×10^4 m/sec. Conductivities were in the range

(over)

of 1000 to 1500 mho/m. Among the principal results of the studies of the interaction of this plasma with the transmission line was the preferential trapping of plasma on the leading portion of the traveling cusp. This result was in sharp contrast to the ineffectiveness of the trailing half of the cusp to retain and accelerate the plasma. Also, there was found direct evidence for the presence of circulating Hall currents in the accelerator. Finally, there is strong evidence for the occurrence of a large-scale instability which developed in the reflected wave.

UNCLASSIFIED

1. Accelerators
2. Propulsion devices
3. Acceleration
4. Plasma sources
5. Inductive plasma accelerators

I. AFSC Project 3141, Task 314103

II. Contract AF 33(616)-8331

III. Aerojet-General Nucleonics, San Ramon, California

IV. Luce, J. S., Gates, D.C., et al.

V. AGN Report No. AN-759

VI. In ASTIA collection

UNCLASSIFIED